Sodium chloride crystallization in drying porous media: influence of inhibitor

Sonia Gupta

Sodium chloride crystallization in drying porous media: influence of inhibitor

Sonia Gupta

geboren te Ludhiana, India

Dit proefschrift is goedgekeurd door de promotoren en de samenstelling van de promotiecommissie is als volgt:

voorzitter: prof.dr.ir. G.M.W. Kroesen
1^e promotor: prof.dr.ir. K. Kopinga
copromotor(en):   dr.ir. L. Pel
                    dr. M. Prat (University of Toulouse)
leden: prof. A. Putnis PhD (University of Münster)
                    PD.Dr.habil. M. Steiger (Hamburg University)
                    prof.dr.ir. D.M.J. Smeulders
                    prof.dr. C.M. Rodriguez Navarro (Granada University)

To my parents

IV

Contents

Sodium chloride crystallization in drying porous media: influence of inhibitor

Chapter 1

Introduction

1.1 Salt weathering

Salt weathering, i.e. damage of the building materials due to the presence of salt. It is one of the most pervasive threats to the long-term survival of porous building materials, historic structures and stone monuments worldwide. Damage of porous materials due to the presence of salt is known since ancient times, see, e.g., Herodotus 420 B.C. [1]. A historic structure has a great cultural and social importance for the history of a country. Their damage, due to the presence of salt, is not only a physical loss of the material but also a loss with significant cultural and economic implications. To avoid these problems, in the last decades there has been increasing scientific interest in building material decay phenomena [2-4]. This interest has led to an increase in research to understand the role of salt in damage.

It is widely recognized that soluble salts such as chlorides, sulphates and nitrates are the sources of damage. The damage is mainly due to the crystallization of these soluble salts inside the porous matrix of the materials. These salt crystals accumulate just beneath the surface of the material or inside the porous layers of the material. The growth of salt crystals exerts pressure on the pore walls, which can exceed the tensile strength of the material. The hazardous consequences of salt crystallization inside the material can be understood by considering the examples shown in fig. 1.1.

Figure 1.1: *Examples of the damage to brickwork in Venice. The buildings in Venice are in a constant state of destruction almost entirely due to marine salt (dominated by NaCl).*

Sodium chloride (NaCl)

The salts responsible for damage can enter or be transported within the porous materials only if dissolved in water. Water ultimately leaves the porous material by evaporation, leaving behind salt crystals inside the material. Sodium chloride (NaCl) is one of the most

abundant and ubiquitous among various salts commonly found in buildings. It can be present in weathered rocks and construction materials in a wide range of environments such as hot, cold and humid coastal areas [5, 6]. Sodium chloride found in porous materials may either originally be present in the materials, e.g., mortars prepared using sand from the sea, or may have penetrated later in the walls, e.g., from external sources. The Netherlands is partially located beneath the sea level. Therefore, sea flooding has often constituted an important source of salts. Consequently, the walls of the buildings located in the flooding area are often contaminated with NaCl. Besides, the presence of sea-salt spray in the coastal areas and the use NaCl as deicing salt causes NaCl to be one of the most commonly present salt in buildings. Therefore, the damage caused by NaCl crystallization is wide spread.

1.2 Damage mechanisms

Many studies have been carried out in the past to understand the underlying salt damage mechanism. However, until now there is no unambiguously accepted hypothesis on the mechanism(s) responsible for the damage. The mechanisms most often addressed as causes of damage will now successively be discussed.

1.2.1 Crystallization pressure

Lavalle published the first scientific study on the relation between salt crystallization and pressure in 1853 [7]. In that work, experiments indicating the ability of salts to push away a certain weight were described. In early 20th century, these results were confirmed and extended [8, 9]. An important conclusion was that a liquid film must exist between the growing salt crystal and the pore wall (denoted by δ in fig. 1.2). Salt ions can diffuse through this film to the surface of the growing crystal. If such a film does not exist, the crystal cannot grow any further and the growth will stop. However, for the existence of this film, a repulsive force must exist between the pore wall and the crystal [10]. The electrostatic forces across the liquid film sandwiched between the salt crystal and the pore walls are held responsible for this repulsion [10]. Another important conclusion was that the growing salt crystal can only exert pressure when it is in contact with a supersaturated solution.

In 1949, Corren's presented a mathematical model that gives a relation between crystallization pressure and supersaturation [11]. He showed that a crystal placed in a supersaturated solution tends to grow. In order to stop its growth, a certain pressure has to be applied which is given by:

$$P_c = \frac{RT}{V_m} ln\left(\frac{C}{C_o}\right) \qquad (1.1)$$

In this equation, P_c is the crystallization pressure, R is the universal gas constant, T is the absolute temperature, V_m is the molar volume of the salt crystal, C and C_o are the concentration of a supersaturated and saturated salt solution, respectively (see fig. 1.2). Corren's also stated that for this condition to hold, no other non-pressurized crystal should be present in the solution, because otherwise it would consume all the supersaturation. He also argued that the interfacial energy between crystal/material interfaces should be higher than

the sum of the interfacial energies between the crystal/liquid and mineral/liquid interface. If this condition is satisfied, a direct contact between the salt crystal and the mineral wall does not occur and a solution layer can enter between the pore wall and the crystal.

Corren's related the crystallization pressure to supersaturation of the solution, whereas Everett [12] related the pore size distribution of the material to the crystallization pressure. Everett's approach is based on the properties of curved interfaces between the crystal and the solution. Considering the chemical potential difference between a bigger and a smaller crystal, he derived the following expression for crystallization pressure:

$$P_c = \gamma_{cl} \frac{dA}{dV} \tag{1.2}$$

Where, γ_{cl} is the solid liquid interfacial free energy, A is the surface area and V is the volume of the crystal. In a first approximation, $dA/dV \sim 1/r$, where r is the radius of the pore. This equation indicates that the crystallization pressure will be lower in larger pores.
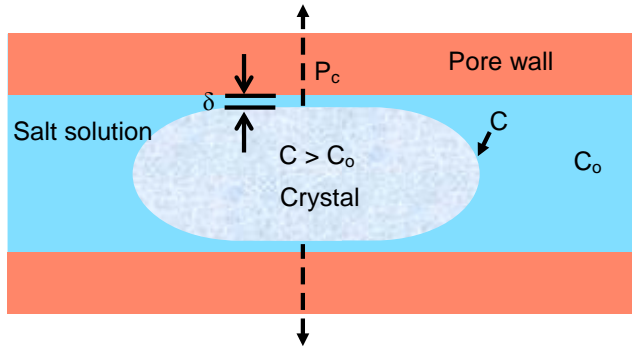
Figure 1.2: *Schematic representation of a crystal confined between the pore walls with a salt solution layer (δ) between crystal and pore wall.*

These two approaches (Corren and Everett) are extensively used in the literature to calculate the crystallization pressure. Recently, Steiger [13, 14] came up with a single equation for the calculation of the crystallization pressure, taking into account both the degree of supersaturation of the solution and the effect of curvature of the crystal liquid interface. The crystallization pressure exerted by a crystal growing from a supersaturated solution of an electrolyte is given by [14]:

$$P_c = \frac{vRT}{V_m}\left(ln\frac{m}{m_o} + ln\frac{\gamma_\pm}{\gamma_{\pm,o}} + \frac{v_o}{v}ln\frac{a_w}{a_{w,o}}\right) - \gamma_{cl}\frac{dA}{dV} \tag{1.3}$$

In this equation, v is the total number of ions released upon dissociation of the salt (e.g. for NaCl, $v = 2$), m_o, $\gamma_{\pm,o}$ and $a_{w,o}$ refer to the molality, the mean activity coefficient and the water activity of the saturated solutions, respectively, and v_o is the number of molecules of water. The last term in eq.(1.3) accounts for the effect of crystal size on the crystallization pressure. This effect becomes significant for crystals smaller than 100 nm [14]. Since the pore size of most natural stones is larger, the influence of crystal size can be neglected. For anhydrous

salts like NaCl, $v_o = 0$, and therefore the last term within the parenthesis vanishes. For ideal solutions, where $\gamma_\pm = 1$, eq. (1.3) can be rewritten as:

$$P_c = \frac{vRT}{V_m}\left(ln\frac{m}{m_o}\right) \tag{1.4}$$

This equation is comparable to eq. (1.1). The first term within the bracket corresponds to the term $ln(C/C_o)$ term in eq. (1.1) describing supersaturation. It should be noted that in eq. (1.1), the dissociation of ions was not considered, and therefore the factor v is not present. However, this can lead to large errors in calculation of crystallization pressure e.g., in case of a 1:1 electrolyte like NaCl, the Corren's equation would underestimate the crystallization pressure by factor 2.

In the thermodynamic approach of the crystallization pressure outlined above, the poromechanic properties of the material are not taken into account. In an alternative poromechanic approach, these properties are included. The expansion of the material is considered to be caused by a poromechanical pressure (P_m). Assuming a uniform distribution of the crystals inside the pores with no preferred direction of the crystal growth, the poromechanical pressure (P_m) exerted by a confined crystal in a porous material is given as [15]:

$$dP_m = \frac{3K}{bS_C}(d\varepsilon - \alpha dT) \tag{1.5}$$

Here K is the bulk modulus, b is the Biot-coefficient, S_c is the volume fraction of the crystals, ε is the expansion of a sample resulting from salt crystallization, α is the linear thermal expansion coefficient, and T is the temperature. The term αdT represents the expansion of a sample resulting from thermal dilation only (no crystallization). If a material has no viscoelastic properties, i.e., there is no delay between the exerted pressure and the mechanical reaction of the material, the poromechanical and thermodynamic approaches become equivalent [15].

From the literature cited above it is clear that supersaturation is one of the plausible mechanisms for salt damage. However, in case of NaCl, the question of supersaturation is controversial. Several experiments have been done to show that NaCl does not supersaturate inside the building materials [16]. It has been shown that relevant crystallization pressure develops in nm pore sizes usually absent in traditional building materials [17]. In addition, NaCl tends to crystallize on foreign nucleation sites (e.g. pore walls) [18]. Therefore, to the development of a high crystallization pressure based on supersaturation and the generation of damage are also not so very likely. Despite this fact, damage has been observed due to the presence of NaCl inside building materials, indicating that other mechanisms need to be taken into account.

1.2.2 Differential thermal expansion

Cooke and Smalley [19] have proposed that differential thermal expansion is a possible damage mechanism. This is because certain salts have a higher coefficient of thermal expansion than the material in the pores of which they are present. A necessary condition for

thermal damage to occur is that the pores are completely filled with salt. Such a type of condition is most likely to be fulfilled for repeated cycles of drying and crystallization. As an example, the thermal expansion coefficient of NaCl is 44×10^{-6} °C^{-1} and for most of the building materials, the expansion coefficient is in the range of $3\text{-}14 \times 10^{-6}$ °C^{-1} [20]. The thermal stress (σ) is in first order equal to:

$$\sigma = E \, d\alpha \, dT \tag{1.6}$$

where E is the Young's modulus, $d\alpha$ is the thermal expansion mismatch between the salt and the brick and dT is the temperature change. For fired-clay brick, $E \sim 8$ GPa and $\alpha \sim 4 \times 10^{-6}$ °C^{-1}. Therefore, the thermal expansion mismatch between NaCl and brick is $\sim 40 \times 10^{-6}$ °C^{-1}. For one °C rise in temperature, a thermal stress of ~ 0.32 MPa will be generated. For a day and night temperature variation where the temperature difference can go up to 10 °C, significant stresses can be generated which exceed the tensile strength of the material.

This type of damage occurs at a variation in temperature and therefore cannot explain the results of durability tests performed on these materials at a constant temperature [21], which show serious decays for NaCl. Consequently, differential thermal expansion is not likely to be the main cause of damage.

1.3 Drying

To understand the damage mechanism, it is important to understand the moisture and ion transport and related salt crystallization phenomena inside the material. Drying has a large effect on the moisture and ion distribution processes inside a porous material. The location of salt crystallization is determined by a dynamic balance between drying at the surface (rate of escape of moisture at the surface) and the rate of supply of moisture to the surface [22].

1.3.1 Moisture transport

Drying is a drainage process, where the non-wetting fluid (gas) replaces the wetting fluid (liquid) [23]. In general, drying of a homogeneous, uniformly wet, porous material has two identifiable stages, a uniform drying period (stage-1 or externally limited drying stage) followed by a receding drying front period (stage-2 or internally limited drying stage). These two stages can be explained with the help of the sketches shown in fig. 1.3. During the externally limited drying stage, there is a continuous capillary flow of water towards the drying surface to meet the demands of the evaporative flux (see fig. 1.3a). At a constant temperature, the drying rate mainly depends on the gradient of the water vapor pressure between the air/material interface and the environment and is given by:

$$\frac{dV}{dt} = D \frac{A}{\rho} \frac{M}{RT} \frac{(P_{sat} - P^{*})}{\delta} \tag{1.7}$$

In this equation, dV/dt is the rate of volume change of the water in the pores, D is the diffusivity of water vapor in air, A is the effective surface area available for evaporation, ρ is the density of liquid water, M is the molar mass of water, R is the gas constant, T is the

temperature, P_{sat} and P^* are the water vapor pressures at the air/material interface and in the environment, respectively, and δ is the thickness of the boundary layer through which the diffusion of water vapor takes place. Due to drying the moisture content decreases and water is redistributed. During redistribution, the bigger pores feed water to the smaller pores because of the pressure gradient. As evaporation proceeds, air will invade the bigger pores, where the capillary pressure (P_c) is lowest as can be seen from the following equation,

$$P_C = \frac{2\gamma\cos\theta}{r} \tag{1.8}$$

In this equation, γ is the surface tension of the liquid vapor interface, θ is the contact angle between the liquid air and liquid solid interface, and r is the pore radius. At a certain time the unsaturated capillary flow can no longer supply water towards the drying surface at a rate high enough to meet the demands of the evaporative flux. Therefore, the liquid continuum i.e., the continuous network of liquid filled pores, breaks up to form disconnected islands, i.e., isolated clusters of liquid filled pores surrounded by air filled pores [23] (see fig. 1.3b). Water can no longer be transported at the required rate, because vapor diffusion is a slow process. As a result, air will invade in the material. This corresponds to the beginning of the internally limited drying stage. The transition between these two drying stages is identified as the critical moisture content [23].

Externally limited drying stage

Internally limited drying stage
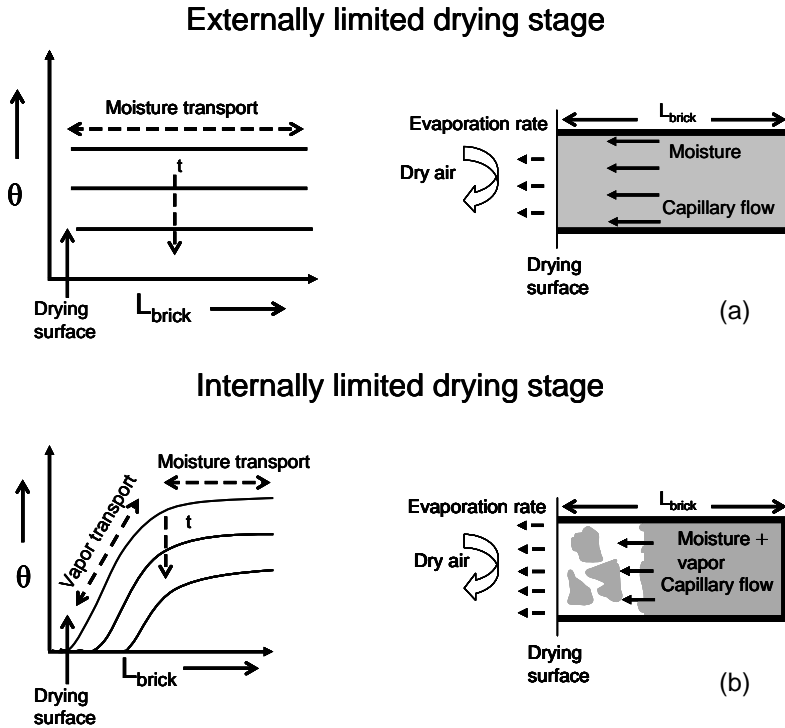
Figure 1.3: *Schematic representation of the two stages of drying: (a) externally limited drying stage (b) internally limited drying stage.*

1.3.2 Ion transport

A detailed knowledge about the ion distribution is required to detect the location of salt crystallization inside the material. During drying, the dissolved salt ions are dragged along with the moisture towards the drying surface. This leads to an accumulation of salt ions near the surface, increasing the local salt concentration in this region. This surface accumulation induces a concentration gradient within the material, which in turn induces diffusion to level off this gradient (see fig. 1.4a). Therefore, there is a competition between advection, which transports ions towards the drying surface, and diffusion, which will try to level off the concentration gradient (see fig.1.4a). This competition can be characterized by the Peclet number (*Pe*) [24]:

$$Pe = \frac{|U| L}{D_{eff}} \qquad (1.9)$$

Where *U* is the fluid velocity, *L* is the characteristic length of the sample, and D_{eff} is the effective diffusion coefficient of the salt ions in the porous medium. For *Pe* < 1, diffusion dominates and salt crystallizes uniformly inside the material whereas for *Pe* > 1, advection dominates and salt crystallizes either just beneath the surface of the material or outside the material as efflorescence. If the rate of escape of moisture at the

surface is smaller than or equal to the rate of supply of moisture to the surface, the liquid/vapor interface remains on the external surface of the sample and salt will crystallize as efflorescence (see fig. 1.4b). However, if the rate of escape of moisture at the surface is larger than the rate of supply of moisture to the surface, the liquid/vapor interface will remain inside the brick and salt will crystallize just beneath the surface of the material as sub-florescence (see fig. 1.4c).
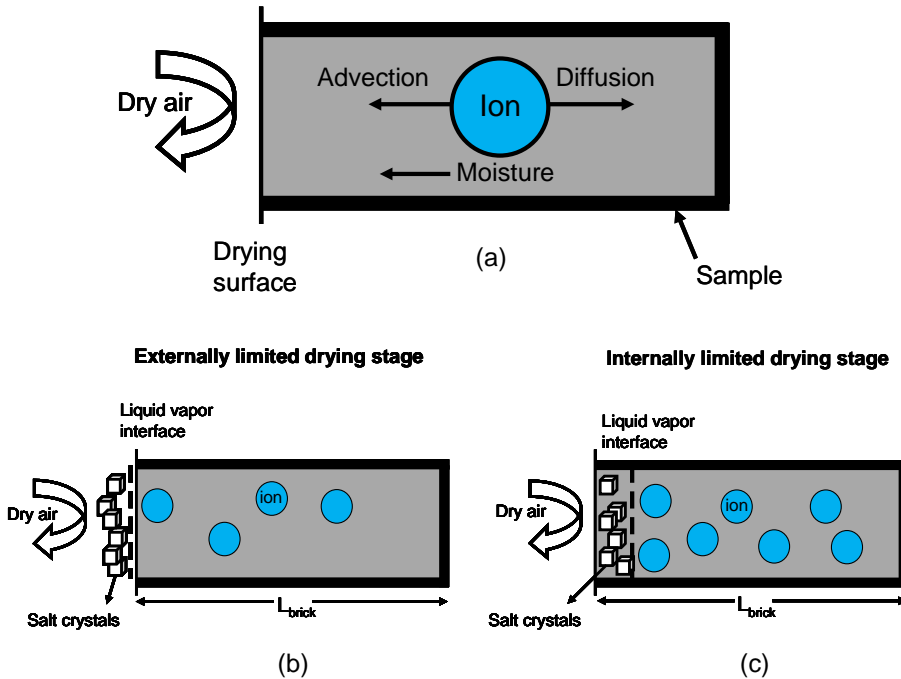
Figure 1.4: *Schematic representation of a) one-dimensional drying of a sample saturated with salt solution, b) salt crystallization during the externally limited drying stage of the material, c) salt crystallization during the internally limited drying stage of the material.*

1.4 Damage prevention

The risk to lose cultural heritage has resulted in dedicated efforts worldwide for their preservation. Although the problem is widespread, proper prevention methods are still not understood well enough for successful remedies. Cultural heritage has a great social importance for the history of a country. The care of historical buildings is not only an aesthetic obligation but is also necessary for the economy of a country with tourism and cultural activities in or around monuments. Limiting salt decay is necessary in order to preserve our cultural heritage.

If possible, avoiding sources of moisture is the fundamental rule in preventing any salt contaminated structure. As an example, physical separation of the porous material from the soil moisture using a plastic sheet or glazed brick can be an option. This might be possible for

relatively small objects. Salt damage presents a particularly difficult challenge for a conservator, because the present options for treatment are extremely limited. Different preventive methods, like controlling environmental conditions [25], and treatment methods, like poulticing [26] and electro kinetic desalination [27] have been tested in the past. However, none of those provides a complete solution to the problem. One of the emerging fields in the conservation of historic monuments and sculptures is the use of crystallization inhibitor. Trace amounts of these inhibitors can dramatically alter the crystallization phenomenon. These inhibitors are known to act either by preventing or delaying the onset of nucleation [28], and hence crystallization, or by changing the crystal growth mechanism by adsorbing onto specific crystal faces [29].

1.4.1 Crystallization inhibitors

The use of inhibitor has been reported in different fields, e.g., the use of polyacrylate for the prevention of crystallization of normal alkanes from diesel fuels [30], polyphosphates and phosphates to control calcium carbonate and calcium sulfate scale formation and deposition [31] and to prevent the spontaneous crystallization of gypsum [32]. Inhibitors are also widely used as scale-inhibitors to prevent undesired effects associated with partially soluble salts (mainly sulfates and carbonates) re-precipitating in oil-extraction pipelines [33], industrial boilers, heat-exchangers, house-appliances or water pipes [34, 35], mining and mineral processing [36], and desalination plants [37]. Mineral precipitation is also a problem in many industrial processes, leading to costly scale formation. Calcium sulphate, calcium carbonate, barium sulphate and sodium chloride are few of the commonly occurring scales in oil and gas industry. Scaling can significantly decrease the permeability and well productivity, which leads to economic losses. It can block flow by clogging of the pipes.

The use of inhibitors in the field of conservation is recent and not yet fully explored. For NaCl different habit modifiers are known since a long time. Since 1783, urea is known to modify the habit of NaCl from cubic to octahedral [38]. Besides, formamide and cadmium chloride are also known as habit modifiers for NaCl [39]. However, the most commonly used additive for NaCl is ferrocyanide. Ferrocyanide salts, such as sodium and potassium ferrocyanide, are highly effective anti-caking agents [40]. Anti-caking agents are generally assumed to be crystal growth inhibitors, preventing crystals from growing together and agglomerating. Calcium chloride and sodium chloride are used extensively in large quantities on roads for snow and ice removal. The problem with using salt, as a deicing compound is that salt is likely to clump or cake during temperature and humidity fluctuations. The caking causes difficulties in dispensing the salt evenly on the roads.

Ferrocyanide ions are known to act as crystal growth inhibitor, nucleation inhibitor and crystal habit modifier for NaCl. In spite of the extensive research done on the influence of ferrocyanide ions on NaCl crystallization, the mechanism of the inhibitor action is still not clear. Different viewpoints have been reported in the literature and it is still an ongoing debate. Steinike [41] proposed that the structural analogy between the NaCl and ferrocyanide lattice leads to the formation of an adsorbed monolayer cover on the NaCl crystals. However, the formation of a monolayer cover is inconsistent with the growth of the crystals [42]. Glasner and Zidon [42] also objected that the monolayer cover theory did not explain the

striking habit modification and the quantitative relation between the concentration of ferrocyanide ions and the supersaturation reported by them. Therefore, they proposed that a good structural and size matching between the $[Fe(CN)_6]^{4-}$ ions and hexachlorosodium $[Na(Cl)_6]^{5-}$ causes cyanoferrate to act as NaCl nucleus in a supersaturated NaCl solution. Consequently, ferrocyanide ions act s a heterogeneous nucleation site for NaCl crystal. The contradiction between the proposed heterogeneous model and the observed supersaturation has been discussed using the argument that that nucleation cannot be immediately followed by visual crystallization. However, this model is not consistent with the conductivity results reported by Navarro et al. [43]. They observed a continuous increase in conductivity with increasing supersaturation till NaCl crystals are visually detected. Recently, it has been proposed that $[Fe(CN)_6]^{4-}$ replaces a $[NaCl_6]^{5-}$ at the surface. Due to the charge mismatch, the charge of a ferrocyanide ion $Fe(CN)_6^{4-}$ is lower than the charge of a $[NaCl_6]^{5-}$ cluster, the further growth of NaCl clusters is inhibited [44].

Although different viewpoints about the molecular level interaction between NaCl and ferrocyanide ions have been presented in the literature, the striking effect of ferrocyanide ions on the NaCl crystal habit is obvious. In the presence of ferrocyanide ions the NaCl crystal morphology changes from cubic to dendrites. In a porous material, a non-destructive efflorescence has been reported in the presence of inhibitor [43, 45]. In bulk droplets a higher NaCl supersaturation has been shown [43, 45]. However, the influence of inhibitor on the salt ion concentration inside the porous material is not yet known. This is a very important aspect of salt damage because, if a higher supersaturation is generated inside the material, the induced crystallization pressure will be higher, as mentioned above. In addition, the effect of inhibitor on the drying and crystallization behavior of salinated porous material is hardly explored.

1.4.2 Salt mixtures

In the past, intensive research has been carried out to understand the crystallization behavior of a single salt and the tendency of single salts to generate a high supersaturation inside a porous building material. However, single salts are rarely found in practice and generally a salt mixture is present. The crystallization behavior of mixed salt systems is much more complex than that of pure single salts. For instance, the crystallization of one salt from a mixture does not occur at a specific value of the relative humidity but rather across a range of relative humidities [46]. The crystallization of salt mixtures occurs at lower humidities than expected in case of pure salts [46]. The rate of deliquescence and crystallization of a salt is also affected by the presence of another salt [47]. In the presence of an additional salt, a rise in the rate of moisture uptake (deliquescence) and a drop in the rate of moisture loss (crystallization) have been reported [47]. This is caused by the reduction of the vapor pressure of the solution in the presence of additional salts. For the salt mixture, where the salts have one ion in common, e.g., the mixture of NaCl and KCl, the saturation concentration of the salts is lower in the mixture than the saturation concentration of the salts individually.

Since the behavior of salt mixtures commonly found in building materials is complicated, only a few studies have been carried out to understand the crystallization behavior of salt mixtures [48, 49]. Linnow et al. [49] have reported a study in which the

complexity of the kinetic and thermodynamic properties of the salt mixtures is considered. They have studied the crystallization behavior of the mixture of Na_2SO_4–$NaNO_3$ in a salt solution droplet. This work has been extended by De Clerq et al. [50], who have studied the crystallization behavior of this mixture in porous limestone's. They studied the drying behavior of two types of limestones loaded with equimolar mixtures of Na_2SO_4–$NaNO_3$ and Na_2SO_4–K_2SO_4. They found that the properties of the materials influence more strongly the crystallization pattern of one type of salt mixture (Na_2SO_4–$NaNO_3$) than that of other (Na_2SO_4–K_2SO_4).

Summarizing, ferrocyanide ions have been tested as a preventive measure against single salts, Whereas single salts are rarely found in nature. In practice, buildings are contaminated with salt mixtures, which present a totally different behavior. This behavior is still poorly understood.

1.5 Outline of the thesis

To understand the damage mechanism it is important to understand the drying and crystallization behavior of salinated porous materials. The aim of this thesis is (a) to understand the drying and crystallization behavior of NaCl saturated bricks (b) to explore the use of ferrocyanide ions as a preventive method to stop/reduce damage caused by NaCl crystallization. These behaviors are hardly explored in the past. In this work, a specially designed Nuclear Magnetic Resonance set-up [51] was used. Using this set-up, we are able to measure non-destructively both, the amount of moisture (H) and dissolved sodium (Na) ions inside a porous media during dynamic measurements.

In chapter 2, paradoxical drying behavior of fired-clay brick due to in-pore salt crystallization is discussed. In chapter 3, the influence of ferrocyanide inhibitors on sodium chloride crystallization under low relative humidity conditions is investigated. This work is further extended in chapter 4, where, the influence of ferrocyanide ions on NaCl crystallization is studied under different relative humidity conditions. For the study performed in chapter 3 and chapter 4, the inhibitor was introduced along with the salt solution inside the porous material. In practice, the inhibitor can only be applied by spraying on the contaminated porous material. For this purpose, the effectiveness of inhibitor is tested by spraying inhibitor on salt contaminated samples and is discussed in chapter 5. In chapter 6, the influence of ferrocyanide ions is tested on NaCl crystallization in salt mixture. In chapter 7, repeated crystallization and dissolution cycles in a salt solution droplet are studied. Conclusions and future work are given in chapter 8.

Chapter 2

Paradoxical drying due to salt crystallization

Abstract

We investigated how salt crystallization inside a porous building material influences the formation of a receding drying front. Nuclear Magnetic Resonance (NMR) is used to measure non-destructively both hydrogen and dissolved sodium ions simultaneously during drying experiments. In this study we focused on the influence of NaCl on the drying. The results show that salt changes the drying process. At low relative humidities (RH ~ 0%), the drying rate of a brick saturated with NaCl solution is much lower than the drying rate of water saturated brick. Moreover, the presence of salt suppresses the development of a receding front. In this case homogenous drying of the material continues till very low saturation values. This is due to salt crystallization near the surface of the brick that causes blockage of the pores. This blockage reduces evaporation rate at the surface and allows maintaining a continuous hydraulic connection between the surface of the porous medium and the liquid present inside the material till low saturation values. Increasing the relative humidity at 55% and 70% RH with the brick saturated with the salt solution leads to a paradoxical situation with evaporation rates greater than for 0% RH. The paradox is explained by the impact of evaporation rate on the efflorescence microstructure, leading to the formation of a blocking crust for sufficiently high evaporation rates and non-blocking efflorescence for sufficiently low evaporation rates. The fundamental difference between the two types of efflorescence is demonstrated from a simple imbibition experiment. Using a simple continuum scale model of drying, critical moisture content was determined and all the essential features of the experimental results are validated. It is shown that critical moisture content can be very low in case of fired-clay brick due to the low threshold of the pore space, which is consistent with the relatively large pore size distribution of the fired-clay brick.

2.1 Introduction

Salt crystallization inside the pores of a building material can cause severe damage [3]. Salt can enter a building material along with moisture in various ways, such as capillary rise of ground water, absorption of sea water, atmospheric pollution etc. Almost all water that enters building materials will leave by evaporation or drying. Due to drying salt crystals will crystallize inside the pores of a building material.

Drying of porous media in the presence of salt is of interest not only to understand the crystallization mechanisms and related salt damage problems, but also in the field of soil physics [52], injecting CO_2 in aquifers [53], and related studies. Vegetation, plant growth and soil organisms can be severely limited in salt-affected land. Despite of the above mentioned problems, drying of porous materials in the presence of salt is still poorly understood. This is due to the complex phenomena involved, e.g., moisture and ion transport phenomena and phase transitions. Therefore, a better insight of the drying process of salt containing porous media is required to understand various salt related damage problems.

Lewin [22] proposed that the location of salt crystallization is determined by a dynamic balance between the rate of escape of water at the surface (evaporation or drying) and the rate of supply of water to the surface. If salt crystallizes inside the material, i.e., the so-called sub-florescence, it can cause damage. On the other hand, if salt crystallizes outside the material, also called efflorescence, it may be unaesthetic but it is not harmful for the buildings. The location of salt crystallization is in general determined by the competition of two forces: diffusive force and advective force. Generally it is characterized in terms of a Peclet number (Pe) [24].

In the past, a significant progress has been made in understanding the drying kinetics of porous materials, especially focusing on the pore level [54, 55]. It is widely mentioned that for irregular pore geometry thick liquid films provide an efficient transport of liquid to the surface [56]. The pores inside the brick are generally not perfectly cylindrical and have edges; consequently thick liquid films will be present. These films are known to contribute significantly to the mass transport phenomenon during stage-1 of drying [57]. The films supply water to isolated liquid clusters, thereby enhancing the mass transfer in comparison to the vapor diffusion transport mechanism [57]. The standard drying behavior of water saturated porous material is well documented in the literature [23]. However, the drying behavior of the porous material in the presence of salt is still a topic of discussion, especially with regard to the impact of salt crystallization on drying. By varying the mean pore size of the porous material, it has been shown that the crystallization of the salt at the porous material surface could either severely reduce the evaporation rate compared to pure water or have no impact at all [58], [59]. This led to identify two main types of efflorescence, referred to as patchy (or non-blocking) and crusty (or blocking). As we shall see, distinguishing these two main types of efflorescence is also a key factor for analyzing our results.

The aim of this work is to study the drying behavior of porous materials saturated with salt. In this study we will focus on NaCl as this is a common salt found in many salt related problems in situ. We will investigate to which extent this drying behavior resembles the standard drying behavior of water saturated materials. In particular, we focus on the effect of

salt crystallization inside a porous material on the development of a receding front during drying. To our best knowledge, no study has been reported in the past to explore this aspect of drying probably because it is difficult to measure the moisture and ion distribution simultaneously in real porous materials. For this purpose a specially designed Nuclear Magnetic Resonance (NMR) set-up with a static magnetic field of 0.78 T was used [60]. With this set-up it was possible to carry out non-destructive, quantitative and simultaneous measurements of both the hydrogen and sodium content in a brick sample.

2.2 Material and methods

2.2.1 Materials

The material used in this study was fired-clay brick. The red fired-clay brick is of a type typically used for construction in the Netherlands, and had an average porosity (as measured by water immersion method) of 0.32 m^3 m^{-3}, and a pore size distribution ranging from a few tens of nanometers to 100 µm (with 80% of the total pore space corresponding to pores in the range 1-10 µm), as determined by Mercury Intrusion Porosimetry (MIP).

2.2.2 Nuclear Magnetic Resonance (NMR)

A specially designed nuclear magnetic resonance (NMR) set-up, for non-destructive, quantitative and simultaneous measurement moisture (^{1}H) and sodium (^{23}Na) profiles in inorganic materials was used. An extensive description of this set-up can be found elsewhere [60]. A schematic representation of the set-up is given in fig. 2.1.
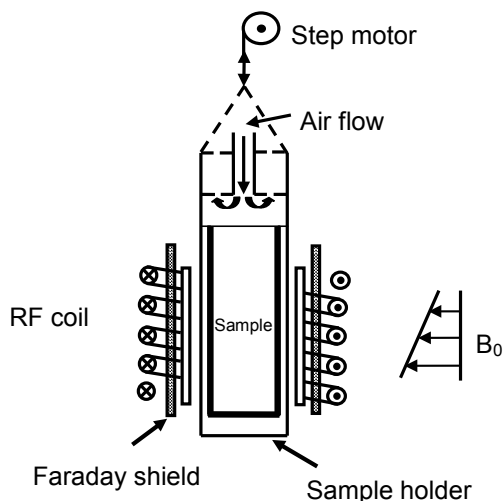

Figure 2.1: *NMR set-up for the drying experiments with cylindrical samples. The Teflon holder with the saturated sample is moved in the vertical direction by means of a step motor. The signal from H or Na nuclei at resonance is received by the RF coil.*

The tuned circuit of the set-up can be toggled between 33 MHz for ^{1}H and 8.9 MHz for ^{23}Na, giving the possibility to quasi-simultaneously measure the H and Na content and thereby the concentration. For the echo time used in the experiment, i.e., T_E = 250 μs for ^{1}H and 450 μs for ^{23}Na, only the dissolved Na and H nuclei are measured and no signal is obtained from the nuclei incorporated in the crystals. The magnetic field gradient was chosen so that a slice of less than 2 mm is measured. The cylindrical samples 20 mm in diameter and 40 mm in length were vacuum saturated with water and 3m NaCl solution. These samples were sealed using Teflon tape on all sides except the top surface and placed in the NMR sample chamber. In this way a one dimensional drying experiment was performed. The samples were then exposed to dry air at a flow rate of 1 l min^{-1}. The relative humidity was varied from 0% to 70%. The sample was moved in the vertical direction using a step motor to allow the measurement of moisture and sodium content throughout the sample length. Measuring one profile takes about 2.26 hours. As the complete drying experiment takes in the order of a few days small variations in the moisture and ion profiles during a single scan can be neglected. After each drying experiment was completed the efflorescence formed on the top of the sample was collected and weighed.

2.3 Results

2.3.1 Drying behavior of water and salt saturated fired-clay brick dried at 0% RH

Initially, the drying behavior of fired-clay brick samples vacuum saturated with water and salt solution (3m NaCl) was studied. The samples were dried at 0% RH and 1 l min^{-1} air flow rate. Fig. 2.2a and 2.2b show the measured moisture profiles during drying of water and salt saturated samples, respectively. The recurrent irregularities in the profiles result from inhomogenities of the sample, e.g., at ~ 15 mm in case of the water saturated sample (fig. 2.2a).
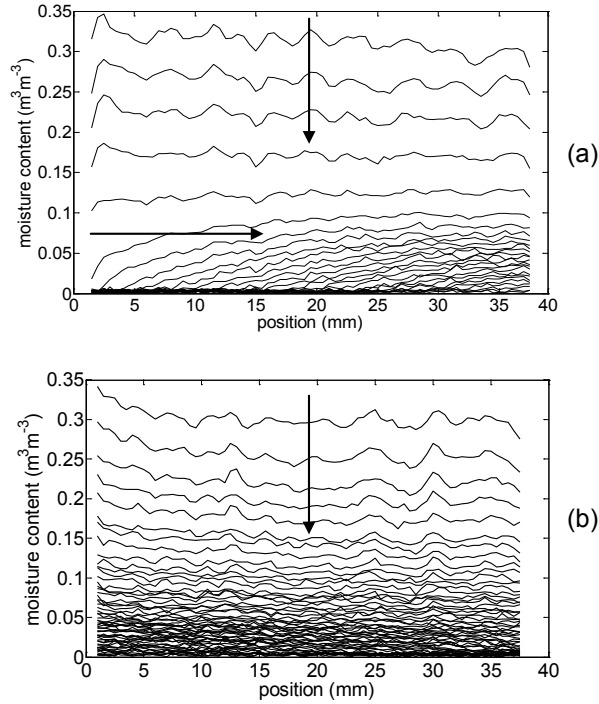
Figure 2.2: *The measured moisture profiles for (a) water saturated (b) 3m NaCl saturated fired-clay brick plotted as a function of position. The profiles are given for every 0.45 h and 2.26 h for water and salt saturated bricks. The samples were dried using dry air with a flow of 1 l min^{-1} and 0% relative humidity. The drying surface is at 0 mm. The vertical arrow shows the homogenous drying of the sample (externally limited) and the horizontal arrow shows the penetration of the receding drying front (internally limited).*

In case of water saturated samples the first few profiles are almost horizontal, representing the first (externally limited) drying stage (shown by a vertical arrow in fig. 2.2a). Afterwards, a drying front develops which recedes below the sample surface (shown by a horizontal arrow in fig. 2.2a). This represents the second (internally limited) drying stage. The addition of salt changes the drying behavior of the fired-clay brick (fig. 2.2b). Two effects were seen. Firstly, the presence of NaCl reduces the drying rate compared to the drying rate of water saturated fired-clay brick. Complete drying of water saturated fired-clay brick took about one day, in comparison to more than one week for NaCl saturated fired-clay brick of the same dimensions and at the same drying conditions. Secondly, the receding drying front vanishes and homogenous drying of the material continued till low saturation values. Hence, drying stage-1 prolongs and homogenous drying is maintained till low saturation values.

2.3.2 Drying behavior of water saturated fired-clay brick at high relative humidity

Since the evaporation rates are markedly different between the pure water experiment and the salt experiment, it is interesting to get insights into the effect of evaporation rate on the drying process. To this end, experiments were performed on water saturated fired-clay brick at high humidity conditions, i.e., at 55% and 70% RH. Because of the depression of the humidity gradient at the surface drying rate should decrease. The evaporation rate is proportional to the difference between the relative humidity at the porous medium surface, which is equal to 100 % when pure liquid water is present at the surface and to 75% for a NaCl saturated solution, and the relative humidity in the external air.

The results of the drying experiments performed on water saturated samples are shown in fig. 2.3. The rate of volume change, i.e., dV/dt, is plotted as a function of moisture content. In this figure two drying stages can be distinguished, a constant drying rate period (stage-1) and a falling drying rate period (stage-2). A constant drying rate corresponds to the externally limited drying stage and a falling drying rate period corresponds to the internally limited drying period. The dashed lines in fig. 2.3 are drawn as a guide to the eye. The dotted vertical line denotes the moisture content at which the front starts to penetrate the sample. It can be clearly seen that at higher humidities the receding front starts to penetrate at lower moisture content values. The moisture content marking the end of stage-1 is classically referred to as the "critical" moisture content [23]. For different materials the critical moisture content must be determined experimentally [61] under a given set of environmental conditions. As can be seen from fig. 2.3 the critical moisture content is in fact not constant but decreases with a decreasing evaporation rate.
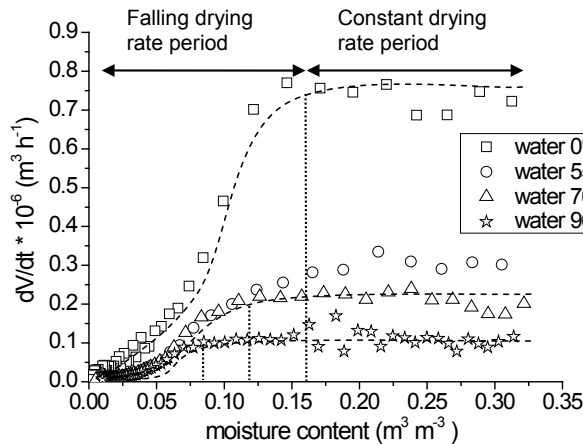

Figure 2.3: The rate of volume change (dV/dt) as a function of moisture content ($m^3 m^{-3}$) for water saturated fired-clay bricks dried at different relative humidity conditions. The dashed lines are a guide to the eye.

In another experiment, a water saturated fired-clay brick was dried at 96% relative humidity while approx. 75% of the brick surface was covered with Teflon tape. Covering the brick surface was done to avoid evaporation and to mimic the situation of salt contaminated materials where the surface is blocked due to salt crystallization (see below). These results are also plotted in fig. 2.3. A significant delay (low saturation value) in the penetration of the receding front is seen. These results clearly confirm that the drying rate at the surface affects the penetration of receding front and the critical moisture content.

2.3.3 Drying behavior of salt saturated fired-clay brick at high relative humidity

An important result of the experiments described in the previous sub-section is that the evaporation rate at the surface of the material affects the formation of a drying front. In a separate study [45] it was found that the evaporation rate of a salt contaminated brick was higher at high relative humidity than at low relative humidity. To investigate this, drying experiments were performed on samples saturated with salt solution at 55% and 70% relative humidity. The samples were vacuum saturated with 3m NaCl solution and dried inside NMR at room temperature and $1\,l\,min^{-1}$ air flow rate. The results are shown in fig. 2.4, where the rate of volume change (dV/dt) is plotted as a function of moisture content.
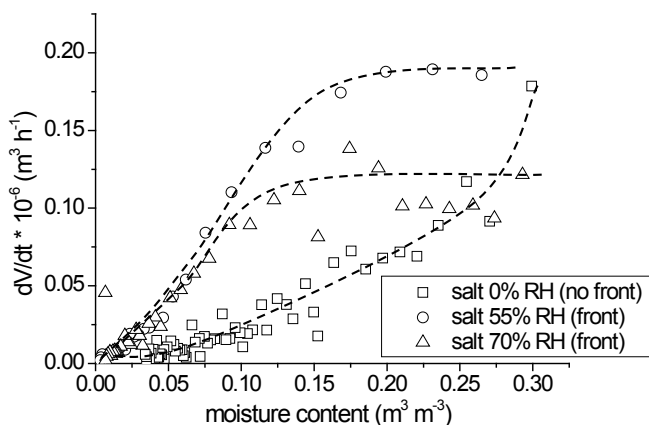
Figure 2.4: The rate of volume change (dV/dt) as a function of moisture content ($m^3\,m^{-3}$) for salt saturated bricks dried at different relative humidity conditions. The dashed lines are a guide to the eye.

For comparison, the result of salt saturated brick dried at 0% RH is also shown. For the brick dried at 0% RH a continuous decrease of the flux with decreasing moisture content is seen. Thus, there is no constant rate period in this case. However, at high humidities initially a constant drying rate is maintained (stage-1) and later a falling drying rate period is observed (stage-2). This leads to a paradoxical drying situation since the evaporation rate is greater for 55% RH and 70% RH than for 0% RH. Thus, in the presence of NaCl a receding front develops again at high humidities. At the end of the experiment, the efflorescence formed on

the surface of the fired-clay brick was collected and weighed. At 0% relative humidity 6% - 7% of the NaCl crystallized as efflorescence. This efflorescence had the form of a very thin crust on the outer surface of the fired-clay brick and was strongly adhered to the substrate. It was not easy to remove the efflorescence from the substrate. On the other hand, at 55% and 70% RH, a significant amount of NaCl crystallized as efflorescence. About 48% and 40% of the salt crystallized as efflorescence at 55% and 70% RH, respectively. The type of efflorescence formed at high humidities was rather fragile and was easy to remove from the substrate by rubbing. Pictures of the efflorescence formed on the surface of the materials are shown in fig. 2.5. The efflorescence is clearly quite different at 0% RH compared to the efflorescence at 55% and 70% RH. Similarly as in [58], this suggests distinguishing two types of efflorescence, referred to as "patchy" and "crusty" in [58] and that can be referred to as well as "non-blocking" and "blocking". The efflorescence obtained at 0% RH is blocking whereas the efflorescence at 55% and 70% RH is non-blocking.
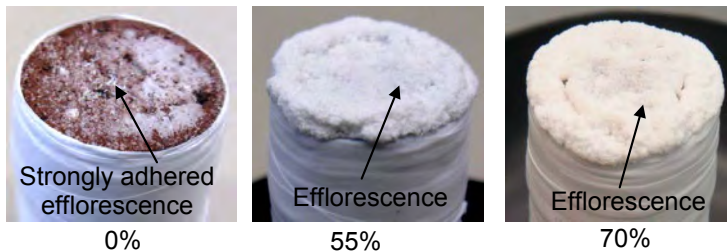
Figure 2.5: *Pictures of the efflorescence formed at the end of drying experiment in the case of 3m NaCl saturated brick dried at 0%, 55% and 70% relative humidity. The amount of efflorescence increases at higher humidities.*

The blocking efflorescence does not form all of sudden, but progressively covers the porous medium surface. This is explained by the non-uniformity of the evaporation flux at the porous medium surface. As explained for instance in [58] or [62], efflorescence starts forming in the region of higher evaporation fluxes at the surface and then progressively colonizes the rest of the surface. Other factors, such as possible local spatial variations of porosity and/or permeability, especially in the top region of sample, may also play a role in the localization and development of efflorescence [63]. Thus, the pore blockage essentially starts where the evaporation flux is the highest and next progressively develops over rest of the surface of the material. The net effect is a progressive reduction of the surface left free for evaporation and consequently a continuous decrease of the flux with decreasing moisture content. As can be seen in fig. 2.4, at low moisture contents (0.15 m^3m^{-3}), the rate of volume change (dV/dt) is very low compared to the NaCl saturated fired-clay bricks dried at high humidities. However, at high humidities NaCl also crystallizes as efflorescence. Because of the formation of efflorescence we might expect a reduced blockage effect near the drying surface. Since we did not see any drop in drying rate after the formation of efflorescence, we expect that the permeability of this efflorescence should be comparable to the permeability of the underlying material. Therefore, the system remains open and a constant volume flux is maintained initially, followed by a receding front. Thus, in this case, the efflorescence is non-

blocking. An important outcome of the results depicted in fig. 2.4 is therefore that not only the mean pore size of the porous medium as in [58] but also the initial drying rate has an impact on t he type of efflorescence that forms at the porous medium surface. This is qualitatively consistent with the crude efflorescence growth model introduced in [58], which "explains" the transition from non-blocking to blocking efflorescence from the consideration of viscous pressure drop into the growing efflorescence. Increasing the evaporation rate increases the pressure drop and thus the maximum height of efflorescence which then expands laterally rather than upwardly for a sufficiently high evaporation rate. A more detailed model of this type is proposed in [59] and is consistent with a transition blocking / non-blocking driven the evaporation rate. The markedly different properties of blocking and non-blocking efflorescence are confirmed from the imbibition experiment described in the next sub-section.

2.3.4 Sorptivity test

To estimate quantitatively the difference in pore blockage of bricks were dried at different humidity conditions and sorptivity tests were performed. The bottom of the test material is touched with the solvent (decane) to let the material absorb the solvent by capillary suction. The mass change is recorded as a f unction of time. The tests were performed on bare fired-clay brick and on fired-clay bricks saturated with 3m NaCl solution and dried at 0 % and 55 % relative humidity. The main idea is that salt crystallization inside the pores causes a reduction of the pore volume and hence the permeability of the material, making solution transport more difficult [64]. Decane was used as a solvent for the sorptivity tests, because NaCl crystals do not dissolve in decane. We expect that blockage due to salt crystallization near the drying surface will generate a surface resistance to decane uptake in case of salt contaminated brick dried at 0% RH. Therefore, a delay in imbibition is expected. In the tests the efflorescence was not removed from the surface of the brick. This was done to check the permeability of the efflorescence also. The surface of the brick above which dry air was blown during the drying experiment was exposed to decane. The results for salt free, salt contaminated brick dried at 0% RH, and salt contaminated brick dried at 55% RH are shown in fig. 2.6, where the imbibition (i) is plotted as a function of the square root of time ($\sqrt{t}$). The imbibition is defined as the cumulative volume of absorbed decane per unit area of inflow surface. For the salt contaminated brick dried at 0% RH, the imbibition initially increases very slowly (slope of the curve is almost flat), indicating resistance to the uptake of decane. This is due to the presence of a dense layer of salt crystals near the drying surface that causes blockage. In depth of the sample the amount of crystallized salt and hence, the resistance to uptake of decane also decreases. Thus, the slope of the curve increases progressively. In case of the fired-clay brick dried at 55% RH, no c hange in the slope of imbibition is observed, indicating that the permeability of the efflorescence does not limit the rate of fluid uptake.
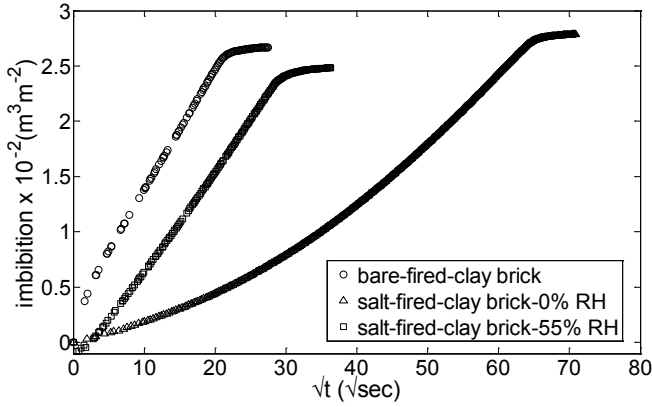
Figure 2.6: *The measured imbibition of decane in the salt-free fired-clay brick and in fired-clay bricks saturated with 3 m NaCl solution dried at different relative humidity conditions.*

2.4 Discussion

As presented in this section, the most important features of the experiments can be understood from a simple continuum scale model of drying.

2.4.1 Water saturated brick

To understand the different drying behavior of NaCl saturated fired-clay brick we first have to understand the standard drying behavior of water saturated fired-clay brick. It is well understood that drying is a drainage process, where the non-wetting fluid (gas) replaces the wetting fluid (liquid). In general, drying of a homogeneous, uniformly wet, porous material has two identifiable stages, a uniform drying period (stage-1) followed by a receding drying front period (stage-2) as exemplified in fig. 2.2a.

During stage-1, there is a continuous capillary flow of water towards the drying surface to meet the demands of evaporative flux [23]. Consequently, the rate of moisture loss from the surface of material is constant as long as the rate of liquid water that can be transported to the surface through the action of capillary forces is equal to the external evaporation demand. With time the unsaturated capillary flow can no longer supply water towards the drying surface at a rate high enough to meet the demands of the evaporative flux. This very classical scenario can be quantified using traditional continuum scale model. A key factor is to determine the "critical" moisture content marking the end of first drying period and thus the beginning of the formation of drying front within the porous medium (fig. 2.2). During stage 1, the fact that the water brought to the surface thanks to capillary effects balances the evaporation demand can be expressed as,

$$A\,K_s(\theta)\,\frac{\partial h}{\partial z} = -\,J \qquad (2.1)$$

Where A is the top surface area of the porous medium, $K_s(\theta)$ is the hydraulic conductivity of the porous medium, h the pressure head ($h = P_c/\rho_\ell g$, where P_c is the capillary pressure, ρ_ℓ is the density of liquid and g the acceleration due to gravity), z is a vertical coordinate increasing downward from the top surface of porous medium, J is the evaporation rate expressed in m/s. For the capillary regime considered in the present study, which is characterized by a spatially uniform moisture content during the first stage of drying, a first order approximation assuming P_c varies linearly over H, the "critical" moisture content can be estimated from Eq.(2.1) expressing $\dfrac{\partial h}{\partial z}$ as $\dfrac{h(\theta)}{H}$, where H is the height of sample. This gives,

$$A\, K_s\,(\theta)\ \frac{h(\theta)}{H} = -\,J \tag{2.2}$$

To make use of Eq. (2.2), it is necessary to characterize the unsaturated hydraulic conductivity $K_s\,(\theta)$ and the retention curve $h\,(\theta)$. Following [65], the moisture retention curve can analytically described by a bimodal function of the van Genuchten type [66]:

$$\theta = \theta_s\left[\ell_1(1+(a_1 p_c)^{n_1})^{-m_1} + \ell_2(1+(a_2 p_c)^{n_2})^{-m_2}\right] \tag{2.3}$$

As can be seen from fig. 2.7, Eq. (2.3) with $\theta_s \approx 0.32$, $a_1 = 5.8\ 10^{-5}$ Pa^{-1}, $a_2 = 9\ 10^{-6}$ Pa^{-1}, $\ell_1 = 0.846$, $\ell_2 = 0.154$, $n_1 = 4.$, $n_2 = 1.69$ and $m_i = 1 - n_i$ leads to a representation of the retention in good agreement with the few experimental data reported in [26].

The unsaturated hydraulic conductance $K_s\,(\theta)$ is estimated from the retention curve using the Mualem model [67]

$$K_s(\theta) = K_s(\theta_s)\left(\frac{\theta}{\theta_c}\right)^{0.5} \int_0^\theta \frac{d\theta}{p_c(\theta)}\ /\int_0^{\theta_s} \frac{d\theta}{p_c(\theta)} \tag{2.4}$$

The saturated hydraulic conductance $K_s\,(\theta_s)$ can be evaluated from the fired-clay brick permeability κ ($\kappa \approx 9.6\ 10^{-14}$ m^2, $K_s\,(\theta_s) = \frac{\kappa \rho_\ell g}{\mu}$). Using the capillary pressure curve for fired-clay brick as given in fig.2.7 the relative permeability $k_r\,(\theta) = K_s(\theta)/K_s(\theta_s)$ can be calculated using Eq. (2.4) and is shown insert in fig. 2.7,
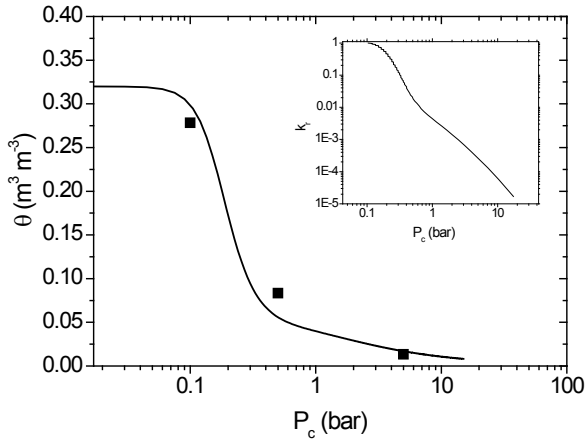
Figure 2.7: *Capillary pressure curve for fired-clay brick material. The filled symbols are experimental data [26]. The solid line is computed using Eq.(2.3). The insert shows the relative permeability computed using the Mualem's model Eq.(2.4).*

In fig. 2.8 the calculated "critical" moisture content as a function of evaporation rate as obtained from inserting Eq.(2.3) and (2.4) into Eq.(2.2) and solving for θ. Note that the intrinsic permeability κ has been a bit modified *($\kappa = 0.6 \ 10^{-14} \ m^2$)* so as to obtain critical moisture contents close to the ones obtained in the experiments (fig. 2.3).

As can be seen the "critical" moisture content decreases with a decreasing evaporation rate. The theoretical lower bound θ_r to the critical water content corresponds to the percolation threshold of the pore space pore network [68] and can be reached for an extremely low drying rate. The retention curve depicted in fig. 2.7 suggests that θ_r is very small for the fired-clay brick that is on the order or smaller than the smallest moisture content reported in fig. 2.2. This is consistent with experimental results at 0% RH with the salt solution depicted in fig. 2.2.

Figure 2.8: *Critical moisture content as a function of evaporation rate as predicted by Eq.(2.2).*

2.4.2 Salt saturated brick

Since the evaporation rate is very low in the presence of NaCl due to the formation of a blocking crust (0% RH), the homogeneous drying can thus take place over most of the drying process in this case.

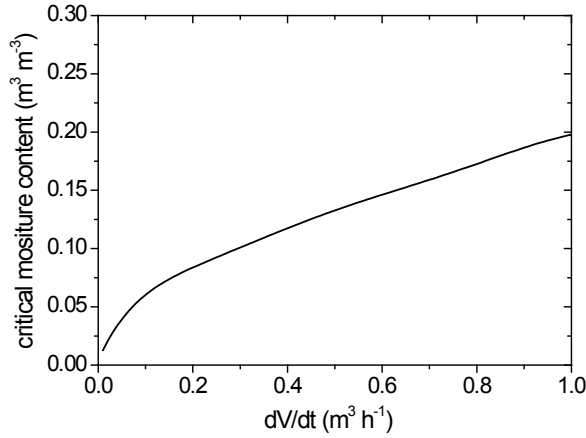However, it can be pointed out that the evaporation rate is not constant, but decreases monotonously during stage 1 (= homogeneous drying) for the fired-clay brick dried at RH = 0% (see fig.2.4). Hence Eq. (2.2) is thus slightly modified,

$$A K_s (\theta) \frac{h(\theta)}{H} = - J(t) \tag{2.5}$$

as to express explicitly the time dependence of evaporation rate in this case. Here we suppose that the salt crystallizes only within a thin layer at the top surface of porous sample. This is supported by the estimate of Peclet number $Pe \approx \dfrac{JH}{AD_s^*}$, where D_s^* is the effective diffusion of the ion in the porous medium ($D_s^* \approx 10^{-9}$ m^2/s). For $J / \rho_\ell = 0.1$ *cm^3/h*, which is a mean representative value for the case 0% RH (see fig. 2.4) this yields *Pe ≈ 3.5*. The Peclet number is greater than 1 and thus the accumulation of the salt at and near the top surface of sample is expected [24]. Thus, most of the sample is not affected by the crystallization process. This is why we keep the same unsaturated hydraulic conductance and retention curve as for the sample without salt crystals.

Using the data displayed in fig. 2.4 for the case 0% RH, Eq. (2.5) gives the variation of the critical moisture content depicted in fig. 2.9. As can be seen, the critical moisture content is never reached, i.e. θ is always greater than θ_c consistently with the evolution of moisture content profile given in fig. 2.2.
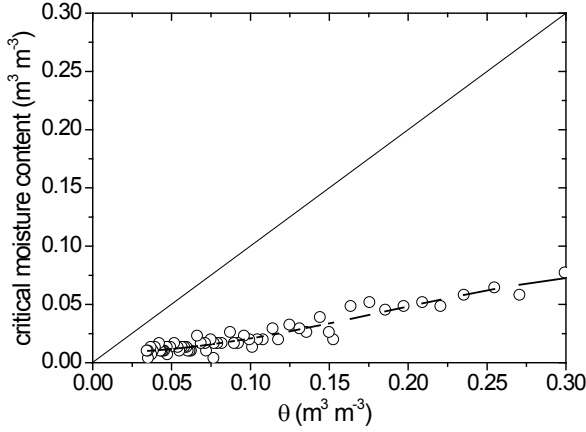
Figure 2.9: *Critical moisture content as a function of water content in the material for salt satured fired-clay brick with 0% RH as predicted by Eq.(2.5).*

Consistently with the experiment with a partial covering of surface with Teflon tape (see section 2.3.2 and fig. 2.3), the reduction of the drying rate is explained by the progressive reduction of the evaporation surface at the top of sample due to the progressive colonization of the surface by the efflorescence blocking crust. The effective evaporation surface of porous medium, which is denoted by $A_{app,}$ can be computed simply from the relationship,

$$A_{app.}\ (t) = A\ \frac{J(t)}{J(0)} \tag{2.6}$$

where $J(0)$ is the evaporation rate at $t = 0$. Using again the data displayed in fig. 2.4 for the case 0% RH, this gives the evolution of apparent evaporation surface shown in fig. 2.10. $A_{app.}$ is called the apparent evaporate surface because other factors may contribute to reducing the evaporation rate as will be briefly discussed in section 2.4.4. The result displayed in fig. 2.10 is consistent with the progressive blocking of sample top by the development of blocking efflorescence. Using this model, the drying process can still be considered as in the constant rate period, by considering the evaporation flux at the surface free of efflorescence $j = J(t)/A_{app.}\ (t),$ which is constant and equal to $J(0)/A$. Thus, the mass transfer at the top surface of sample free of efflorescence is essentially the same at any time.

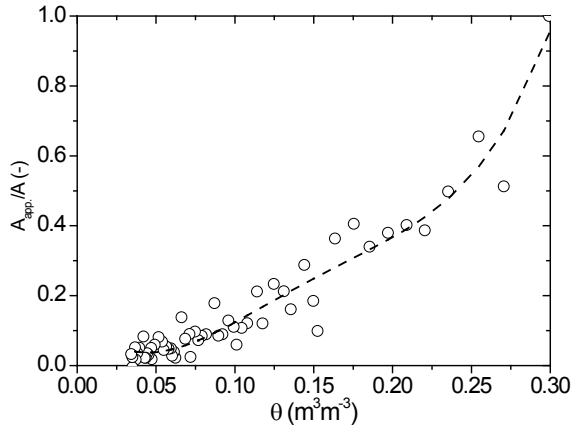**Figure 2.10:** *Variation of apparent evaporation surface area as a function of mean moisture content in sample for the 3m NaCl satured fired-clay brick with 0%RH as predicted by Eq.(2.6).*

2.4.3 Critical moisture content

A key feature in the analysis is that the critical moisture content can be very low in a fired-clay brick as indicated by the retention curve (fig. 2.7). As already mentioned, this can be due to the low percolation threshold of the pore space, which is consistent with the relatively large pore size distribution of the fired-clay brick spanning over more than three decades between a few tens of nanometers and 100 microns [26]. The thick liquid films that can be present along the walls and corners of pore space within the pores invaded in the bulk by the gas phase [56, 57] may also plays a role in maintaining the hydraulic connection all over the pore space at very low moisture contents.

2.4.4 Other effects

The simple model considered in section 2.4.2 essentially assumes that the system becomes a system of two layers in series as a result of crystallization: a porous layer free of crystal corresponding to almost the entirety of fired-clay brick sample connected a t hin crystallization layer formed by the efflorescence crust and probably a very thin layer of the fired-clay brick sample adjacent to the top surface. The image of the crust depicted in fig. 2.5a suggests that the transfers are probably three-dimensional in the top region of sample since the development of salt crust is not homogeneous. Thus, there is some redirection of the flow carrying the ions underneath the porous medium surface toward the part of the surface free of efflorescence. The corresponding effects are included in the apparent surface area $A_{app.}$ depicted in fig. 2.10, which thus may not exactly correspond to the evaporative surface area. It can be also noted that the development of the crust could also modify the structure of the water vapor field in the air above the sample top surface, which may slightly modified the evaporation flux at the surface free of efflorescence. Nevertheless, we believe that the simple

model presented in section 2.4.2 captures the essential of the effects explaining the moisture profiles during the drying of fired-clay brick samples with and without NaCl as depicted in fig. 2.2 and the evaporation rate variations depicted in fig. 2.4.

2.5 Conclusions

In case of water saturated fired-clay brick two drying stages were observed, i.e., a continous drying rate period followed by a receding drying front period. These results are in accordance with the standard drying behavior of water saturated porous media. However, at 0% RH, NaCl suppresses the formation of a drying front. This is due to the extremely low drying rate, which is mainly caused by pore blockage near the drying surface. The low evaporation rate at the surface allows maintaining a continuous hydraulic connection between the surface of the porous medium and the liquid present inside the material till low saturation values. For NaCl salt saturated fired-clay brick the evaporation rate is higher at high relative humidities and salt ions crystallize as efflorescence on the surface of the brick. Because of the higher evaporation rate the water transport cannot be maintained. This leads to the penetration of front at high humidities, also in the presence of salt. The amount of pore blockage was estimated quantitatively using sorptivity tests. The results show that the permeability of the brick dried at high humidities is higher than the permeability of the brick dried at low humidity due to pore blockage in the later case. Using a simple continuum scale model of drying, critical moisture content was determined. It is shown that critical moisture content can be very low in case of fired-clay brick due to the low threshold of the pore space, which is consistent with the relatively large pore size distribution of the fired-clay brick. For salt saturated material it is shown that critical moisture content is never reached inside the brick and is in agreement with the experimental results. Also, using model it is shown that critical moisture content decreases with the reduction in evaporation rate. The reduction of drying rate is explained due to the progressive colonization of the surface due to the formation of crust like efflorescence.

Hence, drying with salt leads to a paradoxical situation in which increasing the relative humidity in the external air and thus reducing the external evaporation demand can increase the evaporation rate. This is explained by the dependence of efflorescence properties with potential evaporation, i.e. the evaporation rate at the very beginning of drying. Sufficiently high evaporation rates lead to the formation of blocking efflorescence (crust) whereas lower rates can lead to non-blocking efflorescence. Although some insights into the blocking – non blocking efflorescence transition are proposed in recent works [58], [59], this topic clearly needs further investigation so as to predict whether efflorescence will be blocking or not blocking in a given situation.

The chapter also indicates that the concept of critical moisture content should be considered with caution. As demonstrated here, the critical moisture content, i.e. the moisture content marking the end of stage 1 in drying, should not be regarded as an intrinsic property of a porous material but varies depending on the evaporation condition. The lower the evaporation rate, the greater the critical moisture content.

Chapter 3

The influence of ferrocyanide on the transport and crystallization processes of sodium chloride

Abstract

We evaluated the effect of crystallization inhibitor on the concentration levels reached by NaCl solutions within the porous media and the associated water and ion transport processes taking place during drying. The results show that NaCl crystal morphology changes from cubic to dendritic crystals in the presence of inhibitor. Consequently, advection becomes the governing process and helps to transport the salt ions outside the material, where they are deposited as a non-destructive efflorescence.

Salt weathering leads to destruction of many valuable cultural heritage monuments and porous building materials. In order to reduce the impact of this, effective treatment methods are required. The use of crystallization inhibitors to mitigate salt damage has been proposed in the past, however to date their effectiveness on cultural heritage objects has not been proven. Therefore a detailed experimental study to see the effect of crystallization inhibitors on the drying behavior of salinated porous materials has been undertaken. Two types of drying experiments were performed to observe the crystallization behavior of salt solutions with and without the presence of inhibitors: 1) in droplets of salt solution 2) in porous supports (brick) contaminated with salt solution. From the droplet drying experiments it is shown that the presence of inhibitor results in higher supersaturation and changes the crystal morphology from cubic to dendritic crystals. In the brick drying experiments, due to the dendritic crystal morphology in the presence of inhibitor, advection becomes the governing phenomenon for ion transport. This results in the transport of salt ions to the outer surface of the brick, where crystallization results in the formation of non-destructive efflorescence. Meanwhile, inside the brick, higher supersaturation levels are not observed.

3.1 Introduction

Soluble salts such as chlorides, sulphates and nitrates are widely recognized as a cause of destruction in porous building materials. The damage is mainly due to the crystallization of these soluble salts inside the porous matrix of these materials. The growth of salt crystals exerts pressure on the pore walls, which can exceed the tensile strength of the material thus leading to damage [3]. Therefore, an effective and practically feasible method is required in order to prevent or reduce this damage. Different methods have been proposed in the past such as controlling the environmental conditions [25], or removal of salts from the substrate e.g. by dry brushing, water bath treatments, poulticing [26] and electro migration [27] with varying degrees of success.

In light of the limited practical options available for the control of salt damage, the use of crystallization inhibitors has been proposed as a potential preventive treatment method. These inhibitors act either by preventing or delaying the onset of nucleation [28] (and hence crystallization) or by changing the crystal growth mechanism by adsorbing onto specific crystal faces [29]. Many applications of these inhibitors have been reported in different fields, including the use of polyacrylate for the prevention of crystallization of normal alkanes from diesel fuels [30], polyphosphates and phosphates to control calcium carbonate and calcium sulfate scale formation and deposition [31] and also to prevent the spontaneous crystallization of gypsum [32]. However, their application in the field of architectural conservation is fairly new and not yet fully explored with very limited studies available.

Some authors have proposed the use of ferrocyanide (FC) ions as a preventive measure for NaCl crystallization as these compounds appear to promote the formation of non-destructive efflorescence rather than destructive sub-florescence [43, 69]. For bulk solutions, increased supersaturation levels in the presence of inhibitor have been reported in the past [43]. However, to our knowledge, to date no studies have been published regarding the effect of these compounds on the concentration of NaCl solutions inside a porous media. This indeed is a very important aspect for salt damage. As it is known that the process behind the damage due to salt crystallization is the growth of salt crystals in confined spaces (e.g. pores), hence exerting crystallization pressure on the pore walls. However, for a salt crystal to grow in a confined space, a thin film of the liquid solution should be present surrounding the crystal [8] that can feed ions to the growing crystal. Also the growing crystal can only exert pressure if the salt solution layer in contact with the growing crystal is supersaturated. Thermodynamically the crystallization pressure can be related to supersaturation (C/C_o) of the solution and is given as [14]:

$$P_c = \frac{vRT}{V_m} ln\left(\frac{C}{C_O}\right) \qquad (3.1)$$

Where P_c is the crystallization pressure, v is the total number of ions released upon dissociation of the salt (e.g. for NaCl = 2), R is the universal gas constant, T is the absolute temperature, V_m is the molar volume of the salt crystal, C and C_o are increasing concentration in vicinity of crystal and saturation concentration of NaCl respectively. The saturation concentration of NaCl is 6.1 m (i.e. 6.1 mole of NaCl / kg of water). Before using inhibitors

to treat historic objects detailed experimental studies are required to assess the effectiveness and safety of their application. In particular, it is important to understand their influence on crystallization behavior of NaCl, moisture and ion transport, and also the development of salt damage in porous media. In this paper, we focus on the effect of hexa-cyanoferrate (II) inhibitor on the concentration levels reached by NaCl solutions within porous media during drying, and the associated water and ion transport processes taking place. This behavior is still not completely understood, because it is not easy to measure non-destructively the concentration of ions inside a porous material during dynamic experiments. Techniques like gravimetric analysis have been used for this type of analysis, but these have the disadvantages of being destructive to the sample and have poor spatial resolution. However, with the help of a specially designed Nuclear Magnetic Resonance set-up [51], we were able to non-destructively measure both hydrogen and sodium ions simultaneously during drying experiments. Two types of drying experiments were performed: the first series on droplets of salt solution with and without inhibitor; and the second on porous materials contaminated with salt solution with and without inhibitor.

3.2 Theory: Moisture and ion transport

When a wet porous material starts to dry due to evaporation a moisture flow is induced within the porous material. If there are dissolved salt ions present, the moisture flow will carry the salt ions along with it towards the drying surface (advection). This leads to an accumulation of salt ions near the surface, thus increasing the local salt concentration in this region. Therefore, a peak in the salt concentration profile is observed near the drying surface of the material, which also explains why salt crystallization is first observed near the material surface. This surface accumulation also induces a concentration gradient within the material, which in turn induces diffusion to level off the gradient. Therefore there is a competition between advection that transports ions towards the surface and diffusion that will try to level off the concentration gradient (see figure 3.1). For ion transport the molar flux J (mol m^{-2} s^{-1}) is given as [70]

$$J = \theta \left(CU - D \frac{\partial C}{\partial x} \right) \tag{3.2}$$

Where, C (mol m^{-3}) is the concentration, θ (m^3 m^{-3}) is the moisture content, D (m^2 s^{-1}) is the diffusion of salt ions in porous material given as $D = T^* D_{bulk}$, where T^* is the tortuosity and D_{bulk} is the bulk diffusion coefficient of salt ions, t (s) is the time, x (m) is the position and U (m s^{-1}) is the fluid velocity. The change in salt content can be calculated using law of mass conservation as:

$$\frac{\partial C\theta}{\partial t} = -\frac{\partial J}{\partial x} \tag{3.3}$$

Combining eq. (3.2) and eq. (3.3) the ion transport is given by following advection diffusion equation [71]

$$\frac{\partial C\theta}{\partial t} = \frac{\partial}{\partial x}\left[\theta\left(D\frac{\partial C}{\partial x} - CU\right)\right] \tag{3.4}$$

This equation shows the competition between advection and diffusion. On the right hand side of the equation the first term represents the diffusion process whereas the other term represents the advection process. The competition between these two processes is given by the Peclet number (*Pe*) [24]:

$$Pe = \frac{|U|L}{D} \tag{3.5}$$

Where L (m) is the length of the sample, D was taken equal to 1.3×10^{-9} m^2 s^{-1} [62]. Using measured moisture profiles the fluid velocity can be calculated [26]. For $Pe < 1$, diffusion dominates and for $Pe > 1$, advection dominates.
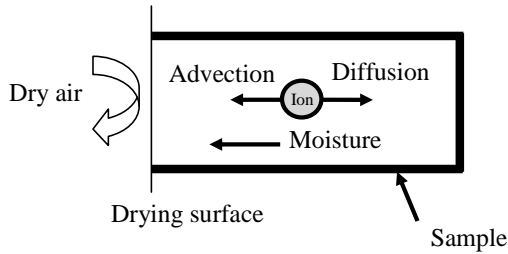

Figure 3.1: *A schematic of one dimensional drying of a sample saturated with salt solution.*

3.3 Experimental

3.3.1 Materials

The materials used in this study were fired-clay brick and Granada limestone. The red fired-clay brick is of a type typically used for construction in the Netherlands, and had an average porosity (as measured by water immersion method) of 0.32 m^3 m^{-3}, and a pore size distribution ranging from 1-10 µm (accounting for ~ 80% of the total pore space), as determined by Mercury Intrusion Porosimetry (MIP) (see fig. 3.2).

The Granada limestone is a buff colored stone commonly used as a building material in Granada, Spain. In this stone calcite is the main component (90 wt%), together with lesser amounts of SiO$_2$ and Al$_2$O$_3$ [72].This material has an average porosity (as measured by water immersion method) of 0.29 m^3 m^{-3}, and a bimodal pore size distribution with pores ranging from 0.3-1 µm (40%) and 1-100 µm (60%) as determined by Mercury Intrusion Porosimetry (MIP) shown in fig. 3.2. In these experiments potassium hexa-cyanoferrate (II) tri-hydrate K$_4$[Fe(CN)$_6$]·3H$_2$O was tested as a crystallization inhibitor. The active species in this chemical is hexa-cyanoferrate (II) [43]. In addition to its function as crystallization inhibitor, hexa-cyanoferrate (II) is also well known commercially as an anti caking agent [40].

3.3.2 Methods

Drying of salt solution droplets

A series of drying experiments to observe the crystallization behavior of NaCl salt solution droplets with and without a crystallization inhibitor were undertaken. A schematic of the set up is shown in fig. 3.3. A cylindrical polymethyl methacrylate (PMMA) sample holder with inner diameter of 16 mm was used. Droplets of 300 µl salt solution (3 m NaCl) with and without inhibitor were dried using 0% relative humidity and about 1 l min^{-1} air flow rate. Time lapse microscopy of the crystallization was performed using a dino-lite digital microscope, with four LED's placed below the substrate as a lighting source for imaging within the NMR setup. The capture of photomicrograph images along with the NMR measurements gives the possibility to visualize the drying of the droplet while simultaneously obtaining information about NaCl concentration of the droplets.
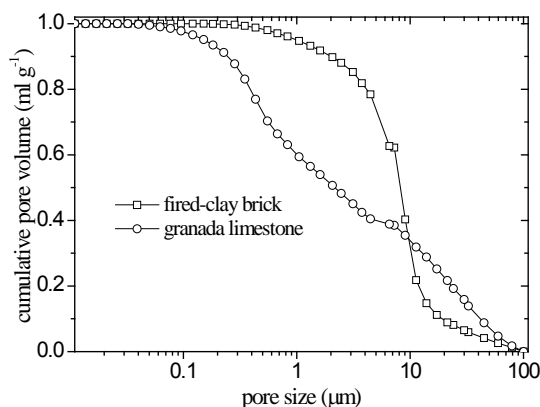

Figure 3.2: *The cumulative pore size distribution of fired-clay brick and Granada limestone as measured by mercury intrusion porosimetry.*

Drying of porous building materials saturated with salt solution

A schematic diagram of the set up is given in fig. 3.4. The cylindrical samples 20 mm in diameter and 40 mm in length were saturated by capillary rise with salt solution (3 m NaCl) containing different concentrations of inhibitor (0.001 m and 0.01 m). These samples were sealed using Teflon tape on all sides except the top surface and placed in the NMR sample chamber where they were exposed to dry air with a flow 1 l min^{-1} and 0% relative humidity, thereby creating one dimensional drying experiment. The sample position was moved in the vertical direction using a step motor to allow measurement of the moisture and Na content throughout the sample length. Measuring one drying profile takes about 3 hours, while the complete drying experiment takes in the order of a few days depending on the composition of the salt solution. Therefore, small variations in the moisture and ion profiles during a single scan can be neglected. After each drying experiment was completed the efflorescence formed on the top of the sample was collected and weighed.
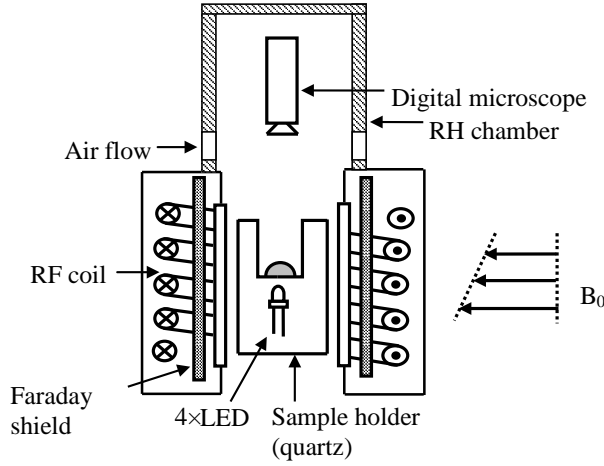
Figure 3.3: *A schematic diagram of the NMR set-up used for droplet drying experiments.*

3.3.3 Nuclear Magnetic Resonance (NMR)

In this study Nuclear Magnetic Resonance (NMR) is used for carrying out non destructive, quantitative and simultaneous measurement of both the hydrogen and sodium ion content in the sample. NMR is based on the principle that in a magnetic field, nuclei have a specific resonance frequency and can be excited by a radio frequency field. The resonance frequency f (Hz) depends linearly on the magnitude of the magnetic field:

$$f = \frac{\gamma}{2\pi} B_O \qquad (3.6)$$

Where $\gamma/2\pi$ (Hz T^{-1}) is the gyro magnetic ratio, B_o (T) is the main magnetic field. For ^{1}H $\gamma/2\pi$ is 42.58 MHz T^{-1} and ^{23}Na is 11.26 MHz T^{-1}. Therefore, by using a specific frequency the method can be made sensitive to a particular type of nucleus, in this case either hydrogen or sodium. The signal intensity S of a spin echo as used in the experiment is given by:

$$S = k\rho \left[1 - exp\left(-\frac{T_r}{T_1} \right) exp\left(-\frac{T_e}{T_2} \right) \right] \qquad (3.7)$$

Where S is the signal intensity, k is the sensitivity of the nuclei relative to hydrogen, ρ is the density of the nuclei, T_r and T_1 are the repetition time of the pulse sequence and spin-lattice relaxation time, T_e and T_2 are the spin echo time and spin-spin relaxation time. To measure the maximum signal i.e. from all pore sizes, T_e should be as short as possible as T_1 and T_2 are proportional to pore size. As the sensitivity of ^{23}Na nuclei is low relative to hydrogen ($k_H = 1$, $k_{Na} = 0.1$), 256 averages of the spin echo measurements are taken for Na nuclei relative to 8 averages of hydrogen to achieve a sufficient signal to noise ratio. In our experiments the T_e used is 250 µs and 450 µs for H and Na respectively. Since the relaxation time for Na in NaCl crystals is of order of 10 µs [73], only dissolved Na ions are measured using the NMR

set up. For the experiments presented here, a home built NMR scanner with a static magnetic field of 0.78 T and gradient up to 0.3 T/m was used [51].In order to perform quantitative measurements a Faraday shield was placed between the coil and the sample [51].
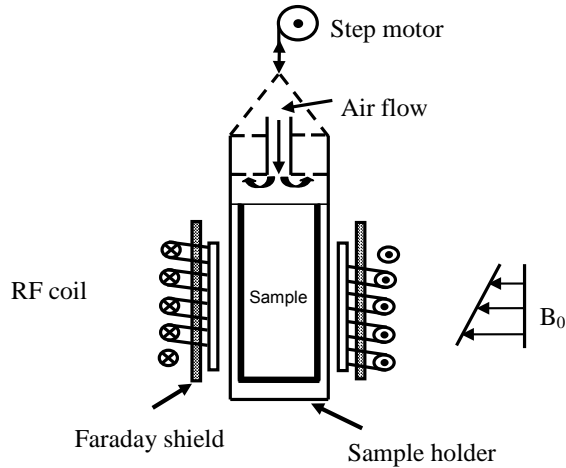

Figure 3.4: *A schematic diagram of the NMR set-up used for the brick drying experiments.*

3.4 Results and discussion

3.4.1 Droplet drying experiments

Drying of salt solution droplet without inhibitor

Initially we started with the drying of a 3 m salt solution droplet without inhibitor. The measured sodium and hydrogen content of the droplet is given in fig. 3.5a, whereas the calculated salt concentration is given in fig. 3.5b. As can be seen, as soon as drying has started the hydrogen content decreases whereas the dissolved sodium content remains constant (see fig. 3.5a) as a result the concentration in the droplet (fig. 3.5b) increases. After about 8 hours a decrease in the sodium content is seen, indicating crystallization. This onset of crystallization was also observed by direct visualization (see picture 3.5c) where cubic structured crystals were seen in the droplet. Also during drying the retraction of contact line was seen. This retraction of the droplet can decrease the effect of advection thereby reducing the concentration gradients in the drop, resulting in a homogenous distribution of the ions in the droplet. This can also be verified by estimating the Peclet number and is discussed in next section. Towards the end of the drying, the decrease in H and Na signals leads to an increase in noise in concentration. Cubic crystals are seen at the end of the experiment (see picture 3.5d).

Figure 3.5: *Drying of a 300 µl of 3 m NaCl salt solution droplet without inhibitor (a) The measured normalized hydrogen (H) content (o) and normalized sodium (Na) content (Δ) (b) calculated NaCl concentration (□) plotted as function of time. The pictures show the crystal morphology (c) at the onset of crystallization (~ 8h) and (d) at the end of the experiment (~ 22h).*

Analysis of advection-diffusion processes in a droplet

In order to do the analyses of advection-diffusion processes in a droplet the data is plotted in a way that is somewhat similar to a so called efflorescence pathway diagram (EPD) [16]. In the case of a droplet drying, the total amount of dissolved salt content in the droplet is plotted as a function of the normalized volume of the droplet ($V/V_{initial}$) and is given in fig. 3.6. In this diagram the competition between advection and diffusion can be shown in terms of the *Pe* number on the microscopic scale (i.e. on the length scale of the droplet). Two extreme situations can be distinguished. In the first case if diffusion dominates ($Pe < 1$) it will result in homogeneous distribution of ions throughout the droplet.
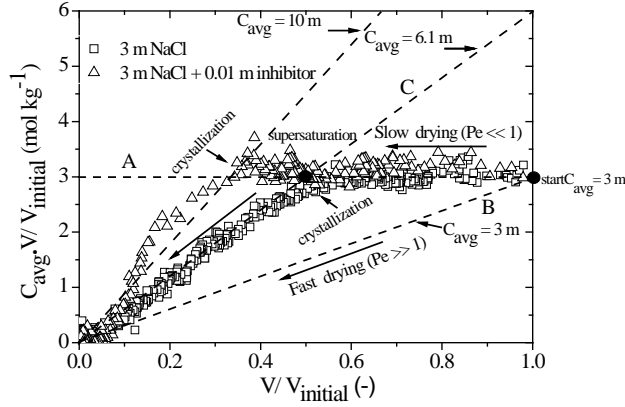
Figure 3.6: *Advection-diffusion analysis diagram for the droplet drying experiment: The total amount of dissolved sodium in the droplet is plotted as a function of the volume of the droplet (V). Both the axes are normalized with respect to the initial volume of the droplet ($V_{initial}$). The division of both the axes gives the average concentration (C_{avg}) of Na in NaCl solution droplet shown by dotted lines in the figure. The results for 3 m NaCl salt solution droplet with ($\triangle$) and without inhibitor ($\square$) are shown.*

Hence, during drying the volume of the droplet will decrease and the concentration will increase homogenously throughout, till the saturation concentration of 6.1 m is achieved. From this moment onwards any further drying will cause crystallization and the concentration would stay constant at 6.1 m. In the second case, if advection dominates ($Pe > 1$), it will result in concentration gradients in the droplet e.g. convective flow of the ions towards the periphery resulting in crystallization patterns somewhat similar to coffee-stain effect will be expected. In this case as soon as the volume of the droplet decreases and if there are enough nucleation sites (e.g. near periphery) immediate crystallization of salt will occur, i.e. the total amount of dissolved salt will decrease. Therefore in this case the concentration of dissolved salt ions inside the droplet will remain almost constant. In figure 6 the data for the 3 m NaCl salt solution droplet is plotted. As can be seen for the salt solution droplet, initially the $Pe < 1$ path is followed indicating diffusion dominance and the concentration increased until nearly the saturation concentration was reached, after which it stayed constant at approximately the saturation concentration 6.1 m.

Drying of salt solution droplet with inhibitor

Next the drying of 3 m NaCl droplet in the presence of 0.01 m inhibitor was studied. In fig. 3.7a the measured sodium and hydrogen signals are given as function of time whereas in fig. 3.7b the corresponding calculated concentration is given. In the presence of inhibitor, during approximately the first 1.5 hours a faster drying rate was observed. During this time the moisture content decreases and sodium content remains constant, thereby resulting in an increase in solution concentration. After approximately 2 hours the concentration in the droplet was in the order of 6.1 m but no crystallization was observed. As the drying

progresses the concentration increased and the system supersaturated slowly. In fig. 3.7b we have also plotted the surface area of the droplet.
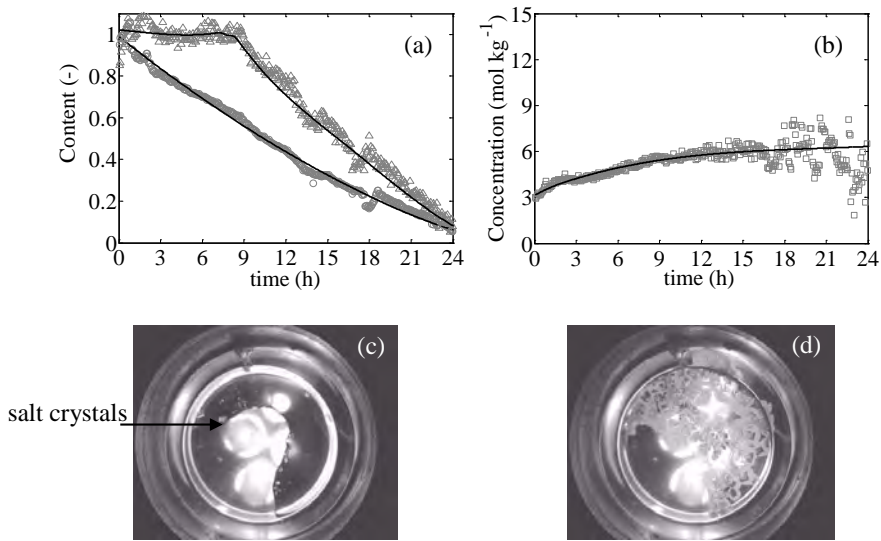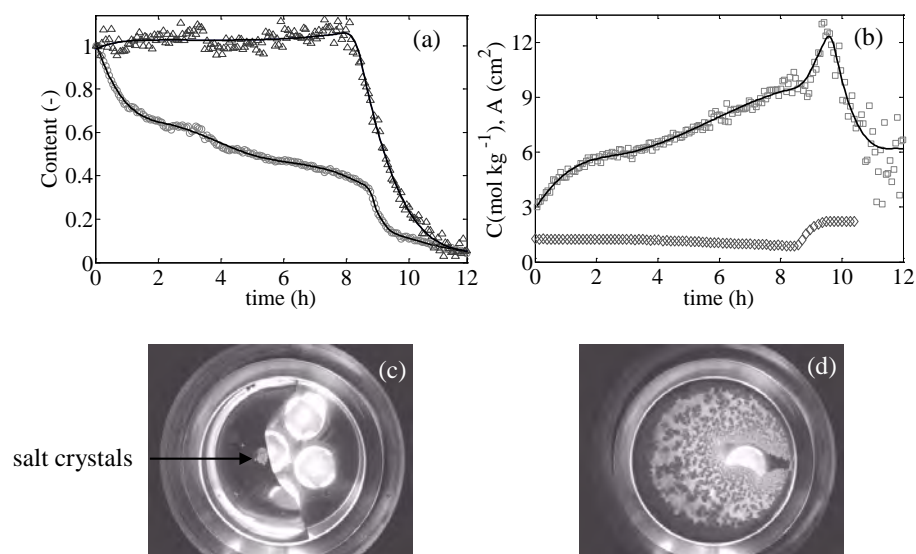

Figure 3.7: *Drying of a 300 µl of 3 m NaCl salt solution droplet with 0.01 m inhibitor (a) The measured normalized moisture (H) content (o) and normalized sodium (Na) content (∆) (b) calculated NaCl concentration (□) and area of the droplet (◊) plotted as function of time. The pictures show the crystal morphology (c) at the onset of crystallization (~ 8 h) and (d) at the end of the experiment (~ 12 h).*

As can be seen due to evaporation the surface area of the droplet decreased continuously. After ~ 8 hours a faster decrease in moisture and sodium content was observed indicating crystallization. This was also observed by direct visualization (see picture 3.7c). A small bunch of dendritic crystals were observed near the edge of the droplet. The corresponding average concentration at this point was nearly 10 m giving a supersaturation of 1.6 (calculated as C/C_o). From this moment onwards the average concentration in the droplet continued to increase as a rapid increase in the surface area of the droplet was observed. This was due to the formation of dendritic crystals, the branches of which provided a pathway for the solution to spread over a much larger surface area, this phenomenon being commonly known as 'salt creep' (see also fig. 3.7d). Due to the enlarged surface area for evaporation a similar increase in the drying rate was observed, and the solution concentration increased to nearly 12 m. After about 9.5 hours the drying rate decreased and no further spreading of the droplets was observed. Meanwhile, the concentration returned to the equilibrium concentration (6.1 m).

The results from the drying of a salt solution droplet with inhibitor are also plotted in fig. 3.6, as can be seen in this case the sodium concentration also remains homogenous until crystallization and the droplet supersaturates, reaching a maximum concentration in the order of 10 m before crystallization. These results show that the ferrocyanide is acting as a strong

nucleation inhibitor, which delays the onset of crystallization resulting in higher solution concentration. The inhibitor's presence also changes the NaCl crystal morphology. The mechanism of the inhibitor action on NaCl nucleation and growth has been studied in detail by Navarro and co-workers [43].

3.4.2 Brick drying experiments

In the previous section we have shown that the presence of an inhibitor significantly increases the supersaturation within salt solution droplets. This delay in onset of crystallization can promote efflorescence growth by inhibiting NaCl nucleation inside the stone. Also this delay may be an advantage in situations where the object is exposed to a fluctuating environment. For such a case the conditions for the crystallization may only be temporarily met. Nevertheless when exposed for periods of sustained low RH the critical supersaturation of the NaCl solution may be reached. As explained earlier higher supersaturation can cause higher crystallization pressure and hence the risk of damage is then greater. Therefore to ascertain the effects of the ferrocyanide inhibitor on the ion transport and crystallization behavior of sodium chloride solution within porous media a series of one dimensional drying experiment were performed using fired-clay brick and Granada limestone substrates.

Drying of samples saturated with pure water

First, the drying behavior of fired-clay brick and Granada limestone capillary saturated with pure water was studied. The measured moisture profiles for both porous materials during the drying process are given in fig. 3.8. Some recurrent irregularities can be seen in the profiles, e.g. at ~ 20 mm in both the fired-clay brick and the Granada limestone. These variations are most likely to be the result of inhomogenities of the sample. For both materials, two drying stages can be observed i.e. externally limited and internally limited. The first 3-4 profiles in both the samples are almost flat representing the first externally limited drying stage (shown by a vertical arrow in fig. 3.8a and 3.8b). During this stage there is continuous capillary flow of water to the surface and drying is limited by external conditions such as relative humidity and air flow. Afterwards, the drying front starts to recede below the sample surface, and the moisture profiles are no longer flat (shown by a horizontal arrow in fig. 3.8a and 3.8b). This represents the second internally limited drying stage where the continuous capillary network of water breaks up to form liquid islands. During this stage drying occurs by vapor diffusion through the porous medium, in response to the relative humidity gradient between the vicinity of the liquid island and the external drying surface of the material [23]. The transition point between these two drying stages can be identified as the critical moisture content. In case of fired-clay brick and Granada limestone, the critical moisture content was observed to be near 0.1 $m^3 m^{-3}$ and 0.12 $m^3 m^{-3}$ respectively.
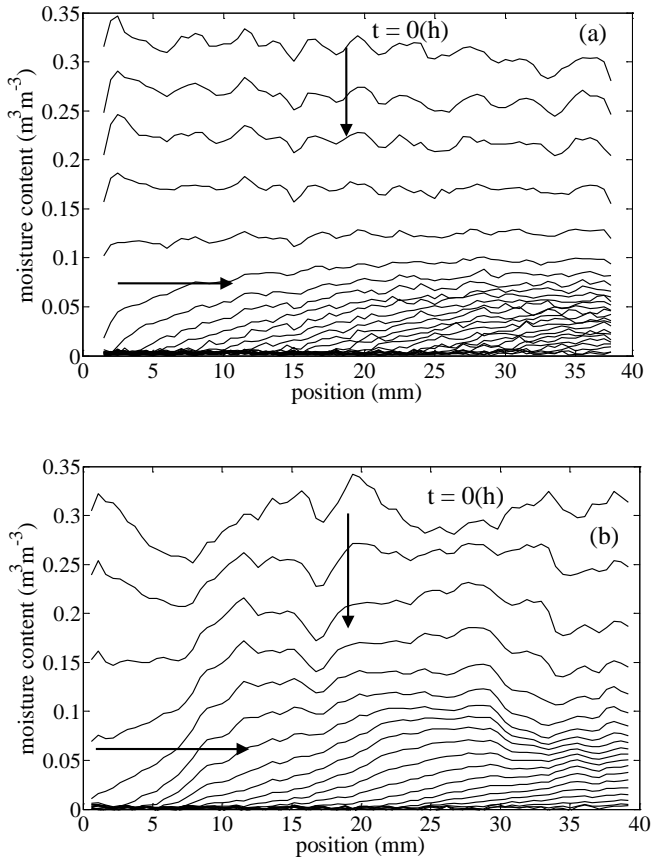
Figure 3.8: *The measured moisture profiles for (a) fired-clay brick and (b) Granada limestone plotted as a function of position during drying. The profiles are given for every 0.45 h. The samples were initially capillary saturated with water and dried using dry air with flow 1 l min^{-1} and 0% relative humidity. The drying surface is at 0 mm. The vertical arrow shows the homogenous drying of the sample and the horizontal arrow shows the penetration of the receding drying front.*

Drying of samples saturated with 3 m NaCl solution

To study the effect of salt on the drying behavior, the samples were capillary saturated with salt solution. The measured moisture profiles and the calculated concentration profiles for the fired-clay brick are given in fig. 3.9a and 3.9b and for Granada limestone in fig. 3.9c and 3.9d. The dotted line in the concentration profiles (fig. 3.9b and 3.9d) is a reference line showing the initial solution concentration (3 m). For both samples, the presence of salt slows down the drying relative to water loaded samples. For example, fired-clay brick saturated with salt solution took 10-11 days to dry in comparison to only 4-5 days for the water

saturated bricks. This difference in behavior can be explained by looking at the boundary conditions as given by:

$$q_v = \frac{\beta}{\rho}(h_a - h_{al}) \qquad (3.8)$$

Where q_v (m^3 m^{-2} s^{-1}) is the vapor flux at the air/material interface, β (mol m^{-2} s^{-1}) the mass transfer coefficient, ρ (mol m^{-3}) the molar density of liquid water, h_a is the partial pressure of water vapor in the surrounding and h_{al} is the partial pressure of water vapor at the air/material interface.

In case of water saturated samples, the air in direct contact with water at material/air interface is saturated with water vapor. The corresponding relative humidity is 100%. If there is a relative humidity gradient between the interface and the surrounding, the water vapor moves away from the surface, thereby causes drying of the material. However, the presence of salt lowers the saturated water vapor pressure due to solute solvent interaction. Therefore the local relative humidity at the air/material interface becomes less than 100% (for saturated NaCl 75%). This in turn reduces the relative humidity gradient [23], thereby causing slower drying of the salt saturated samples. During drying an increase in concentration was seen (see fig. 3.9b and 3.9d) near the drying surface indicating advection of ions towards the top. Using the measured moisture profiles the fluid velocity was calculated and the corresponding *Pe* number was determined [24]. *Pe* ~ 4 in fired-clay brick and *Pe* ~ 6 in Granada limestone confirms advection is dominant. Due to advection salt ions accumulate near the drying surface. When this salt ion accumulation exceeds the saturation concentration crystallization will occur. These salt crystals can block the pores near the drying surface. Especially for fired-clay brick which has smaller pores the effect of blockage is seen on the drying rate. As the moisture content approaches 0.1 m^3 m^{-3}, the drying slows down to such an extent that diffusion dominates, and the salt concentration starts to level off. We found in this case *Pe* ~ 0.8. However, in Granada limestone the blockage effect was not seen due to the presence of bigger pores. No leveling off of the concentration was seen in Granada limestone during the experiment and the Peclet number remained greater than one.
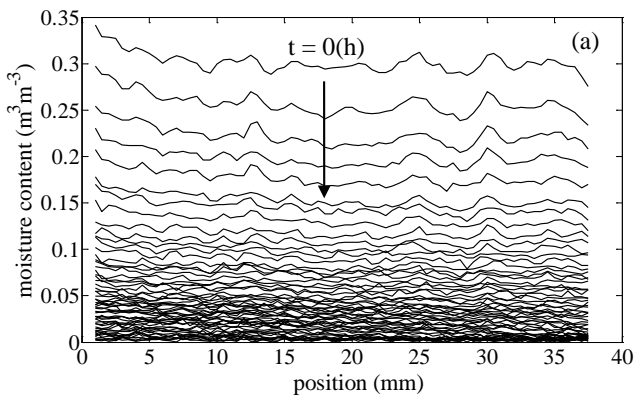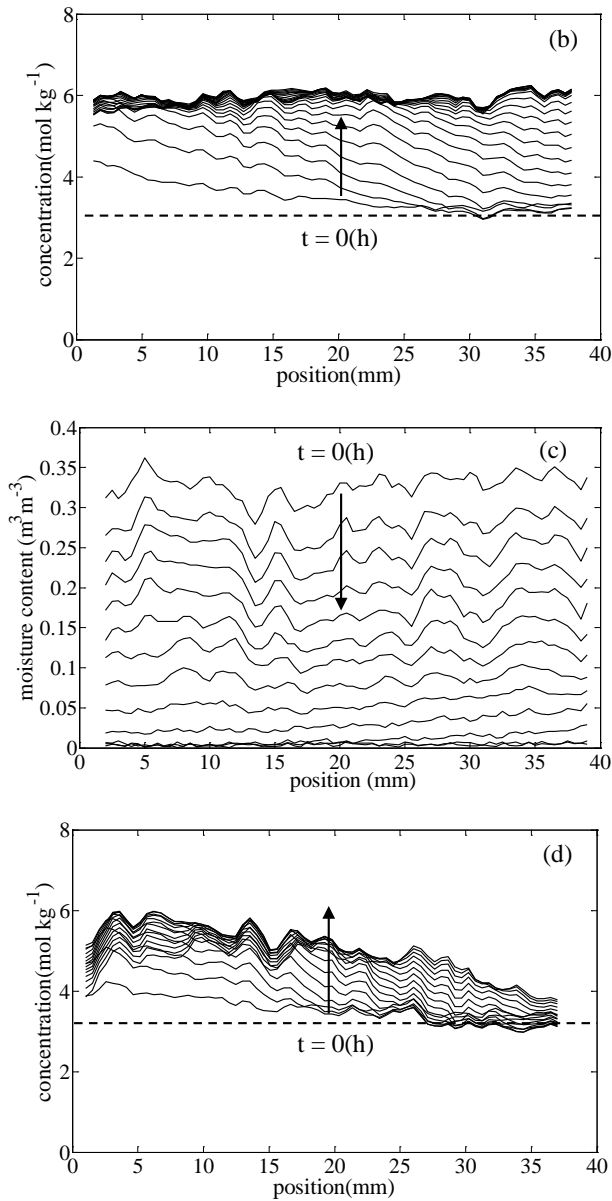
Figure 3.9: *The measured moisture profiles (a) and the corresponding concentration profiles (b) for fired-clay brick, and t he measured moisture profiles (c) and t he corresponding concentration profiles (d) for Granada limestone, plotted as a function of position during drying. These samples were initially capillary saturated with 3 m NaCl solution and dr ied using dry air with flow 1 l min⁻¹ and 0% relative humidity. The profiles are given for every 3 h. The drying surface is at 0 m m. Efflorescence up t o ~ 7% and ~ 10% was seen on the surface of the fired-clay brick and Granada limestone respectively.*

Also, no receding drying front was observed in case of salt saturated samples in contrast to water saturated samples. The slower drying rate and change in the wetting properties of the solution in the presence of NaCl might be responsible for this [16]. The efflorescence formed on the surface was collected at the end of the experiment and weighed to calculate the amount of salt coming out of the sample. Approximately 7% and 10% of the initial salt content came out of the fired-clay brick and Granada limestone respectively.

Efflorescence pathway diagram (EPD)

To understand the crystallization processes during brick drying the data was plotted on a so called efflorescence pathway diagram (EPD) [16]. In this case we have calculated the Peclet number on the macroscopic scale i.e. on the length scale of the brick. The dissolved salt content is plotted as a function of normalized moisture content of the brick. The EPDs for both drying experiments are given in fig. 3.10. As in the case of the droplet two extreme situations can be distinguished on this macroscopic scale. In the first case when the system dries very slowly ($Pe < 1$); diffusion dominates resulting in a homogeneous distribution of ions throughout the sample. For this situation, starting from an initial concentration of 3 m the salt solution concentration will increase throughout the sample, until the saturation concentration 6.1 m is achieved. From this moment onwards any further drying will cause crystallization. Furthermore, the concentration will stay constant at 6.1 m. In the second case the system dries very fast ($Pe > 1$), i.e. advection dominates. In this case, ions will be transported along with the moisture flow towards the drying surface. Thus, the concentration will increase near the drying surface. If there are enough nucleation sites, accumulation of ions beyond the saturation concentration will immediately result in crystallization near the surface as efflorescence. Efflorescence preferentially occurs in the regions where the evaporation is fastest. It also acts as a porous network and increases the effective surface area for evaporation. Thus, causing higher evaporation flux [62,74]. Due to higher evaporation flux, the underlying velocities also increase and thereby pumping more dissolved salt ions towards the surface. In this way, efflorescence acts as a sink for the ions. If rate of crystallization (efflorescence) is high enough, the ratio of transported Na to hydrogen ions remains constant and the dissolved salt ion concentration (ratio of dissolved sodium to hydrogen ions) inside the material will remain almost constant at the initial concentration.

In the brick drying experiments, for the materials saturated with salt only a path in between the extreme cases ($Pe < 1$ and $Pe > 1$) is followed. For fired-clay brick after some time as the drying slows down the $Pe < 1$ path is followed. During this time the salt concentration levels off at ca. 6.1 m. For the Granada limestone, a path in between the two extreme situations is followed throughout the experiment and no leveling off of the concentration is seen due to the presence of bigger pores.
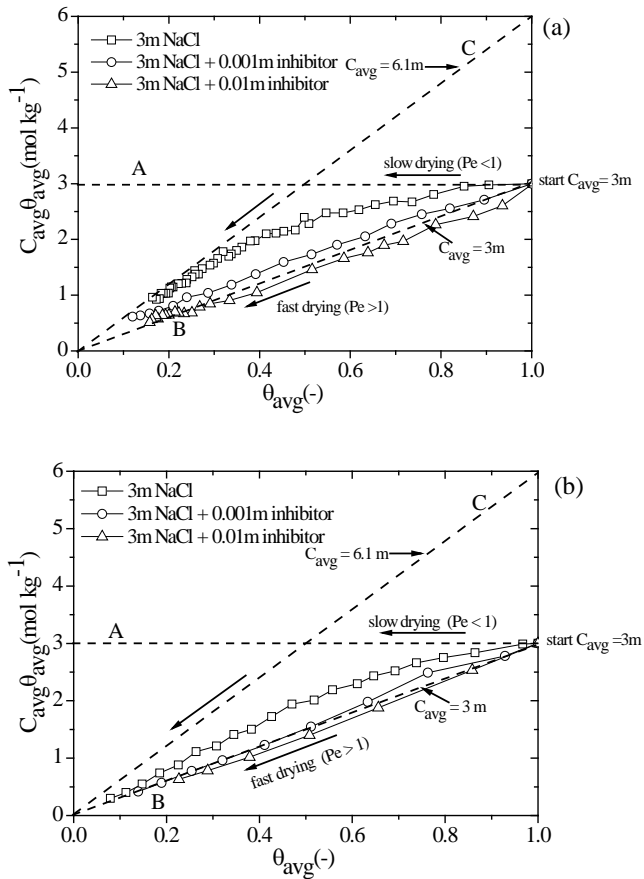
.

Figure 3.10: *Efflorescence pathway diagram for the brick drying experiment: The total amount of dissolved sodium content is plotted as a function of time dependent average moisture content (θ_{avg}) in the brick. Both the axes are normalized with respect to the initial average moisture content. The division of both the axes gives the average concentration (C_{avg}) of Na in the brick as shown by dotted lines in the figure. The results are shown for (a) fired-clay brick and (b) Granada limestone. The materials were capillary saturated with 3 m NaCl solution without and with (0.001 m and 0.01 m) inhibitor.*

Drying of samples saturated with 3 m NaCl solution + 0.001 m inhibitor

In order to see the effect of inhibitor on the salt transport behavior and the concentration of ions inside the materials, samples were capillary saturated with 3 m salt solution mixed with 0.001 m inhibitor. The measured moisture profiles and the calculated concentration profiles for the fired-clay brick are given in fig. 3.11a and 3.11b and for Granada limestone are given in fig. 3.11c and 3.11d respectively. In this case due to somewhat noisy moisture measurement, a few local peaks are seen in the concentration profiles at the end of drying experiment. Fig. 3.11e and 3.11f show the efflorescence seen at

the end of drying on the surface of fired-clay brick and Granada limestone respectively. The drying of the materials saturated with salt solution + 0.001 m inhibitor was faster than the materials saturated with salt solution only. The concentration increases near the drying surface due to advection (see fig. 3.11b and 3.11d). The calculated value of *Pe* ~ 10 (as determined in section 3.2) in both the cases confirms advection is the dominant phenomenon and causes salt crystallization near the drying surface. Due to dendritic crystal growth morphology in the presence of inhibitor, the effective surface area for evaporation increases. The salt solution creeps along the branches of the dendrites and transports more and more dissolved salt ions towards the drying surface which was seen as efflorescence by the end of drying experiment. Also, the crystals were seen to form a salt ring around the material. Approx. 36% of salt in fired-clay brick and 47% of salt in limestone was deposited out of the sample as efflorescence. For fired-clay brick a distinct moisture peak starts building up near the drying surface. Initially this peak increases in height but afterwards near the end of drying it starts to diminish. This peak was probably due to the presence of moisture in the salt ring formed around the material at nearly top 5 mm of the sample (see fig. 3.11e).
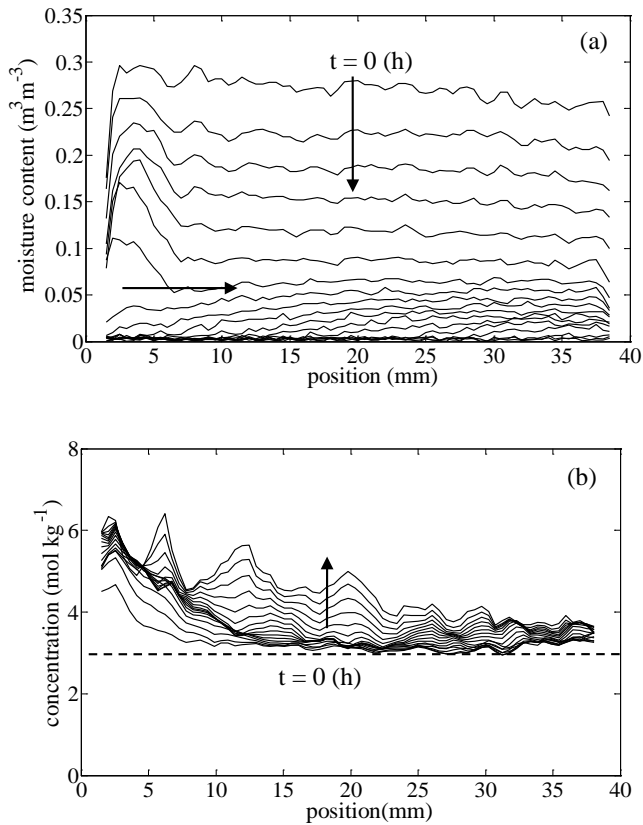
Figure 3.11: The measured moisture profiles (a), the corresponding concentration profiles (b), and the efflorescence seen at the end of the drying on the surface of the sample (e) for fired-clay brick; and the measured moisture profiles (c), the corresponding concentration profiles (d), and the efflorescence seen at the end of the drying on the surface of the sample (f) for Granada limestone, plotted as a function of position during drying. These samples were initially capillary saturated with 3 m NaCl solution + 0.001 m inhibitor and dr ied using dry air with flow 1 l min^{-1} and 0% relative humidity. The profiles are given for every 3 h. The drying surface is at 0 mm.

As this outer salt ring was in the scanning region of the NMR it also contributes to the signal. Therefore it is hard to draw a firm conclusion in the first few mm of the material. However, no supersaturation is seen inside the materials. In the presence of inhibitor a receding moisture front starts penetrating again near 0.08 $m^3 m^{-3}$ in both the samples. This is probably due to faster drying and lower salt content inside the sample. These results are also plotted in the EPD (see fig. 3.10). For both the materials in the presence of the inhibitor the boundary line $Pe > 1$ is followed indicating faster drying compared to salt saturated samples and the concentration stays almost constant at around the starting concentration. A constant decrease in the dissolved sodium content is seen and advection is the governing process throughout the drying.

Drying of the samples saturated with 3 m NaCl solution + 0.01 m inhibitor

Next, the inhibitor concentration was increased by 10 fold. The measured moisture profiles and the corresponding calculated concentration profiles for fired-clay brick are shown in fig. 3.12a and 3.12b and for Granada limestone are shown in fig. 3.12c and 3.12d. The vertical black lines in fig. 3.12a and 3.12c indicate the sample boundaries. The drying surface is at 0 mm. We have also shown the moisture content outside the sample boundaries (see fig. 3.12a and 3.12c). Fig. 3.12e and 3.12f show the efflorescence seen at the end of drying experiment on the drying surface of fired-clay brick and Granada limestone respectively.

In the presence of 0.01 m inhibitor, for both fired-clay brick and Granada lime stone, drying was faster than the salt saturated samples. A distinct moisture peak was seen on the drying surface of the materials. This peak was probably due to the moisture present in the efflorescence found on the surface of material.

In fired-clay brick, the salt concentration up to 10 m is seen near the drying surface (see fig. 3.12 b). As discussed before, it is difficult to draw conclusions on the basis of the measured concentration in first few mm of the material.

In rest of the material the concentration stays constant nearly at the starting concentration i.e. 3 m and no supersaturation was observed In Granada limestone (see fig. 3.12d), the concentration remains nearly constant at the starting concentration and no supersaturation was observed. Approximately 69% of the salt in fired-clay brick and approximately 51% salt in limestone were deposited at the surface in the form of efflorescence. Here also a receding moisture front starts penetrating near 0.1 $m^3 m^{-3}$ for both cases.

From these results it is concluded that in the presence of inhibitor the drying conditions near the material/air interface change due to the change in crystal morphology. The immediate crystallization near the drying surface provides a sink for the salt ions and as a result the concentration of the dissolved salt ions stays constant at the initial concentration inside the material.
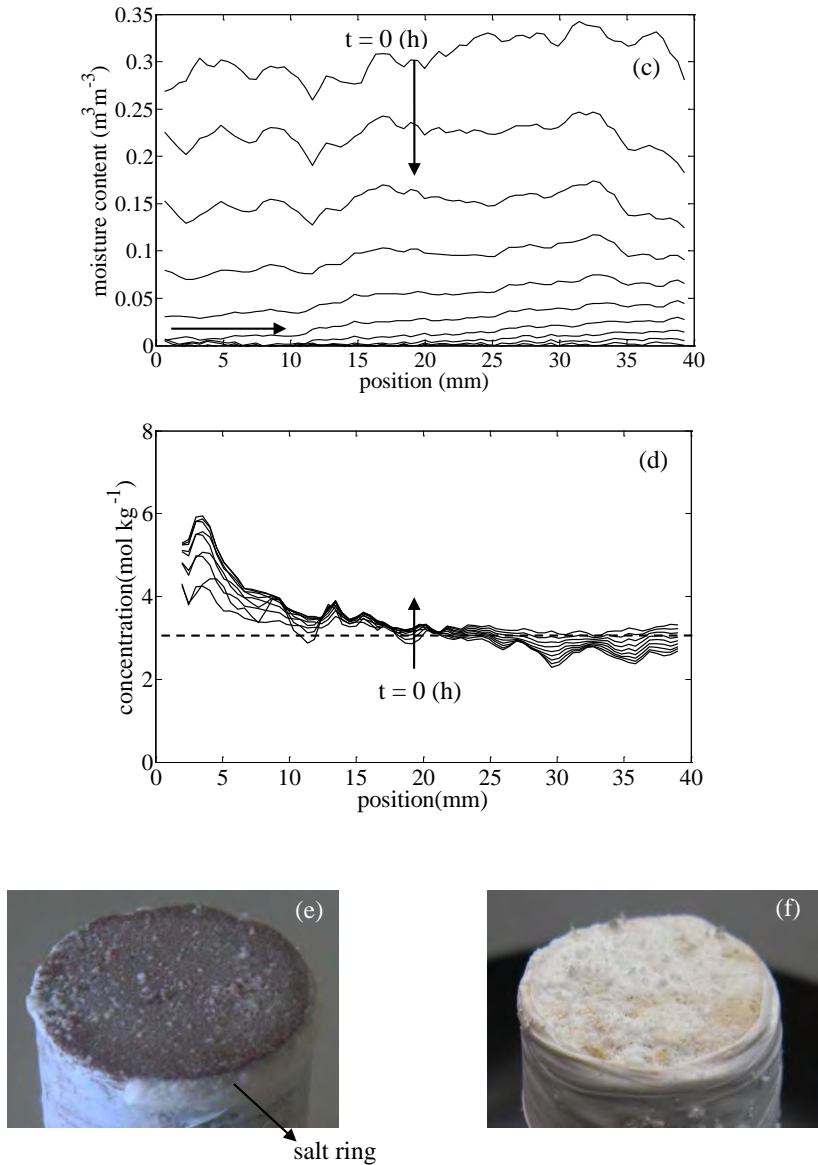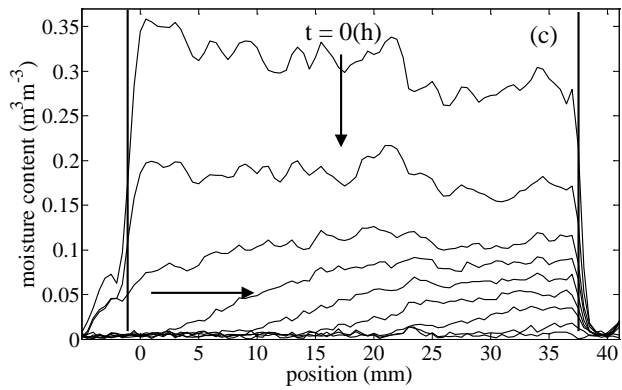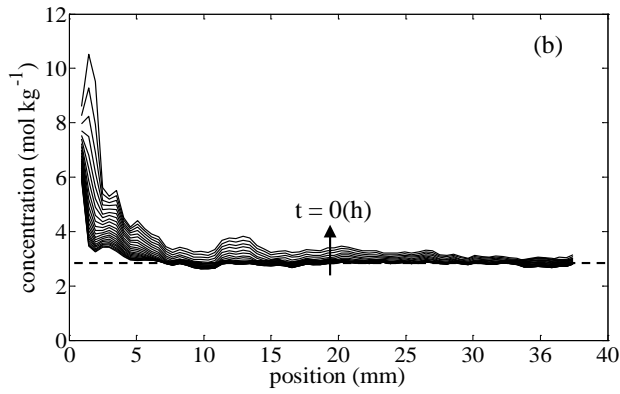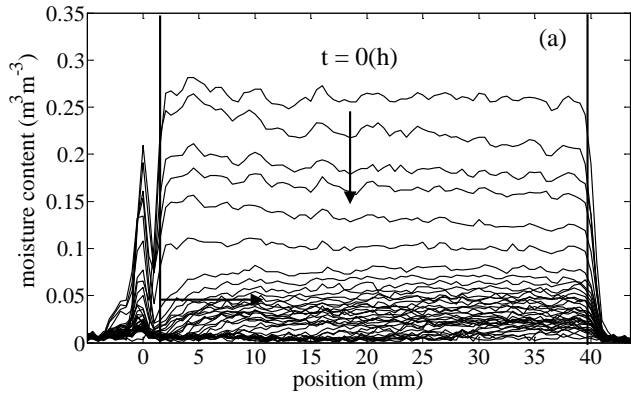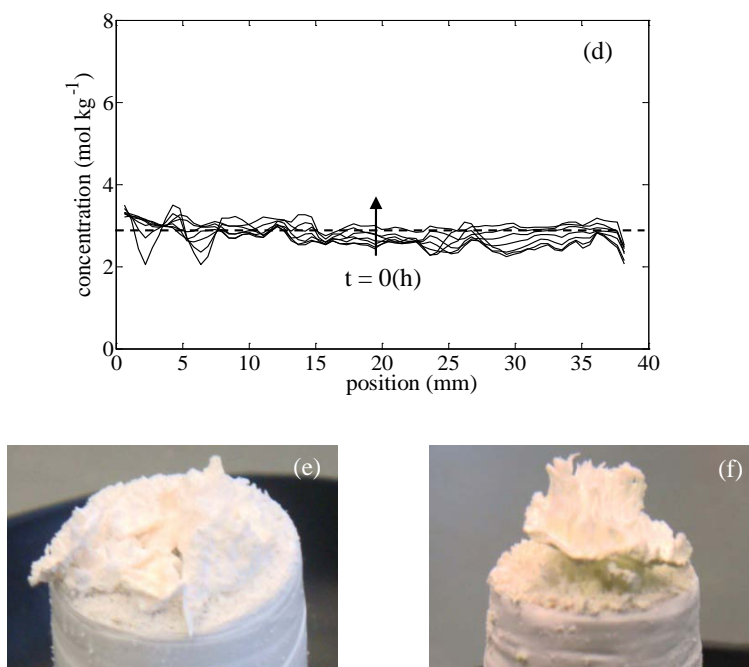
Figure 3.12: *The measured moisture profiles (a), the corresponding concentration profiles (b), and the efflorescence seen at the end of the drying on the surface of the sample (e) for fired-clay brick; and the measured moisture profiles (c), the corresponding concentration profiles (d), and the efflorescence seen at the end of the drying on the surface of the sample (f) for Granada limestone, plotted as a function of position during drying. These samples were initially capillary saturated with 3 m NaCl solution + 0.01 m inhibitor and dried using dry air with flow 1 l min^{-1} and 0% relative humidity. The drying surface is at 0 mm. The vertical black bars indicate the sample boundary.*

3.5 Conclusions

From the droplet drying experiments it is concluded that the presence of inhibitor makes the drying process faster. Higher supersaturation and change in crystal morphology were observed. After attaining supersaturation the salt concentration returns to the equilibrium concentration (6.1 m). This clearly shows that the system goes from a metastable state to stable equilibrium state and NMR provides sufficient signal to noise ratio to determine this transition. Besides this, a tremendous spreading of the salt crystals in the form of efflorescence was observed. This increase in efflorescence formation was related to the inhibitor concentration, and resulted in elevating the drying rate.

From the brick drying experiments it is concluded that the presence of inhibitor changes the drying conditions near the material/air interface due to changes in crystal morphology. Dendrite crystals provide much larger surface area for evaporation and advection becomes the governing phenomenon throughout the drying process. Advection of

dissolved salt ions causes crystallization of salt near the drying surface as non-destructive efflorescence. As a result the concentration inside the material stays almost constant at the initial concentration. This indicates that ferrocyanide ions could potentially be affective against NaCl damage in building materials as they promote non-destructive efflorescence rather than destructive sub-florescence.

At the same time there are many questions still to be addressed such as a) the effect of varying environmental conditions on the inhibitor action and b) the effect of the inhibitor on salt mixtures present in building materials, since in practice there is not only the single salt present in the building materials but indeed mixture of salt is present.

Chapter 4

How ferrocyanide influences NaCl crystallization under different humidity conditions

Abstract

The effect of ferrocyanide ions on moisture/ion transport and salt crystallization processes in salinated porous materials under different environmental conditions has been studied. A Nuclear Magnetic Resonance technique (NMR) has been used for carrying out non-destructive, quantitative and simultaneous measurements of both the hydrogen and sodium ion content.

For salt saturated bricks without inhibitor the slowest drying rate was observed at low relative humidity (0%). This is due to the blockage of pores near the drying surface that reduces the effective surface area available for evaporation. At high humidity (55% and 70%), due to low evaporative flux at the surface, the drying front is located on the surface of the material. Due to this, salt crystallizes as efflorescence and blockage effects were less significant and consequently the drying rate was higher. With the addition of inhibitor at low relative humidity, due to distinct crystal morphology, salt crystallizes as efflorescence and the saturation concentration was attained very slowly inside the brick. At higher relative humidity, in the presence of inhibitor no significant difference either in the amount of efflorescence formed or the speed at which the saturation concentration was attained inside the brick was found.

4.1 Introduction

Salt weathering leads to the destruction of many valuable cultural heritage monuments and of the porous building materials. Soluble salts such as chlorides, sulphates and nitrates are known to be the reason behind damage. Among the various salts commonly found in buildings, sodium chloride (NaCl) is one of the most abundant and ubiquitous. The damage of the porous materials is mainly due to the crystallization of these soluble salts inside the porous matrix of the materials. The growth of salt crystals exerts pressure on the pore walls, which can exceed the tensile strength of the materials thus leading to damage [3]. In order to prevent or reduce the structural damage of the materials, an effective and practically feasible method is required. Because of the limited amount of practical options available for the control of salt damage, the use of crystallization inhibitors has been proposed as a potential preventive treatment method. These inhibitors act either by preventing or by delaying the onset of nucleation [28] (and hence crystallization) or by changing the crystal growth mechanism by adsorbing onto specific crystal faces [29]. Their application in the field of architectural conservation is fairly new and not yet fully explored. Some authors have proposed to use ferrocyanide (FC) ions as a preventive measure against NaCl damage, since these compounds appear to promote the formation of non-destructive efflorescence rather than destructive sub-florescence [43, 69]. Because of the formation of efflorescence the amount of salt crystallized inside the material decreases. It is known that efflorescence changes the drying kinetics of porous media by changing the boundary conditions near material/air interface [62]. Eloukabi et al. [75] have reported two types of efflorescence; crusty efflorescence, when a salt crystal crust forms at the surface of the porous medium and severely limits the evaporation rate; and patchy efflorescence, when the evaporation is not significantly limited by the presence of the crystallized salt at the surface of the porous medium. The evaporation rate can be in fact even greater than with pure water owing to the enhanced evaporation surface [75]. Consequently, efflorescence contributes significantly in changing the drying behavior of porous materials.

For bulk solutions, in the presence of inhibitor increased supersaturation levels have been reported in the past [43]. However, it is important to see the effect of these compounds on the concentration of NaCl solutions inside a porous media. As it is known that the process behind the damage due to salt crystallization is the growth of salt crystals in confined spaces (e.g. pores), hence exerting crystallization pressure on the pore walls. Thermodynamically, for an anhydrous salt the crystallization pressure (P_c) can be related to supersaturation (C/C_o) of the solution as [14]:

$$P_c = \frac{vRT}{V_m} ln\left(\frac{C}{C_o}\right)$$

(4.1)

Where, v is the total number of ions released upon dissociation of the salt (e.g. for NaCl = 2), R is the universal gas constant, T is the absolute temperature, V_m is the molar volume of the salt crystal, C and C_o are increasing concentration in vicinity of crystal and saturation concentration of salt respectively. Hence, if inhibitor brings supersaturation inside a porous material, it can cause damage to the material. However, recently, a study has been performed on the influence of ferrocyanide ions on N aCl crystallization and moisture/ion transport phenomena inside a porous brick [45]. It was reported that the presence of inhibitor changes the drying conditions near the material/air interface due to change in crystal morphology and most of the dissolved salt ions crystallize as non-destructive efflorescence. No high supersaturation has been reported inside the material in the presence of inhibitor. Hence, it was concluded that the use of ferrocyanide ions against NaCl damage is effective under low humidity conditions. However, in that study drying tests were performed at 0 % RH, whereas in practice the humidity can be much higher. Consequently, before using inhibitors to treat a historic object there is an urgent need to assess the effectiveness of their application at different environmental conditions.

In particular, it is important to understand their influence on c rystallization, moisture and ion transport behavior. This behavior is still poorly understood, because it is not easy to measure non-destructively the concentration of ions inside a porous material during dynamic experiments. Techniques, like gravimetric analysis have been used, but these have the disadvantages of being destructive to the sample and have a poor spatial resolution. However, with the help of a specially designed Nuclear Magnetic Resonance set-up [60], we were able to non-destructively measure both the hydrogen and sodium ion profiles simultaneously during dynamic drying experiments. From the ratio of the local sodium and hydrogen content the time evolution of the salt ion concentration inside the porous material can be determined as a function of position. The aim of the study reported in this paper, is to understand the drying and crystallization behaviour of NaCl saturated porous materials in the presence of inhibitor at different environmental conditions.

4.2 Theory

Drying of a porous material occurs due to the humidity gradient between the air/material interface and the environment. The water vapor moves away from the surface, thereby causing drying of the brick. The rate of volume change of water dV/dt (m^3 s^{-1}) across the material/air interface under isothermal conditions is given by the Fick's law:

$$\frac{dV}{dt} = D \frac{A}{\rho} \frac{M}{RT} \frac{(P_i - P^*)}{\delta} \tag{4.2}$$

Where A (m^2) is the effective surface area available for evaporation, ρ (g m^{-3}) is the density of liquid water, D (m^2 s^{-1}) is the diffusivity of water vapor in air, M (g mol^{-1}) is the molar mass of water, R (J mol^{-1} K^{-1}) is the gas constant, T (K) is the temperature, P_i and P^* (N m^{-2}) are the water vapor pressures at the air/water interface at the material surface and in the surrounding air respectively, and δ (m) is the thickness of the boundary layer through which the diffusion of water vapor takes place. Therefore, at a constant temperature the drying rate

mainly depends on the difference between the water vapor pressures at the interface and the environment (i.e. the relative humidity gradient), the effective area available for evaporation and on the air flow that determines the thickness of the boundary layer δ. So, for a given material at a given air flow, drying should be proportional to the relative humidity gradient. This holds good only in the first phase of drying when there is a continuous network of liquid inside the material to meet the demands of evaporitive flux at the surface. During this stage the rate of evaporation is controlled by external conditions rather than by the rate of transport within the material.

For a water saturated brick, the air in direct contact with water at the air/water interface is saturated with water vapor and therefore, $P_i = P_{sat}$ where, P_{sat} is the saturated vapor pressure of the liquids having planar surfaces. For the curved surfaces, e.g., in capillaries and drop, the saturated water vapor pressure changes. The Kelvin equation tells us how the saturated vapor pressure depends on the curvature of the liquid. For cylindrical capillaries of radius r, Kelvin equation is given as:

$$ln\left(\frac{P_i}{P_{sat}}\right) = \frac{\gamma}{r}\frac{V_m}{RT} \tag{4.3}$$

Where, γ is the surface tension, V_m is the molar volume of the liquid, and r is the radius. However, in case of fired-clay brick the pore sizes are in the range of 1-10 μm [45]. So, the influence of the capillary pressure on the P_i is negligible, So, P_i can be taken as equal to P_{sat} in equation (4.2). However, for the materials with smaller pore sizes in the order of nm, this effect should be kept in mind.

The location of salt crystallization in a material is determined by the competition of two mechanisms; diffusion and advection. Due to evaporation, a moisture flow is induced within the porous material. If there are dissolved salt ions present, the moisture flow will carry the salt ions along with it towards the drying surface (advection). This leads to an accumulation of salt ions near the surface, thus increasing the local salt concentration in this region. This surface accumulation induces a concentration gradient within the material, which in turn induces diffusion to level off the gradient. Therefore, there is a competition between advection that transports ions towards the surface and diffusion that will try to level off the concentration gradient. Generally, this competition is written in terms of a Peclet number given by [24]:

$$Pe = \frac{|U|L}{D_{eff}} \tag{4.4}$$

Where U (ms^{-1}) is the fluid velocity, L (m) is the length of the sample, D_{eff} (m^2 s^{-1}) is the effective diffusion coefficient of the salt ions in a material and is given by τD, where τ is the tortuosity and D is the diffusion coefficient. Initially, the evaporative flux at the drying surface is balanced by the liquid flow due to capillary action, thus an average value of fluid velocity can be estimated by using $J/\varphi\rho$ Where, J (kgm^{-2}s^{-1}) is the average mass flux, φ is the porosity of the material and ρ (kgm^{-3}) is the density of water. For $Pe < 1$, diffusion dominates and salt crystallizes uniformly inside the material as sub-florescence and for $Pe > 1$,

advection dominates and salt crystallizes either just beneath the surface of the material or outside the material as efflorescence.

4.3 Experimental section

4.3.1 Nuclear Magnetic Resonance (NMR)

In this study Nuclear Magnetic Resonance (NMR) is used for carrying out non-destructive, quantitative and simultaneous measurement of both the hydrogen and sodium ion content in the sample. NMR is based on the principle that in a magnetic field, nuclei have a specific resonance frequency and can be excited by a radio frequency field. The resonance frequency f (Hz) depends linearly on the magnitude of the magnetic field:

$$f = \frac{\gamma}{2\pi} B_O \qquad (4.5)$$

Where $\gamma/2\pi$ (Hz T^{-1}) is the gyro magnetic ratio, B_o (T) is the main magnetic field. For ^{1}H $\gamma/2\pi$ is 42.58 MHz T^{-1} and ^{23}Na is 11.26 MHz T^{-1}. Therefore, by using a specific frequency the method can be made sensitive to a particular type of nucleus, in this case either hydrogen or sodium. The signal intensity S of a spin echo as used in the experiment is given by:

$$S = k\rho \left[1 - exp\left(-\frac{T_r}{T_1} \right) exp\left(-\frac{T_e}{T_2} \right) \right] \qquad (4.6)$$

Where S is the signal intensity, k is the sensitivity of the nuclei relative to hydrogen, ρ is the density of the nuclei, T_r and T_1 are the repetition time of the pulse sequence and spin-lattice relaxation time, T_e and T_2 are the spin echo time and spin-spin relaxation time. As the sensitivity of ^{23}Na nuclei is low relative to hydrogen ($k_H = 1$, $k_{Na} = 0.1$), 256 averages of the spin echo measurements are taken for Na nuclei relative to 8 averages of hydrogen to achieve a sufficient signal to noise ratio. Since the relaxation time for Na in NaCl crystals is of order of 10 µs [73], only dissolved Na ions are measured using the NMR set up. For the experiments presented here, a home built NMR scanner with a static magnetic field of 0.78 T and gradient up to 0.3 T/m was used [51, 60]. The details of the set-up can be found elsewhere [51, 60].

4.3.2 Materials

The material used in this study was a red fired-clay brick. This red fired-clay brick is of a type typically used for construction in the Netherlands, and had an average porosity (as measured by water immersion method) of 0.32 m^3 m^{-3}, and a pore size distribution ranging from 1-10 µm (accounting for ~ 80% of the total pore space), as determined by Mercury Intrusion Porosimetry (MIP). In the experiments described in this study potassium hexa-cyanoferrate (II) tri-hydrate K_4[Fe(CN)$_6$]·3H$_2$O was tested as a crystallization inhibitor.

4.3.3 Method

A schematic diagram of the set up is given in figure 4.1. The cylindrical samples, 20 mm in diameter and 40 mm in length, were vacuum saturated with water, 3m NaCl solution without inhibitor and 3m NaCl solution with inhibitor. Two concentration of inhibitor were tested 0.001 m and 0.01 m. These samples were sealed using Teflon tape on all sides except the top surface and placed in the NMR sample chamber. The samples were then exposed to dry air at a flow rate of 1 l min^{-1}. The relative humidity was varied at 0%, 55% and 70%. In this way a one dimensional drying experiment was performed. The sample was moved in the vertical direction using a step motor to allow the measurement of moisture and sodium content throughout the sample length. Measuring one profile takes about 2.26 hours, while the complete drying experiment takes in the order of a few days depending on the composition of the salt solution. Therefore, small variations in the moisture and ion profiles during a single scan can be neglected. At the end of each drying experiment the efflorescence on top of the sample was collected and weighed.
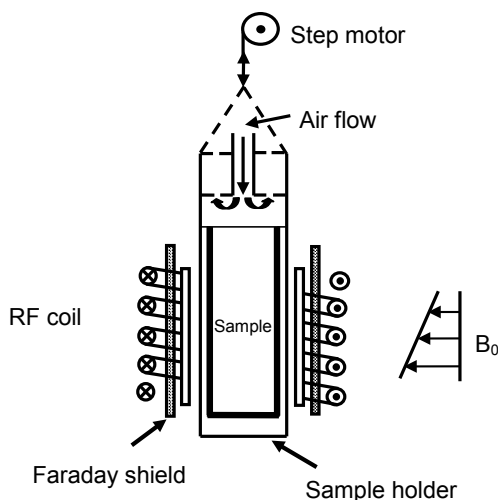
Figure 4.1: *A schematic of the NMR set-up for one dimensional drying of a sample saturated with salt solution.*

4.4 Results and discussion

Our main focus was to understand the influence of inhibitor on the crystallization and drying behavior of salinated porous materials under different environmental conditions. For this purpose, initially the drying behavior of water and salt saturated material was studied under different environmental conditions.

4.4.1 Drying behavior of fired-clay brick saturated with water

First, the drying behavior of water saturated bricks was studied. Drying was carried out at three different relative humidity (RH) conditions, i.e., at 0%, 55% and 70% RH. Using NMR the moisture profiles were measured during measurements. The measured moisture profiles for water saturated material dried at 0% RH and an air flow rate of 1 l min^{-1} are shown in fig. 4.2. The first rather flat profiles (denoted by the vertical arrow in fig. 4.2 represent the externally limited drying stage often called stage-1 of drying. After some time a receding drying front starts to penetrate into the sample and the profiles are not flat anymore (denoted by horizontal arrow in fig. 4.2 representing the internally limited drying stage often called stage-2 of drying. The transition between these two drying stages occurs at the so-called critical moisture content [23]. During stage-1 the drying rate is controlled by external conditions such as RH, temperature and air flow rates and is independent of the capillary processes inside the material [23]. During this stage there is a continuous capillary flow of water to the surface. In stage-2, however, the continuous capillary network of water breaks up to form liquid islands. During this stage drying occurs by vapor diffusion through the porous medium, in response to the relative humidity gradient between the vicinity of the liquid island and the drying surface.
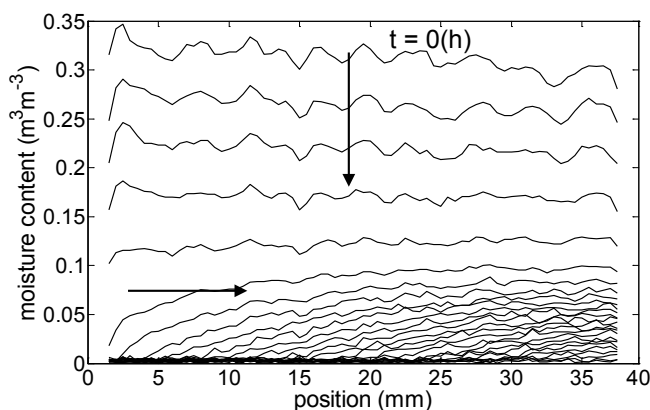

Figure 4.2: *Measured moisture content for a water saturated fired-clay brick as a function of position during drying. The profiles are given for every 0.45 h for a total time of ~ 22 hours. The samples were dried using dry air with a flow of 1 l min^{-1} and 0% relative humidity. The drying surface is at 0 mm. The vertical arrow indicates the homogenous drying of the sample (stage-1) and t he horizontal arrow indicates the penetration of the receding drying front (stage-2).*

Similar moisture profiles were recorded for water saturated samples dried at high humidity. Instead of showing moisture profiles of the samples dried at different relative humidity conditions, the results from various experiments are given in a graph shown in fig. 4.3a, where the normalized integrated hydrogen signal (S_H) is plotted as a function of time (t). The integrated hydrogen signal at a given time represents the total amount of water in the brick. As can be seen in fig. 4.3a, the drying rate of water saturated bricks was slower at high

relative humidity, which can be understood by considering the flux eq. (4.2). As mentioned before for water saturated samples, the air in direct contact with water (at the air/water interface) is saturated with water vapor and therefore $P_i = P_{sat}$ and $P^* = P_{sat} \times RH/100$, where RH is the relative humidity of the environment. With increasing environmental humidity, the water vapor pressure in the surrounding air also increases ($P^* = P_{sat} RH/100$). This decreases the humidity gradient between the air/material interface and the surrounding air and slows down the drying.

To confirm if humidity is the only factor responsible for the observed decrease in drying rate, a scaling of the time axis was done. For this purpose the time axis was multiplied by a scaling factor ($P_i - P^*$). The results are shown in fig. 4.3b, where the normalized integrated hydrogen signal is plotted as a function of ($P_i - P^*$) t. This figure shows that the drying curves of water saturated bricks dried under different relative humidity conditions coincide very well, especially at the initial stage of drying. This confirms that the decrease of the drying rate results from the depression of the humidity gradient only. The experimental value of δ is calculated in the beginning of drying using equation (4.2). The value of δ is found to be ~ 700 μm. The pore sizes in fired-clay brick are in the order of 1-10 μm, which is much smaller than the average boundary layer thickness (~700μm). Therefore, an approx. homogenous boundary layer can be assumed to be present at the surface of the material.
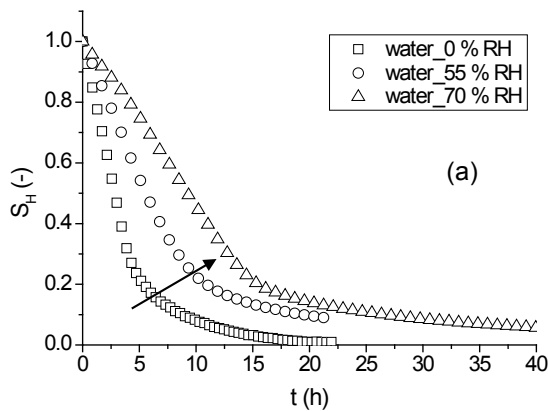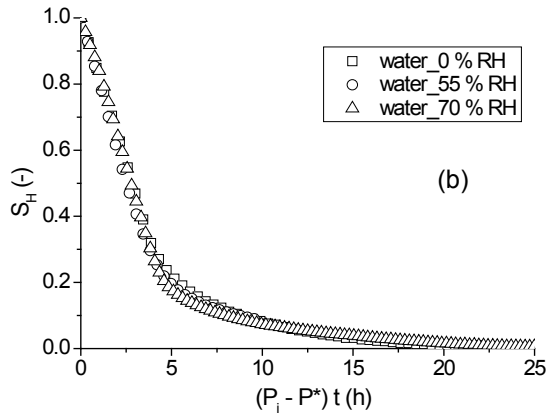
Figure 4.3: *(a) Normalized integrated hydrogen signal (S_H) as a function of time (t) for water saturated fired-clay bricks dried at different relative humidity conditions (b) Normalized integrated hydrogen signal (S_H) as a function of the scaled time ($P_i - P^*$) t. P_i and P^* are the water vapor pressures at the air/water interface at the material surface and i n the surrounding air respectively.*

4.4.2 Drying and crystallization behavior of salt saturated fired-clay brick without inhibitor

In order to understand the drying and the crystallization behavior of bricks in the presence of salt, the samples were saturated with 3 m NaCl solution and were dried at different relative humidity conditions (0%, 55% and 70%).

Drying behavior of salt saturated fired-clay brick at different relative humidity conditions

In fig. 4.4a, the normalized integrated hydrogen signal is plotted as a function of time. The drying rate of salt saturated bricks is lower than that of water saturated bricks (compare fig. 4.4a and fig. 4.3a). The drying rate of a salt saturated brick at 0% relative humidity slows down dramatically (see fig. 4.4a).
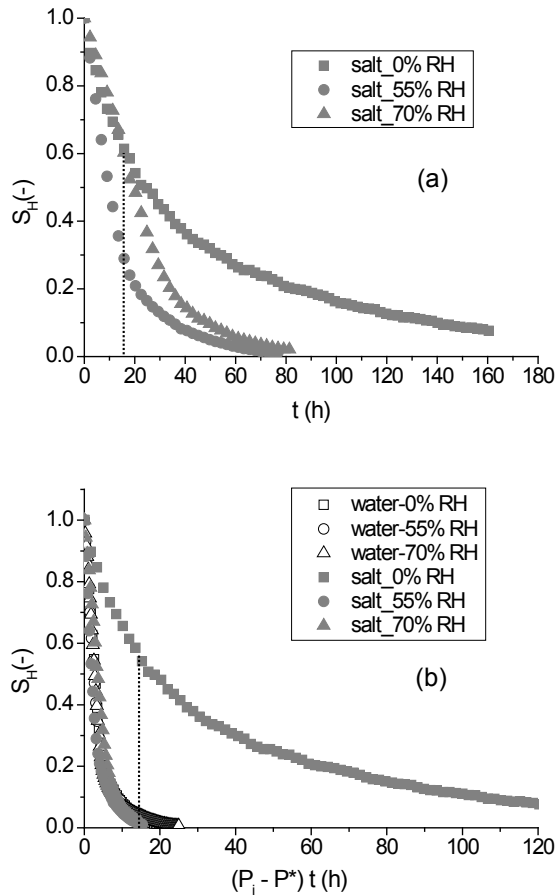
Figure 4.4: *(a) Normalized integrated hydrogen signal (S_H) as a function of time (t) for salt loaded bricks dried at different relative humidity conditions (b) Normalized integrated hydrogen signal (S_H) as a function of the scaled time ($P_i - P*$) t. P_i and $P*$ are the water vapor pressures at the air/water interface at the material surface and in the surrounding air respectively.*

After approx. 15 hours the drying rate of the fired-clay brick dried at low humidity became even lower than that of the bricks dried at higher humidity. On the other hand, the drying rate of bricks dried at 70% RH was lower than that of bricks dried at 55% RH. Besides this, a difference in the amount of efflorescence formed was seen. A negligible amount of salt crystallized as efflorescence at 0% RH in comparison to the amount of efflorescence formed at high humidity. Approx. 48% and 40% of salt crystallized as efflorescence at 55% and 70% RH respectively, compared to 6% efflorescence formed at 0 % RH. The pictures of the salt crystallized as efflorescence taken at the end of the experiments are shown in fig. 4.5a, 4.5b and 4.5c for the brick dried at 0%, 55% and 70% RH respectively. A quantitative data

showing the percentage of salt crystallized as efflorescence is plotted as a function of relative humidity in fig. 4.6.

One of the reasons behind lower drying rate of salt saturated bricks in comparison to water saturated bricks is the dependence of the drying rate on the equilibrium relative humidity, given in eq. (4.2). In the presence of salt the equilibrium relative humidity at the air/material interface decreases (the equilibrium relative humidity of saturated NaCl solution is 75% and that of water 100%) and consequently the drying rate also decreases. In order to check if the depression of relative humidity gradient is the only factor responsible for the slow drying of salt saturated bricks in comparison to water saturated bricks, a scaling of the time axis was done. The results are plotted in fig.4.4b, where the normalized integrated hydrogen signal is plotted as a function of scaled time. For comparison, the results for water and salt saturated samples are also included in fig. 4.4b. Except from the brick dried at 0% RH, the drying curves coincides well, indicating that for 55% and 70% RH the decrease of the drying rate indeed results from the depression of the relative humidity gradient. However, for the fired-clay brick dried at 0% RH, the drying rate was exceptionally lower.
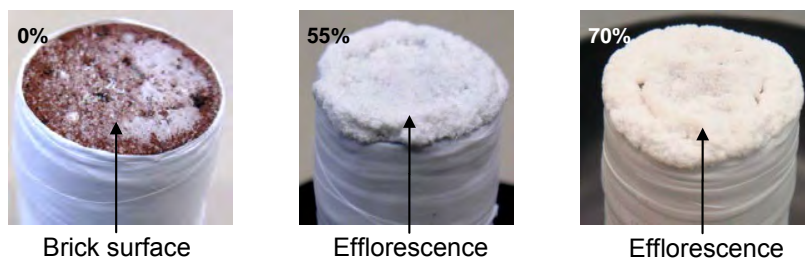

Figure 4.5: *Pictures of the efflorescence formed at the end of drying experiment in case of salt saturated brick dried at 0%, 55% and 70% RH. The amount of efflorescence increases at higher humidity.*

For better understanding of the results, the rates of initial volume change of the solution for water and salt saturated samples dried at different relative humidity conditions were compared. The results are given in fig. 4.7. The values of the volume change are obtained from the slope of a straight line fitted to the time dependent integrated volume for stage-1 drying only. A linear fit is drawn through the values of volume change for water saturated samples. This line shows, as expected, a decrease of water vapor flux with increasing relative humidity and the flux becomes zero at 100% RH. For NaCl solution saturated samples the flux should be zero at 75% RH. Considering this fact a theoretical dashed line is drawn parallel to the solid line for salt saturated samples. The values of the volume change for salt saturated samples should lie on this line, if the decrease in drying rate only results from the depression in of the relative humidity gradient. The figure shows that for samples dried at high relative humidity i.e. 55% and 70%, the values of volume change are close to the expected values. For the salt saturated brick dried at 0% RH the initial volume change is exceptionally low. This clearly indicates that another mechanism is causing the slow drying of the brick at 0% RH. This behavior can be understood from the observed salt efflorescence.
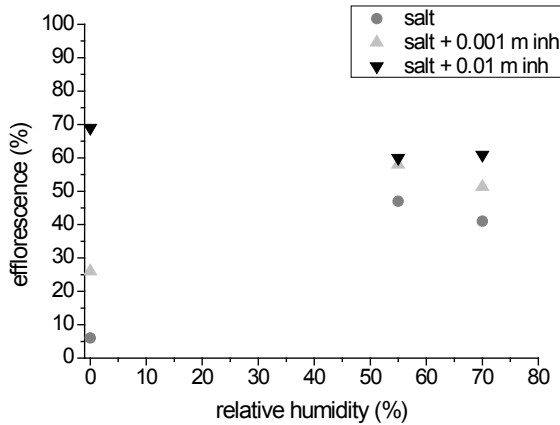
Figure 4.6: *The percentage efflorescence formed during the drying experiment as a function of the relative humidity for salt saturated bricks with and without inhibitor. The percentage efflorescence represents the ratio of the amount of salt crystallized as efflorescence and the initial amount of dissolved salt.*

The observed drying behavior of the material can be explained with the help of a schematic representation of the drying process shown in fig. 4.8. Fig. 4.8a, 4.8b and 4.8c represents a schematic for water saturated brick; salt saturated brick dried at 0% RH and salt saturated bricks dried at 55% / 70% RH respectively. In these pictures, L is the length of sample and δ (m) is the thickness of boundary layer through which the water vapor diffusion takes place. In case of water saturated brick the whole surface is available for evaporation (shown by vertical arrows in fig. 4.8a). However, for salt saturated bricks dried at 0% RH, a part of the surface is blocked by salt crystallization.
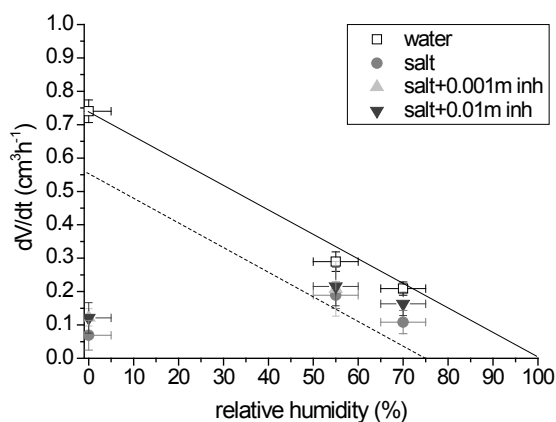
Figure 4.7*: The rate of initial volume change of the solution (dV/dt) as a function of the relative humidity for the bricks saturated with water, salt and salt + inhibitor solution (see fig. 4.3a and 4.4a). The solid line and the dashed line represent a linear fit to the data where the flux gets zero i.e. at 100% for water saturated samples and at 75% for salt saturated samples. The values of the volume change are obtained from the slope of a straight line fitted to the time dependent integrated volume for stage-1 drying only (see fig. 4.1). The solid line drawn through the values of volume change for water saturated samples is a guide to eye. For NaCl solution saturated samples the flux should be zero at 75% RH. Considering this fact a theoretical dashed line is drawn parallel to the solid line.*

This can be understood by considering the *Pe* number. The value of the salt diffusion coefficient is taken as a first approximation equal to 1.3×10^{-9} m^2 s^{-1} [75] assuming $D_{eff} = D$. In practice the D_{eff} will be less than D (as the tortuosity will be less than 1) and therefore the *Pe* number will be higher than the value estimated here. The average value of the flux is taken equal to the theoretical value (see figure 5, the theoretical value of the volume change is represented by a dashed line). At $t = 0$ h, the calculated value of the Peclet number is 46. Therefore, advection is dominant at the start of the experiment. Consequently, salt ions will be advected along with the moisture towards the drying surface. As the evaporation proceeds, the liquid flux continues to transport more and more dissolved salt ions towards the drying surface, where the salt ions accumulate. At a certain moment, the solubility limit will be exceeded and salt crystallization will occur. These salt crystals will block the pores near the drying surface, as shown in figure 4.8b. Due to this blockage the effective surface area available for evaporation reduces (shown by vertical arrows) compared to the surface area available for evaporation for water saturated bricks (refer eq. 4.2). Since for a salt saturated brick the rate of initial volume change was small (see fig. 4.7) we expect a rapid formation of a thin layer of salt crystals in the first few minutes, with a very low permeability near the drying surface. The thickness of this layer is obviously too small to be observed within our experimental resolution.

At high relative humidity, the evaporative flux at the surface of material is lower providing more time for the salt ions to migrate along with the moisture to the drying surface

and crystallize as efflorescence. The calculated value of Peclet number ~16 and ~8.4 in case of 55% and 70% RH respectively confirms advection and hence the salt crystallizes as efflorescence. Efflorescence has two effects. Firstly, it reduces the blockage of pores near the drying surface, keeping the system open, and secondly, the porous network of efflorescence increases the effective surface area available for evaporation [75]. This is the reason that no decrease in the drying rate was seen at high humidity.
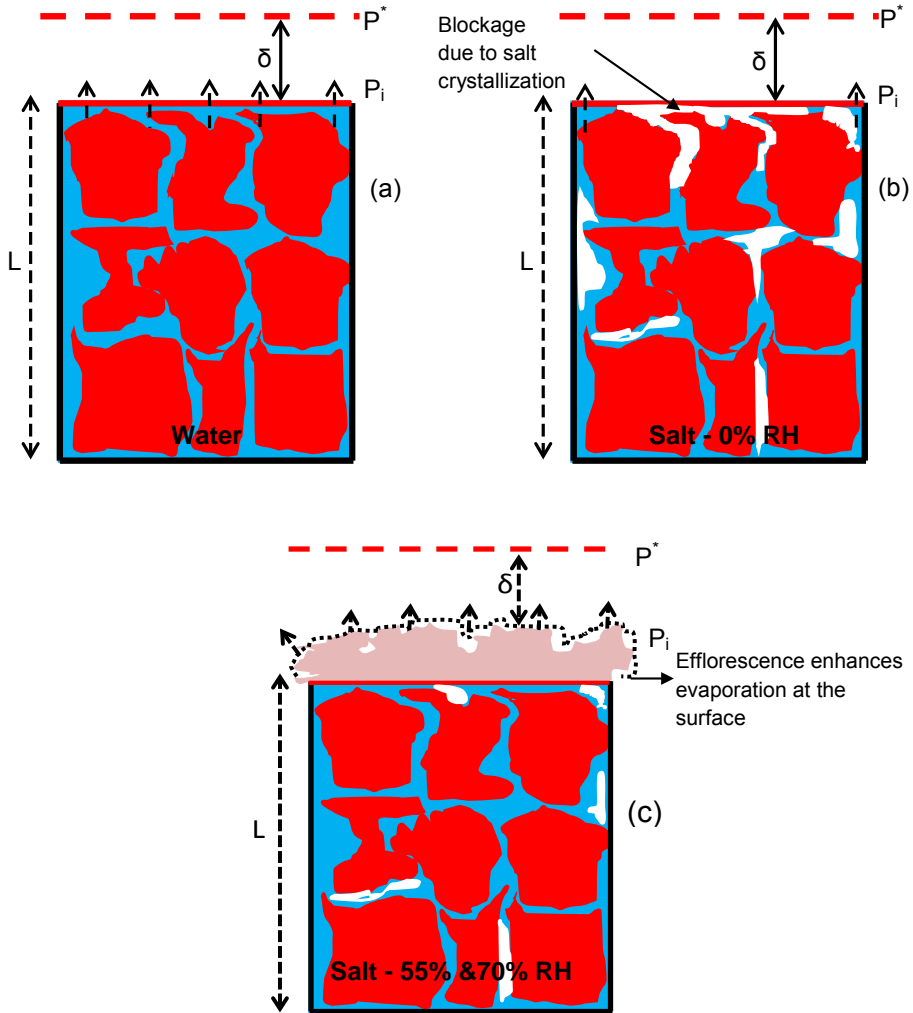
Figure 4.8: *A schematic representation of the drying process for (a) water saturated brick, (b) salt saturated brick dried at 0% RH and (c) salt saturated bricks dried at 55% and 70% RH. L is the length of sample, δ (m) is the thickness of air boundary layer through which the water vapor diffusion takes place, P_i and P* are the water vapor pressure at air/water interface at the material surface and i n the surrounding air respectively. The number of arrows at the surface is indicating the intensity of evaporative flux.*

Crystallization behavior of salt saturated fired-clay brick at different relative humidity conditions

After understanding the drying processes of salt saturated material, the concentration levels reached by NaCl solutions within porous media was determined. For this purpose the data is plotted in a so called efflorescence pathway diagram (EPD) [16]. The results are shown in fig. 4.9, where the dissolved salt content is plotted as a function of normalized average moisture content. Two extreme situations can be distinguished. In the first case, when the system dries very slowly ($Pe < 1$), diffusion dominates, resulting in a homogeneous distribution of salt ions throughout the sample. For this situation, starting from an initial concentration of 3 m , the salt solution concentration during drying will increase homogenously throughout the sample, until the saturation concentration 6.1 m is achieved. Once the saturation concentration is achieved any further drying will cause crystallization. Furthermore, the concentration will stay constant at 6.1 m. In the second case, the system dries very fast ($Pe > 1$); i.e. advection dominates and ions will be dragged along with the moisture flow towards the drying surface. As a result, the salt concentration near the drying surface increases. If there are enough nucleation sites, accumulation of ions beyond the saturation concentration will immediately result in crystallization on the surface as efflorescence. Efflorescence acts as a porous network and increases the effective surface area for evaporation, thereby causing a higher evaporation flux [62]. If the rate of crystallization (efflorescence formation) is high enough and the ratio of transported sodium and hydrogen ions remains constant, the dissolved salt ion concentration (ratio of dissolved sodium and hydrogen ions) inside the material will remain almost constant at the initial concentration, here at 3 m.

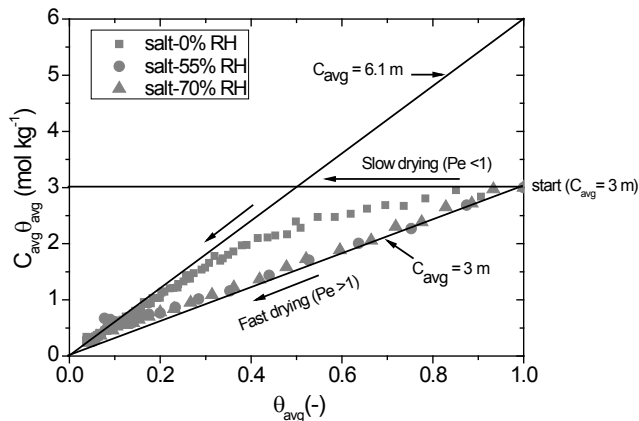***Figure 4.9:*** *Efflorescence pathway diagram for salt saturated brick dried under different RH conditions. The total amount of dissolved sodium is plotted as a function of the average moisture content (θ_{avg}) in the brick.*

For salt saturated brick dried at 0 % RH, initially a pathway in between the extreme cases ($Pe < 1$ and $Pe > 1$) is followed, indicating advection of ions towards the drying surface.

This has been confirmed by calculating the Peclet number, which at time t = 0h equals 46. Hence, the salt ions will crystallize near the drying surface, causing blockage of the pores near the drying surface. This reduces the evaporative flux and causes the drying rate to decrease. Eventually, the drying becomes so slow that diffusion of ions dominates a pathway corresponding to $Pe < 1$ is followed. The calculated value of the Peclet number at this stage equals 0.2, which confirms that diffusion is dominant. Since diffusion tries to level off the concentration gradients within the brick, back diffusion of salt ions from the surface to inside the brick will occur, leading to the formation sub-florescence. Because of this a negligible efflorescence was observed in case of salt saturated brick dried at 0% RH.

The data on salt saturated bricks dried at high humidity follow the boundary line $Pe > 1$. This indicates that advection was the governing process, and ions are transported along with the moisture towards the outer surface of brick. This salt was observed at the end of the experiment as efflorescence on the surface of the brick. Because of the formation of efflorescence the average salt concentration remained below saturation for a longer time than that inside a brick dried at 0% RH. For 55% and 70% RH the dissolved salt ion concentration remains almost constant at about the starting concentration, i.e., 3 m. However, near the end of the drying (approx. near θ_{avg} = 0.3), drying becomes slower and a pathway in between the two extreme situations is followed, which ultimately ends on the $Pe < 1$ pathway. This indicates that near the end of the drying diffusion becomes dominant. This is caused by the penetration of a receding drying front. Because of this drying becomes so slow that back diffusion of salt ions dominates. At this time approx. 30-40 % of the initially dissolved salt is still present inside the brick and cannot be transported to crystallize as efflorescence.

4.4.3 Drying behavior of salt saturated fired-clay brick with inhibitor

To explore the influence of inhibitor on the drying and crystallization behavior of NaCl at different humidity conditions, the drying experiments were performed on salt saturated bricks containing inhibitor.

Drying behavior of salt + inhibitor saturated fired-clay brick at 0% relative humidity

The drying curves for the samples saturated with salt + inhibitor solution dried at 0% RH are given fig. 4.10, where the normalized integrated hydrogen signal is plotted as a function of time. Based on our previous results [76], two concentrations of inhibitor were tested, i.e., 0.001 m and 0.01 m. For comparison, results for water and salt saturated bricks dried at 0% RH are included in fig. 4.10.

Three main observations can be made. Firstly, in the presence of inhibitor the initial drying rates of salt and salt + inhibitor saturated materials were similar. Secondly, after approx. 15 hours a dramatic decrease in the drying rate of the salt saturated material without inhibitor was observed. However, in the presence of inhibitor at this time no drop in the drying rate was seen. Thirdly, in the presence of 0.01 m inhibitor after approx. 25 hours a dramatic decrease in drying rate occurred. No such drop in flux was seen in case of 0.001 m inhibitor.
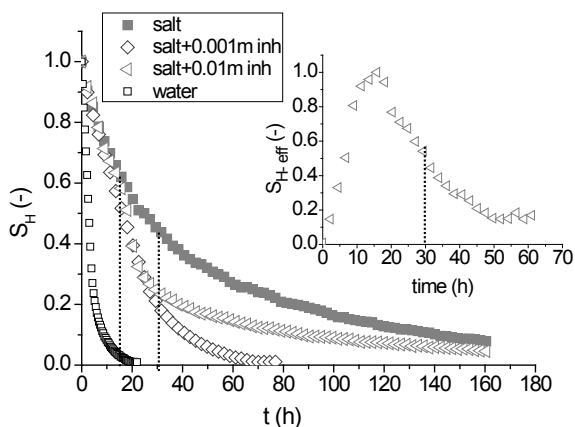
Figure 4.10: *Normalized integrated hydrogen signal (S_H) as a function of time (t) for salt loaded bricks with and without inhibitor dried at 0% relative humidity. In the inset the hydrogen signal from the efflorescence (S_{H-eff}) formed on the outer surface of the brick (in case of 0.01 m inhibitor) is plotted as a function of time.*

The initial drying behavior of the systems with and without inhibitor was the same. This is caused by the fact that with the addition of inhibitor the equilibrium relative humidity of salt solution does not change. Therefore, the humidity gradient and hence the evaporative fluxes remain the same. The rate of initial volume change of the solution in various samples is plotted in fig. 4.7. This figure shows that, at 0% RH, initially the volume change with and without inhibitor is approximately the same. Even in the presence of inhibitor the values are much lower than expected on ba sis of the humidity gradient. This is attributed to the formation of a thin layer of salt crystals near the surface of the material which has a low permeability, as was expected to be formed in case of salt saturated bricks without inhibitor (see section 4.4.2). For such a cas e, the initial drying behavior of the material with and without inhibitor should be the same. This has been confirmed by performing a droplet drying experiment (for the details of the experimental procedure see [45]). The brick powder was added (as nucleation sites) to a salt solution droplet containing inhibitor. This droplet was dried inside the NMR set-up simultaneously measuring the H and Na signal. In the presence of these external nucleation sites the onset of crystallization was observed when the salt concentration reached 6m which is the saturation concentration of NaCl, so no supersaturation occurred. This is different from the high supersaturation that has been reported [45], when a salt solution droplet containing inhibitor was dried without brick powder. This indicates that NaCl solution will not supersaturate in most practical situations.

No drop in the drying rate was seen in the presence of inhibitor in contrary to what was observed in the absence of inhibitor. In the absence of inhibitor after approx. 15 hours, the saturation concentration was achieved in the top few mm of the sample (confirmed from the measured concentration profiles (for details see [45]). This causes a dramatic drop in the drying rate for salt saturated brick. Since, most of the salt crystallized as sub-florescence, it causes a more severe blockage of the pores near the drying surface. However, in the presence

of inhibitor the crystal morphology changes from cubic to dendritic [45]. The salt solution creeps along the branches of the dendrites and transports more and more dissolved salt ions towards the drying surface causing the efflorescence observed at the end of drying experiment. Pictures of the materials with efflorescence are shown in fig. 4.11. Approx. 26% and 69% of the salt crystallized as efflorescence in the presence of 0.001 m and 0.01 m inhibitor respectively. These results are included in fig. 4.6. Because of the formation of efflorescence in the presence of inhibitor the average salt ion concentration inside the brick remained below saturation. Therefore, the system remained open and less blockage occurred compared to the salt saturated system without inhibitor. As a consequence of this no dramatic drop in drying rate was seen.
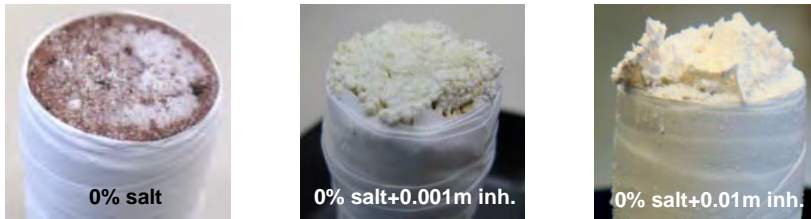

Figure 4.11: *Pictures of the efflorescence formed at the end of a drying experiment in case of salt saturated brick with and without inhibitor dried at 0% RH. The amount of efflorescence increases significantly with the addition of inhibitor.*

An extremely low drying rate was seen at later stages of drying (t >30h) in case of 0.01m inhibitor (see fig. 4.10). This is attributed to drying out of the efflorescence at the end of the drying process. In the inset of fig. 4.10, the hydrogen signal from the efflorescence formed on the outer surface of the brick (in case of 0.01 m inhibitor) is plotted as a function of time. This inset shows that initially, the hydrogen signal increases indicating the growth of the efflorescence. Note that the hydrogen signal comes from the water present in and on the efflorescence. After approx. 30 h (the time after which drying became extremely slow) the hydrogen signal from the efflorescence dropped significantly, indicating that the efflorescence was drying out. Dry efflorescence acts as a water vapor diffusion barrier, slowing down the drying process. Our results are in line with the observations made by previous authors [74]. At lower concentration of inhibitor (0.001m) no such dramatic drop in drying rate was seen. As the thickness of the efflorescence for 0.001m inhibitor is much smaller than for a high concentration of inhibitor (0.01m).
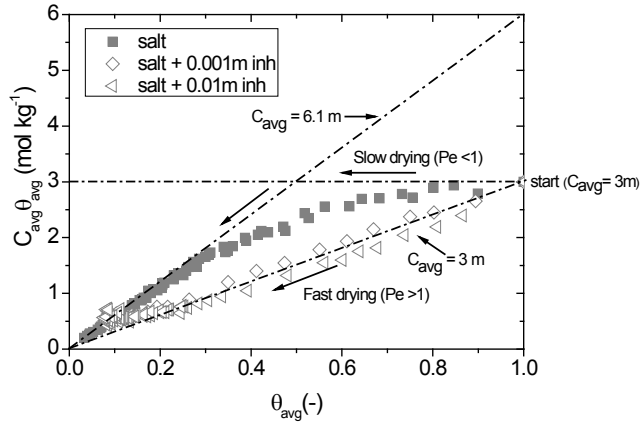
Figure 4.12: *Efflorescence pathway diagram for salt saturated brick with and without inhibitor dried at 0% RH. The total amount of dissolved sodium is plotted as a function of the average moisture content (θ_{avg}) in the brick.*

Crystallization behavior for salt + inhibitor saturated fired-clay brick dried at 0% RH

To obtain the information about the moisture/ion transport phenomena and the salt crystallization processes inside the material the data is plotted in an EPD as shown in fig. 4.12. For comparison the data from salt saturated brick without inhibitor is also plotted. The behavior of salt saturated brick without inhibitor has already been discussed in section 4.4.2. In the presence of inhibitor, initially the boundary line *Pe* > 1 is followed for both 0.001 m and 0.01 m indicating that advection is the governing process during drying. Although the initial drying rate for the materials with and without inhibitor is almost the same (see fig. 4.10), a faster decrease in sodium content is observed in the presence of inhibitor. This is attributed to the formation of efflorescence that has dendritic crystal morphology [45]. This type of morphology has the tendency to spread all over the surface and pushes more and more dissolved salt ions out of the material. In this case, advection remains the governing process during drying. However, for such a case we expect a faster initial drying rate in the presence of inhibitor, which is not observed in our experiments. This is still an open question for future research. Because of the formation of efflorescence the average salt ion concentration inside the brick remained below the solubility limit for a longer period of time. Near the end of the drying (approx. near θ_{avg} = 0.3), the drying of bricks with inhibitor becomes slower and diffusion starts to dominate. This is due to the penetration of a receding drying front that causes back diffusion of ions. At this time approx. 30% of the amount of the initially dissolved salt was still present inside the brick. This remaining salt cannot be transported to the outer surface of bricks to crystallize as efflorescence. This is the reason that we never observed more than 70% efflorescence (see fig. 4.6).

Drying behavior of salt + inhibitor saturated fired-clay brick at 55% and 70% relative humidity

In practice the humidity is much higher than 0%, so the drying behavior of salt + inhibitor saturated brick was studied at higher humidity. The results for salt + inhibitor saturated brick dried at 55% and 70% RH are shown in fig. 4.13a and 4.13b, respectively, where the normalized integrated hydrogen signal is plotted as a function of time. At a high relative humidity, no significant difference in the drying behavior of brick with and without inhibitor was seen. A comparable efflorescence was formed for both the cases with and without inhibitor.

The lower drying rate of the salt and salt + inhibitor saturated bricks compared to the water saturated brick at high humidity results from the depression of the humidity gradient. After correcting for this effect the curves coincide rather well, as similar to the case of salt saturated brick (see fig. 4.4b).

The drying behavior of the materials with and without inhibitor at high humidity was about the same. The values of the initial volume change for salt saturated material in the presence of inhibitor have been included in fig. 4.7. These values are close to the expected values of the drying rates. This is caused by the fact that at high humidity conditions for salt saturated materials the drying front is located at the surface of the material. Therefore, salt crystallizes as efflorescence. Because of the formation of efflorescence the system remains open and no prominent blockage of pores near the drying surface is expected. As the system remains open it extracts more dissolved salt ions out of the material to crystallize as efflorescence. The addition of inhibitor does not alter this situation.
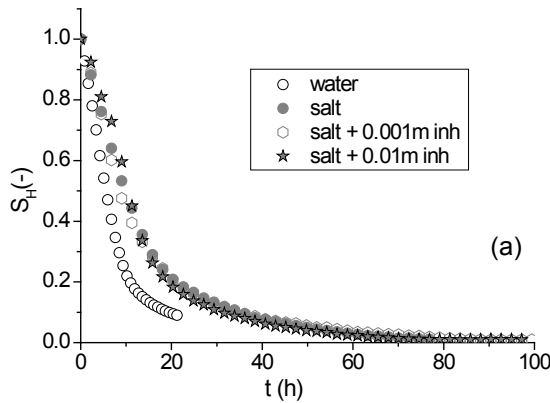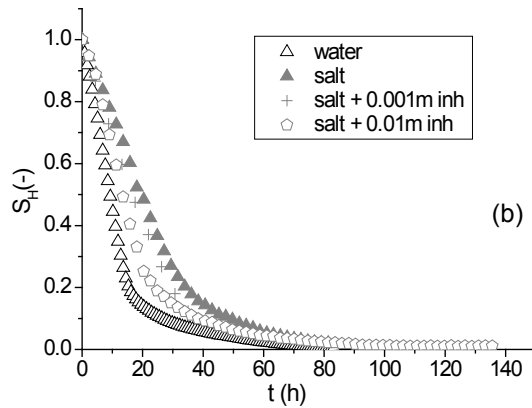
Figure 4.13: *Normalized integrated hydrogen signal (S_H) as a function of time (t) for salt loaded bricks with and without inhibitor dried at (a) 55% relative humidity and (b) 70% relative humidity.*

Since, the evaporative flux is the same for the bricks with and without inhibitor, the velocity of the salt solution should also be the same and about the same amount of efflorescence is expected for both the cases. This indeed is observed at the end of drying experiment. Fig. 4.14 shows the pictures of efflorescence for brick dried at 55% relative humidity. Approx. 48% of salt without inhibitor and 60% of salt with inhibitor crystallized as efflorescence. As can be seen in fig. 4.7, at 70% RH, approx. 40% of salt without inhibitor and 60% of salt with inhibitor crystallized as efflorescence (see fig. 4.6).

Figure 4.14: *Pictures of the efflorescence formed at the end of drying experiment in case of salt saturated brick with and without inhibitor dried at 55% RH. A comparable amount of efflorescence was formed in both cases, i.e., with and without inhibitor.*

Crystallization behavior for salt + inhibitor saturated fired-clay brick dried at 55% and 70% RH

To understand the salt crystallization processes inside the materials at higher humidity the data is plotted in an EPD. The results are shown in fig. 4.15a and 4.15b for salt saturated bricks with and without inhibitor dried at 55% and 70% RH respectively.

The behavior of salt saturated brick without inhibitor has already been discussed in section 4.4.2. For the materials with inhibitor, advection remained the governing process throughout the drying process. In the presence of inhibitor the sodium content was decreasing at the same rate as without inhibitor, and therefore salt crystallization was delayed for the same amount of time. Addition of inhibitor causes no de lay in attaining the saturation concentration inside the brick. Towards the end of the drying process (approx. near θ_{avg} = 0.3), diffusion started to be dominant because of the penetration of a receding drying front. Therefore, after this time no more salt can be transported towards the outer surface of brick to crystallize as efflorescence.
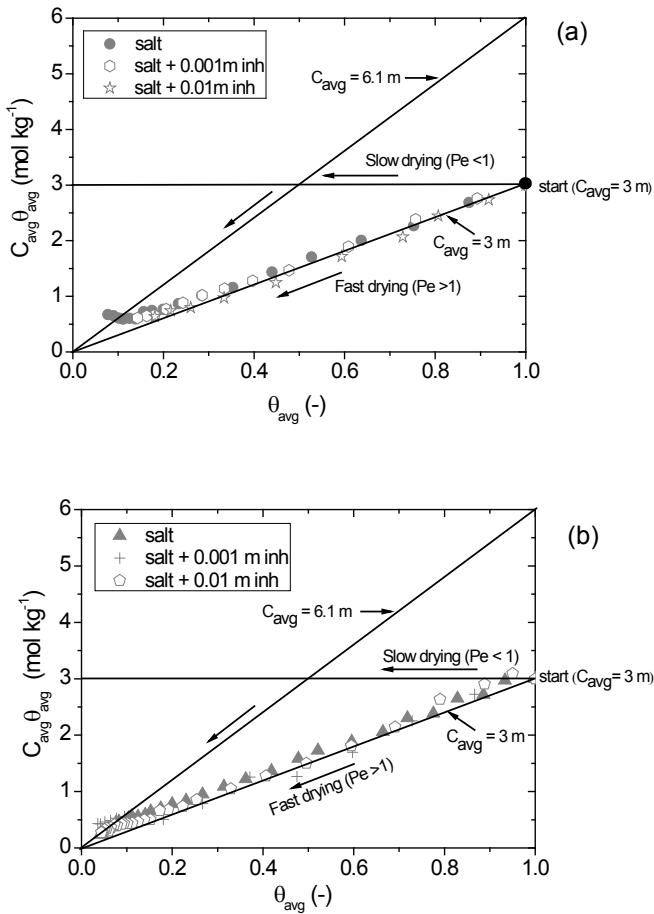

Figure 4.15: *Efflorescence pathway diagram for salt saturated brick with and without inhibitor dried at (a) 55% RH and (b) 70% RH. The total amount of dissolved sodium ($C_{avg}\theta_{avg}$) is plotted as a function of the average moisture content (θ_{avg}) in the brick.*

4.5 Conclusions

Drying of a salt loaded fired-clay brick is faster at high humidity than at low humidity. This is caused by the fact that at low humidity, advection is so dominant in the initial stage of drying process and that ions quickly crystallize and block the surface. At a later stage of the drying, back diffusion of ions dominates which levels off the salt ion concentration inside the brick. This causes the salt to crystallize inside the brick as sub-florescence. At high humidity, salt crystallizes outside the material as efflorescence. This prevents blockage of the pores, thereby keeping the system open to transport more and more salt outside the material. Advection remains the governing process for ion transport and no drop in the drying rate is seen. Addition of inhibitor was found to be useful at low humidity conditions. At low humidity, due to the crystal morphology in the presence of inhibitor salt crystallizes as non-destructive efflorescence. This prevents a severe blockage as was seen for salt loaded material at low humidity.

At high humidity conditions addition of inhibitor to the salt loaded bricks had no significant effect on the drying behavior, the amount of efflorescence formed, the moisture and ion transport and the salt concentration levels attained inside the brick. This is caused by the fact that because of the slow dying at high humidity, the salt ions crystallize outside the material as non-destructive efflorescence. Consequently, the system remains open and the addition of inhibitor has no effect.

This study helps to understand that the success of adding an inhibitor strongly depends on the local climate. The effect of inhibitor on the sheltered areas of a monument would be different from that on the areas exposed to sun and wind. Before using inhibitor in practice these aspects should be considered carefully.

Chapter 5

Effect of spraying ferrocyanide ions on NaCl contaminated samples

Abstract

Salt weathering leads to destruction of many valuable cultural heritage monuments. To reduce the impact of destruction, effective treatment methods are required. The use of crystallisation inhibitors to mitigate salt damage has been proposed in the past, however to date the effectiveness and safety of their application on cultural heritage objects has not been proven. Therefore, a detailed experimental study is performed to see the effect of spraying potassium hexa-cyanoferrate (II) tri-hydrate inhibitor on NaCl contaminated samples. We focus on the concentration levels reached by NaCl solutions within porous media during drying, and the associated water and ion transport processes taking place.

Two types of drying experiments were performed (1) droplet drying experiments, and, (2) salt contaminated brick drying experiments. For droplet drying experiments the salt solution droplets with and without inhibitor were dried. In brick drying experiments salt contaminated materials were sprayed with inhibitor solution and dried afterwards. From droplet drying experiments it is shown that in the presence of inhibitor higher supersaturation is achieved and supersaturation increases with increase in inhibitor concentration. Also, a change in crystal morphology from cubic to dendritic crystals is seen. Dendritic crystals occupy much larger surface area compared to cubic crystals. The spreading effect increases with increase in inhibitor concentration. From the brick drying experiments it is shown that in the presence of inhibitor, due to the dendritic crystal morphology, advection becomes the governing phenomenon for ion transport. It results in the transport of the salt ions to the outer surface of the brick, where it crystallises in the form of non-destructive efflorescence. No higher supersaturation is observed within the materials sprayed with inhibitor solution. These results show that ferrocyanide ions could potentially be affective against NaCl damage.

5.1 Introduction

Soluble salts such as chlorides, sulphates and nitrates are widely recognized as a cause of destruction in porous building materials, mainly due to crystallization inside the porous matrix. The growth of salt crystals exerts pressure on the pore walls, which can exceed the tensile strength of the material thus leading to damage [3]. Among various salts present inside the porous material sodium chloride (NaCl) is one of the most damaging salt. The source of salt can be ground water, flooding, rain and also chemical composition of the material itself. It is well known that the deterioration occurs only if the salt crystals deposits within the pores of the material often known as sub-florescence. This happens when migration of the salt solution to the surface is slower than the evaporation of the solution from the surface. On the other hand, when salt crystallizes on the external surface of the material it is known as efflorescence. Efflorescence is unsightly but in most cases not harmful for the materials. Different methods have been tested in the past to control salt damage but with varying degree of success. Recently, the use of crystallization inhibitors has been proposed as a potential preventive treatment method. For bulk solutions, increased supersaturation levels in the presence of inhibitor have been reported in the past [43]. However, to our knowledge, to date no study has been published regarding the effect of these compounds on the concentration of NaCl solutions inside a porous media. This indeed is a very important aspect for salt damage. As it is known that the process behind the damage due to salt crystallization is the growth of salt crystals in confined spaces (e.g. pores), hence exerting crystallization pressure on the pore walls. Thermodynamically, the crystallization pressure can be related to supersaturation (C/C_o) as given by following equation [14]:

$$P_C = \frac{vRT}{V_m} ln \frac{C}{C_O}$$

(5.1)

Where P_c is the crystallization pressure, v is the total number of ions released upon dissociation of the salt (e.g. for NaCl = 2), R is the universal gas constant, T is the absolute temperature, V_m is the molar volume of the salt crystal, C and C_o are increasing concentration in vicinity of crystal and saturation concentration of salt respectively. Before using inhibitors to treat historic objects detailed experimental studies are required to assess the effectiveness and safety of their application. In the past, a detailed study was performed to test the effectiveness of ferrocyanide ions as inhibitor against NaCl damage [45]. For this study, the sample materials were initially saturated with salt and inhibitor solution. However, in practice for the monuments already contaminated with salt the only way to test the effectiveness of inhibitors is by spraying inhibitor solution on the contaminated walls. Therefore, in this work a systematic study has been undertaken to see the effect of spraying hexa-cyanoferrate (II) ions as inhibitor on the salt contaminated walls. We focused on the concentration levels reached by NaCl solutions within porous media during drying and the associated water and ion transport processes taking place. This behavior is not completely understood, because it is not easy to measure non-destructively the concentration of ions inside a porous material during dynamic experiments. However, with the help of a specially designed Nuclear

Magnetic Resonance set-up [51], we were able to non-destructively measure both hydrogen and sodium ions simultaneously during drying experiments.

5.2 Nuclear Magnetic Resonance (NMR)

In this study Nuclear Magnetic Resonance (NMR) is used for carrying out non-destructive, quantitative and simultaneous measurement of both hydrogen and sodium ion content in a sample. NMR is based on the principle that in a magnetic field, nuclei have a specific resonance frequency and can be excited by a radio frequency field. The resonance frequency f (Hz) depends linearly on the magnitude of the magnetic field:

$$f = \frac{\gamma}{2\pi} B_O \qquad (5.2)$$

Where $\gamma/2\pi$ (HzT^{-1}) is the gyromagnetic ratio, B_0 (T) is the main magnetic field. For ^{1}H $\gamma/2\pi$ is 42.58 MHzT^{-1} and ^{23}Na is 11.26 MHzT^{-1}. Therefore, by using a specific frequency the method can be made sensitive to a particular type of nucleus, in this case either hydrogen or sodium. The signal intensity S of a spin echo as used in the experiment is given by:

$$S = k\rho \left[1 - exp\left(-\frac{T_r}{T_1} \right) exp\left(-\frac{T_e}{T_2} \right) \right] \qquad (5.3)$$

Where S is signal intensity, k is the sensitivity of the nuclei relative to hydrogen, ρ is the density of the nuclei, T_r and T_1 are the repetition time of the pulse sequence and spin-lattice relaxation time, T_e and T_2 are the spin echo time and spin-spin relaxation time. To measure the maximum signal, i.e. from all pore sizes, T_e should be as short as possible as T_1 and T_2 are proportional to the pore size. As the sensitivity of ^{23}Na nuclei is low relative to hydrogen ($k_H = 1$, $k_{Na} = 0.1$), 256 averages of the spin echo measurements are taken for Na nuclei relative to eight averages of hydrogen thereby giving the possibility to obtain sufficient signal to noise ratio. Since the relaxation time for Na in NaCl crystals is of order of 10 μs [73] only dissolved Na ions are measured using the NMR set-up. For the presented experiments, a home-built NMR scanner with a static magnetic field of 0.78 T and gradient up to 0.3 T/m is used. To perform quantitative measurements a Faraday shield is placed between the coil and the sample [51].

5.3 Droplet drying experiments

In the beginning, a series of droplet drying experiments was performed to observe the crystallization behavior of NaCl salt solution droplets with and without crystallization inhibitor. The aim behind this study was to see the influence of increasing inhibitor concentration on NaCl supersaturation, crystal morphology and also to find out the optimum inhibitor concentration for spray drying experiments.

5.3.1 Experimental set-up

A schematic of the setup is shown in fig. 5.1. A quartz sample holder with inner diameter of 16 mm was used. Droplets of 300 µl salt solution (3 m NaCl) with and without inhibitor were dried using 0 % relative humidity and about 1 l min^{-1} air flow rate.
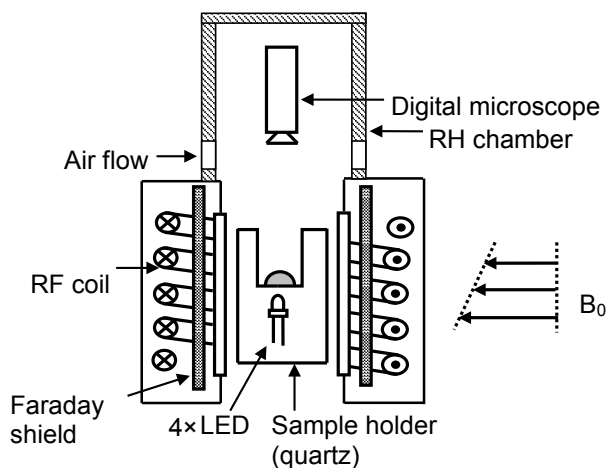

Figure 5.1: *A schematic diagram of the NMR set-up used for droplet drying experiments.*

The effect of increased inhibitor concentration on the nucleation and crystal morphology of NaCl was studied. Time lapse microscopy of the crystallization was performed using a dino-lite digital microscope. Four LED's were placed below the substrate as a lighting source for imaging within the NMR setup. The capture of photomicrograph images along with the NMR measurements gives the possibility to visualize the drying of the droplet while simultaneously obtaining information about NaCl concentration within the droplets. NMR is used to measure hydrogen (H) and sodium (Na) and from their ratio (Na/H) the concentration of dissolved sodium ions in the droplet is calculated. As we are doing simultaneous time lapse microscopy, we can see exactly at what concentration the salt crystal appears. Thus, we can relate the onset of crystallization with the Na concentration in a droplet. The supersaturation is calculated as C/C_o where C and C_o are increasing concentration in vicinity of crystal and saturation concentration (6.1 mol/kg of water) of NaCl respectively.

5.3.2 Results

Initially, we started with drying of a salt solution droplet with and without inhibitor. For salt solution droplet without inhibitor the onset of crystallization was seen at a concentration of 6.2 ± 0.5 m giving a supersaturation of 1.06 ± 0.04 (see fig. 5.2). In the presence of inhibitor, the crystallization was seen at a concentration higher than the saturation concentration of NaCl and thus the droplet supersaturates. The results are shown in fig. 5.2, where the supersaturation is plotted as a function of inhibitor concentration.
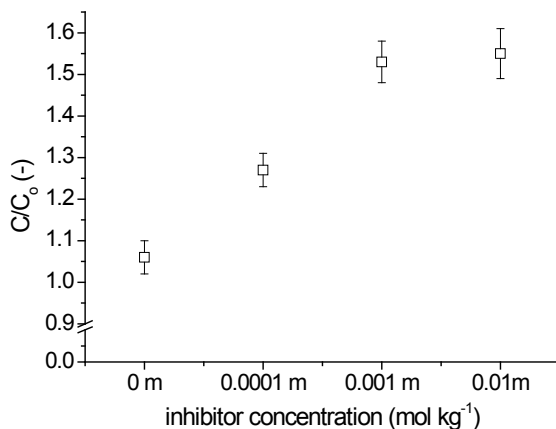
Figure 5.2: *The figure shows the supersaturation plotted as a function of inhibitor concentration.*

As can be seen in fig. 5.2, supersaturation increases with increase in inhibitor concentration. We found a maximum supersaturation up to 1.55 m in the presence of 0.01 m inhibitor. In addition, due to the presence of inhibitor NaCl crystal morphology changes from cubic crystal morphology to dendritic crystal morphology. The pictures showing NaCl crystal morphology at the end of drying experiment are shown in fig. 5.3. In case of drying of a NaCl solution droplet without inhibitor, cubic crystals were seen growing at the liquid/air interface. Whereas, in the presence of inhibitor dendritic crystals first forms at the liquid/air interface. These crystals then spread very rapidly all over the substrate. Spreading of the crystals was more at higher inhibitor concentration. The branches of dendritic crystals provide a pathway for spreading of solution to much larger surface area. This phenomenon is commonly known as 'salt creep' (see also fig. 5.3). Due to the enlarged surface area for evaporation at higher inhibitor concentration a similar increase in the drying rate was observed. So, at higher inhibitor concentration faster drying was seen.
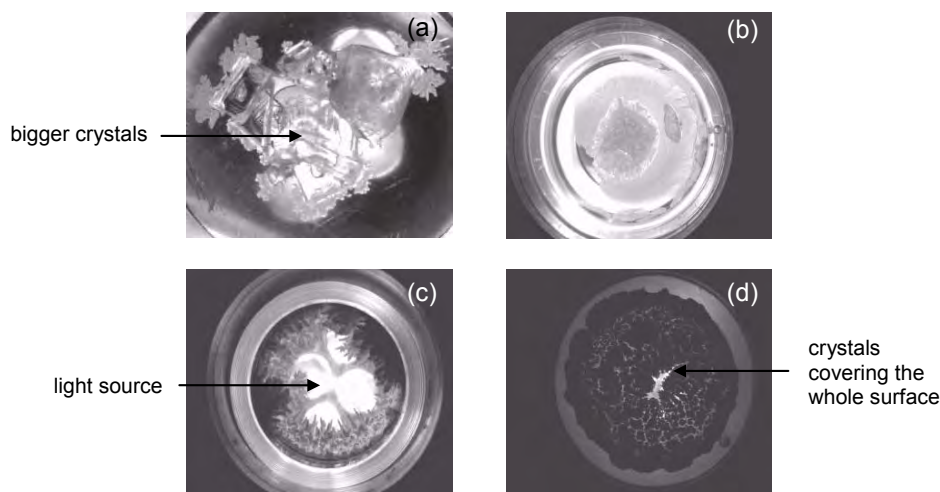
Figure 5.3: *Images showing the crystal morphology at the end of droplet drying experiment (a) with no inhibitor (b) 0.0001 m inhibitor (c) 0.001 m inhibitor (d) 0.01 m inhibitor. These images are captured using dino-lite digital microscope. At higher inhibitor concentration more spreading of the crystals were seen.*

5.4 Brick drying experiment

5.4.1 Material

The materials used in this study were fired-clay brick and Granada limestone. The red fired-clay brick is of a type typically used for construction in the Netherlands, and had an average porosity (as measured by water immersion method) of 0.32 $m^3 m^{-3}$, and a pore size distribution ranging from 1-10 µm (accounting for ~ 80 per cent of the total pore space), as determined by Mercury Intrusion Porosimetry (MIP). The Granada limestone is a buff colored stone commonly used as a building material in Granada, Spain. In this stone calcite is the main component (90 wt%), together with lesser amounts of SiO_2 and Al_2O_3. This material has an average porosity (as measured by water immersion method) of 0.29 $m^3 m^{-3}$, and a bimodal pore size distribution with pores ranging from 0.3-1 µm (40 per cent) and 1-100 µm (60 per cent) as determined by MIP. In this study potassium hexa-cyanoferrate (II) tri-hydrate $K_4[Fe(CN)_6]\cdot 3H_2O$ was tested as a crystallization inhibitor.

5.4.2 Experimental set-up

A schematic diagram of the brick drying experiments is given in fig. 5.4. The cylindrical samples 20 mm in diameter and 40 mm in length were vacuum saturated with salt solution (3 m NaCl). In order to have homogenous distribution of the salt crystals inside the samples, the saturated samples were freeze dried for approx. 10 days. For freeze drying, the samples were initially immersed in liquid nitrogen at temperature -196 ^{o}C. This causes

immediate freezing of the salt solution inside the material. After that the frozen samples were placed in an ultra-high vacuum at 10^{-2} mb for about 8-10 days. This causes direct sublimation of the solid water to water vapor thus leaving behind the salt crystals at their initial place. The sample weight was monitored after every 24 h. After about 7-8 days the sample attains constant weight indicating complete absence of water. In this way salt contaminated samples were prepared. Afterwards, the contaminated samples were sprayed with inhibitor solution prepared in water. For spraying 0.01 m inhibitor solution was used.
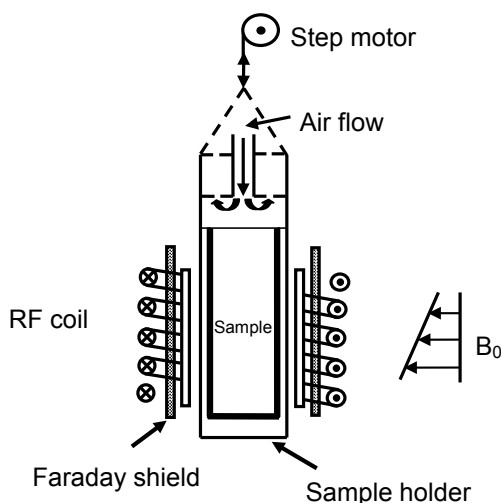

Figure 5.4: *A schematic diagram of the NMR set-up used for spray drying experiments.*

This is due to the fact that maximum effect of inhibitor on supersaturation and crystal morphology was seen at this concentration. To avoid evaporation of water after spraying the samples were covered in an aluminum foil and were placed inside a sealed polythene bag for about 4 h. The procedure of spraying inhibitor and covering the contaminated sample was repeated for about 2 days. The aim behind doing so was to give sufficient time to inhibitor to penetrate inside the material through diffusion. First order approximation about the timescales of diffusion was made using $x = \sqrt{2Dt}$, where x (m) is the length, D (m^2 s^{-1}) is the diffusion coefficient of the salt ions and t (s) is the time. After that the prepared samples were sealed using Teflon tape from all sides except from the top surface and placed inside the NMR sample chamber. Samples were exposed to dry air with a flow 1 l min^{-1} and 0 % relative humidity, thereby creating one-dimensional drying experiment. The sample position was moved in the vertical direction using a step motor to allow measurement of the H and Na content throughout the sample length. Measuring one drying profile takes about 3 hours, while the complete drying experiment takes in the order of a few days depending on the composition of the salt solution. Therefore, small variations in the moisture and ion profiles during a single scan can be neglected. After each drying experiment was completed the efflorescence formed on the top of the sample was collected and weighed.

5.4.3 Results

In the previous section we have shown that the presence of inhibitor significantly increases the supersaturation within the salt solution droplets. As explained earlier higher supersaturation can cause higher crystallization pressure and hence the risk of damage is then greater. Therefore, to ascertain the effects of inhibitor on NaCl ion transport and crystallization behavior within porous media, a series of one dimensional drying experiment were performed. In the past a detailed study was performed where ferrocyanide ions were tested as an inhibitor against NaCl damage. For this study the materials were initially saturated with salt and inhibitor solution. The results show that in the presence of inhibitor most of the salt crystallizes as non-destructive efflorescence [45]. However, in practice for the materials that are already contaminated with salt the only way to test inhibitor is by spraying inhibitor solution on the contaminated walls. So, laboratory experiments were performed to simulate practical situation. The measured moisture profiles and the calculated concentration profiles for fired-clay brick are given in fig. 5.5a and 5.5b and for Granada limestone are given in fig. 5.5c and fig. 5.5d respectively. The recurrent irregularities in the profiles are the result of inhomogenities of the sample. For both materials, two drying stages can be observed i.e. externally limited and internally limited shown by a vertical and a horizontal arrow in fig. 5.5a and 5.5c.
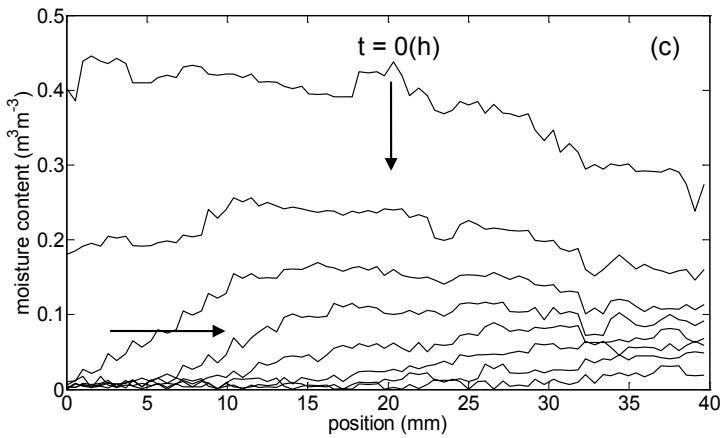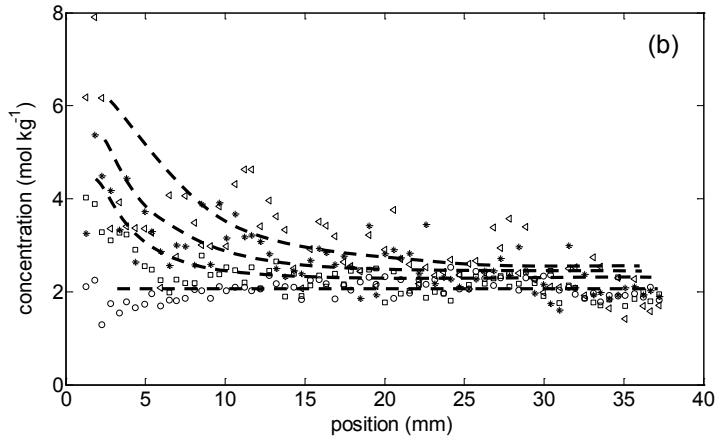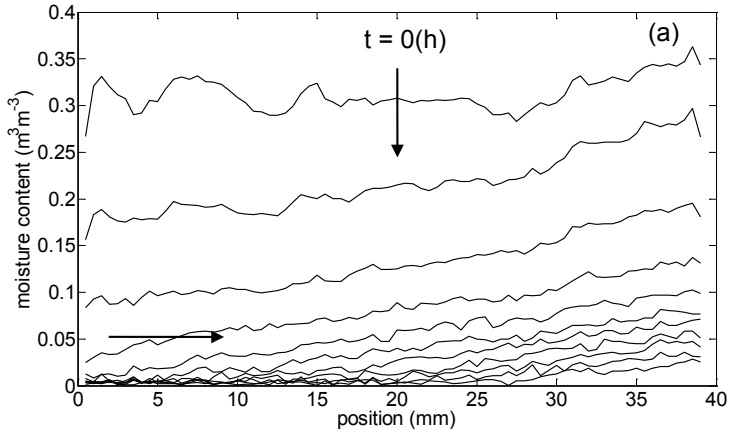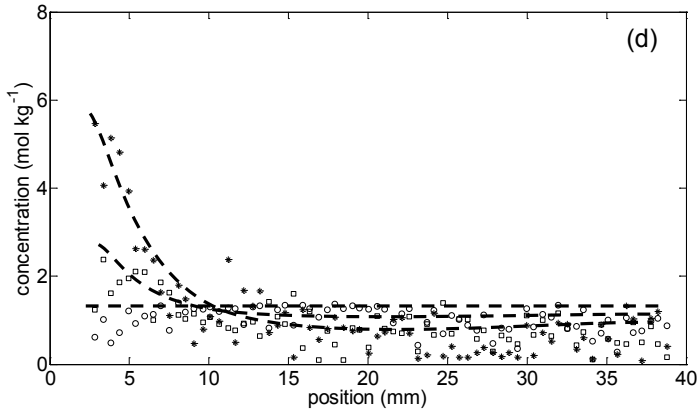
Figure 5.5: *(a) The measured moisture profiles (b) the corresponding concentration profiles for fired-clay brick and (c) the measured moisture profiles (d) the corresponding concentration profiles for Granada limestone plotted as a function of position during drying. The samples were intially contaminated with salt and then sprayed with 0.01 m ihibitor solution and dried using dry air with flow 1 l min⁻¹ and 0% relative humidity. The profiles are given for every 3 h. The drying surface is at 0 mm. The dotted lines in the concentration profiles are guide to the eye.*

The first 2-3 profiles in both the samples are almost flat representing the first drying stage. During this stage there is continuous capillary flow of water to the surface and drying is limited by external conditions such as relative humidity and air flow. Afterwards, the drying front starts to recede below the sample surface, and the moisture profiles are no longer flat. This represents the second drying stage where the continuous capillary network of water breaks up to form liquid islands. During this stage drying occurs by vapor diffusion through the porous medium, in response to the relative humidity gradient between the vicinity of the liquid island and the drying surface [23]. The transition point between these two drying stages can be identified as critical moisture content. Critical moisture content was observed to be near 0.08 m^3m^{-3} in both the samples. In fig. 5.5b the initial concentration of NaCl is 2 m, whereas the sample material was initially vacuum saturated with 3 m NaCl solution. The lower concentration of salt is due to the fact that after freeze drying the sample was sprayed with inhibitor solution. It was not possible to reach the same saturation level as was done initially by vacuum saturation. Due to this all the crystallized salt inside the material was not dissolved and thus the concentration of NaCl was lesser than the initial concentration of 3 m. During drying an increase in salt solution concentration is seen near the drying surface (see fig. 5.5b and fig. 5.5d). This is due to the advection of salt ions along with the moisture towards the drying surface. This is confirmed by calculating the Peclet number. The Peclet number is dimensionless number that shows the competition between diffusion and advection and is given as [24]:

$$Pe = \frac{|U|L}{D} \tag{5.4}$$

Where U (m s^{-1}) is the fluid velocity, L (m) is the length of the sample and D (m^2 s^{-1}) is the diffusion coefficient of salt ions in porous materials and taken equal to 1.3×10^{-9} m^2 s^{-1} [62]. Using measured moisture profiles the fluid velocity is calculated [26]. For $Pe < 1$, diffusion dominates and for $Pe > 1$, advection dominates. The calculated value of $Pe \sim 5$ in both the cases confirms that advection is the dominant phenomenon and causes salt crystallisation near the drying surface. Due to dendritic crystal morphology in the presence of inhibitor, the effective surface area for evaporation increases [62]. The salt solution creeps along the branches of the dendrites and transports more and more dissolved salt ions towards the drying surface which was seen as efflorescence by the end of drying experiment. This efflorescence was collected and weighed. The efflorescence formed in the spray experiments is compared with the efflorescence formed in the saturation experiment (in saturation experiments the samples were vacuum saturated with salt and inhibitor solution [45]. The results are shown in fig. 5.6 where the efflorescence formed is plotted as a function of inhibitor concentration. As shown in fig. 5.6 the amount of efflorescence formed increases with increasing inhibitor concentration. This is due to more pronounced spreading of dendritic salt crystals at high inhibitor concentration. However, no supersaturation was seen within salt contaminated materials sprayed with inhibitors.
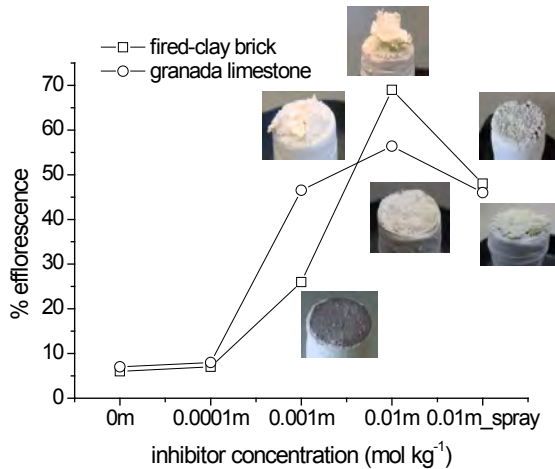

Figure 5.6: *Figure shows the efflorescence formed at the end of drying plotted as a function of inhibitor concentration. With increasing inhibitor concentration the amount of salt crystallized as efflorescence also increases. Significant efflorescence is seen in spray drying experiments.*

From the results it is concluded that spraying of inhibitor on salt contaminated materials helps to remove the salt as non-destructive efflorescence. However, it should be kept in mind that it is very important to give time to the inhibitor molecules to diffuse inside the material. In our case we did so by covering the material after spraying with inhibitor. This helped the inhibitor to diffuse inside the material and causes the crystallisation of salt as efflorescence. In a previous study done by [69] this effect was not taken into account. This might be the reason that they did not observe much efflorescence in their experiments [69].

Regarding the action of inhibitor we concluded that the presence of inhibitor changes the drying conditions near the material/air interface due to the change in crystal morphology. The immediate crystallization near the drying surface provides a sink for the salt ions and as a result most of the salt crystallizes as non-destructive efflorescence.

5.5 Conclusions

From the droplet drying experiments it is concluded that in the presence of inhibitor higher supersaturation is attained. The supersaturation increases with increase in inhibitor concentration. NaCl crystal morphology changes from cubic to dendritic crystals. The branches of dendrite crystals provide much larger surface area for evaporation of the water and consequently make the drying process faster.

From the spray drying experiments it is concluded that it is important to give sufficient time to the inhibitor molecules to diffuse inside the contaminated material. In the presence of inhibitor the drying conditions changes near the material/air interface due to changes in crystal morphology. Dendrite crystals provide much larger surface area for evaporation and advection becomes the governing phenomenon throughout the drying process. Advection of dissolved salt ions causes crystallization of salt near the drying surface as non-destructive efflorescence. This indicates that application of ferrocyanide ions on NaCl contaminated walls could potentially be affective against damage in building materials. However, at the same time it must be kept in mind that in practice there is not only the single salt present in the building materials but indeed mixture of salt is present. Therefore it is important to explore the effect of inhibitor on the mixture of salt. This will be studied in future work.

Chapter 6

The effect of ferrocyanide ions on sodium chloride crystallization in salt mixtures

Abstract

The use of crystallization inhibitors has been proposed as a potential preventive treatment method against damage and is extensively tested for crystallization of single salts. However, in practice always mixtures of salts are present. Therefore, before using inhibitors in practice there is a strong need to explore their effect on salt mixtures. In this research, we studied the effect of ferrocyanide ions on NaCl crystallization in single salt and in salt mixtures of NaCl - KCl and NaCl - LiCl.

A series of micro droplet drying experiments were undertaken. Time lapse microscopy of the crystallization was performed along with NMR measurements of hydrogen, sodium and lithium ions. This gives the possibility to visualize the drying of the droplet while simultaneously obtaining information of both the NaCl and LiCl concentration in the droplet. For a NaCl solution droplet, in the presence of inhibitor, a significantly higher supersaturation prior to the onset of crystallization and a change in crystal morphology were observed. On the other hand, for the salt mixtures NaCl - KCl and NaCl - LiCl, the NaCl supersaturation was much lower in the presence of inhibitor than for the single salt. However, a significant change in the crystal morphology was seen in the presence of inhibitor for these salt mixtures.

6.1 Introduction

Deterioration of porous building materials such as stone, brick and concrete due to in pore salt crystallization has been identified as a major cause of damage to these materials since several decades [3, 8]. The main cationic agents detected inside these materials are sodium, potassium, calcium and magnesium. Their main anionic counterparts are sulphate, nitrate and chloride. One of the most widely accepted damage mechanisms is the existence of supersaturation in the pores of the building material during crystallization. Thermodynamically, the crystallization pressure can be related to the supersaturation (C/C_o) as [14]:

$$P_c = \frac{vRT}{V_m} ln\left(\frac{C}{C_O}\right) \tag{6.1}$$

where P_c is the crystallization pressure, v is the total number of ions released upon dissociation of the salt (e.g. for NaCl = 2), R is the universal gas constant, T is the absolute temperature, V_m is the molar volume of the salt crystal, C and C_o are the actual and the saturation concentration of the salt, respectively. Consequently, at a higher supersaturation a higher crystallization pressure will be generated.

In order to stop/reduce salt damage, preventive methods are required. In the past, intensive research has been carried out to test various preventive/treatment methods against salt damage [25-27, 45]. However, all these tests have been performed on single salts, which are rarely found in practice, where always salt mixtures are present. The crystallization behavior of mixed salt systems is much more complicated than that of pure single salts. For instance, the crystallization of one salt from a mixture does not occur at a specific value of the relative humidity but rather across a range of values [49, 46]. The crystallization of salt mixtures occurs at lower humidities than expected in case of pure single salts [46]. The rate of deliquescence and crystallization of single salts is also affected by the presence of another salt [47]. In the presence of additional salt, an increase of the rate of moisture uptake (deliquescence) and a decrease of the rate of moisture loss (crystallization) have been reported. This is caused by the reduction of the solution vapor pressure in the presence of additional salts [47]. For a salt mixture, where the salts have one ion in common, the saturation concentration of the salts in the mixture is lower than the saturation concentration of the salts individually. For example, in case of a mixture of NaCl - KCl, having Cl ions in common, the saturation concentration of NaCl is less than 6.14 m [77].

The ternary phase diagram of NaCl-KCl-H$_2$O at 25 ^{o}C is given in Fig. 6.1, where the KCl concentration (m) is given as a function of the NaCl concentration (m) [78]. For this mixture the saturation concentration of NaCl depends on the concentration of KCl and is less than 6.14 m. The equilibrium solubility line is indicated by a solid red line. Below this line a liquid phase exists, i.e., salt solution where salt ions are dissolved in water, and above this line both solid salt and salt solution, i.e., NaCl/KCl crystals and salt solution exist. Depending on the initial molar concentrations either KCl or NaCl will crystallize first.
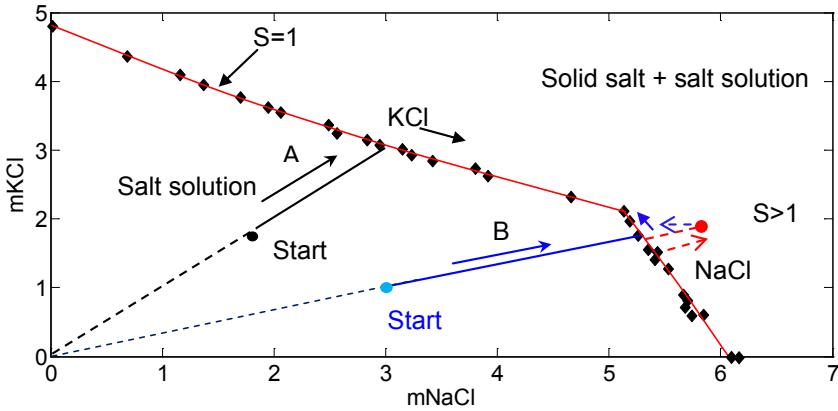
Figure 6.1: *The ternary phase diagram of NaCl-KCl-H$_2$O at 25°C. During evaporation the paths A and B (shown by solid black and blue lines) will be followed for the salt mixture of composition 2m NaCl - 2m KCl and 3m NaCl - 1m KCl, respectively. If no crystal appears at the intersection of path B and the equilibrium line (S = 1), the concentration will keep on increasing (supersaturation), as indicated by the dotted red arrow. After the onset of crystallization the system will return to the equilibrium line, as shown by the dotted blue arrow.*

For example, for a solution of composition 2m NaCl - 2m KCl, upon evaporation the concentration of both NaCl and KCl will increase equally until the solubility line is reached. The path followed is shown by the solid black line A in Fig. 6.1. Upon reaching the equilibrium line KCl will start to crystallize out and the amount of dissolved KCl in the solution decreases. As evaporation proceeds, the NaCl concentration in the solution increases and the KCl concentration will continue to decrease. The NaCl concentration increases up to a maximum concentration of 5.1 m. Any further drying will cause crystallization of both NaCl and KCl and the concentration will stay constant at this point. In case of 3m NaCl - 1m KCl, upon evaporation the concentration of the salt mixture will increase, following a path shown by the solid blue line B. Upon touching the equilibrium line, NaCl will crystallize out at a concentration of 5.3 m. If, upon touching this line, NaCl crystals do not appear and the concentration of the salt mixture keeps rising beyond the equilibrium line (shown by the dotted red line), the solution of the salt mixture is supersaturated. Supersaturation promotes nucleation and growth of crystals. After crystallization the concentration of the supersaturated mixture will return to the equilibrium line (shown by the dotted blue arrow). Next, the equilibrium line will be followed (shown by solid blue arrow). Upon reaching a NaCl concentration of 5.1 m, further drying will cause crystallization of both NaCl and KCl. Note that in the presence of KCl the saturation concentration of NaCl is less than 6.14 m because of the common ion effect mentioned before.

In the past, a few studies have been carried out to understand the crystallization behavior of salt mixtures [50, 79]. Linnow et al. [49] have reported a study in which the complexity of the kinetic and thermodynamic properties of the salt mixtures is considered.

The authors investigated the crystallization sequence of complex salt mixtures using Raman microscopy and polarization microscopy. This work has been extended by Hilde de Clerq et al [50], who studied the crystallization behavior of this mixture in porous limestones. The drying behavior of two types of limestones loaded with equimolar mixtures of Na_2SO_4-$NaNO_3$ and Na_2SO_4-K_2SO_4 was studied. They concluded that the properties of the materials have a larger effect on the crystallization pattern of Na_2SO_4-$NaNO_3$ than on that of Na_2SO_4-K_2SO_4.

Although the study of the drying and crystallization behavior of salt mixtures is an ongoing research, until now, no studies have been reported where preventive methods are explored for salt mixtures. Recently, the use of crystallization inhibitors has been proposed as a potential preventive treatment method. These inhibitors are known to act either by preventing or by delaying the onset of nucleation [28] and hence crystallization. or by changing the crystal growth mechanism by adsorbing onto specific crystal faces [29]. Ferrocyanide is one of the most researched crystallization inhibitors against NaCl damage. Its effect on NaCl crystallization and drying behavior in bulk and in porous materials has been studied. For bulk solutions an increase in NaCl supersaturation has been reported in the presence of ferrocyanide ions [43, 45]. If such a supersaturation can be sustained inside a porous material it can be dangerous for this material. However, recently it has been shown that no high supersaturation is generated inside building materials in the presence of ferrocyanide ions [45]. Additionally, ferrocyanide ions promote the formation of non-destructive efflorescence on building materials [43, 45]. However, all these tests were performed on single salts. To the best of our knowledge, no studies have been reported so far where the influence of ferrocyanide ions on salt mixture has been studied. The reason is the difficulty to measure different types of ions together during in-situ measurements. However, with the help of a specially designed NMR set-up, we are able to measure H, Na and Li ions simultaneously during dynamic drying experiments. The concentration of dissolved salt ions can be calculated from the ratio of the Na/H content and the Li/H content. In this work, we focused on the effect of ferrocyanide ions on the drying and crystallization behavior of NaCl in the salt mixtures NaCl - KCl and NaCl - LiCl.

6.2 Experimental

In this study, a specially designed Nuclear Magnetic Resonance (NMR) set-up was used. NMR is used for carrying out non-destructive, quantitative and simultaneous measurements of hydrogen (H), sodium (Na) and lithium (Li) ions in the droplet. NMR is based on the principle that in a magnetic field, nuclei have a specific resonance frequency and can be excited by a radio frequency field. The resonance frequency f (Hz) depends linearly on the magnitude of the magnetic field:

$$f = \frac{\gamma}{2\pi} B_O \qquad (6.2)$$

where $\gamma/2\pi$ (HzT^{-1}) is the gyromagnetic ratio and B_0 (T) is the main magnetic field. The gyromagnetic ratio ($\gamma/2\pi$), the magnitude of the nuclear spin (I), the relative NMR

sensitivity, and the values of T_1 (spin-lattice relaxation time) and T_2 (spin-spin relaxation time) of the H, Na and Li nuclei are given in table 6.1.

Table 6.1: The gyromagnetic ratio, magnitude of the nuclear spin, relative NMR sensitivity, and T_1 and T_2 values for H, Na and Li nuclei.

Nucleus	^{1}H	^{23}Na	^{7}Li
Spin (I)	1/2	3/2	3/2
$\gamma/2\pi$ (MHz/T)	42.58	11.26	16.55
Relative sensitivity	1	0.093	0.29
T_1 (ms)	2670	75	2502
T_2 (ms)	2000	30	1793

For the experiments presented in this chapter, a home-built NMR scanner with a static magnetic field of 0.78 T was used. An extensive description of this set-up can be found elsewhere [60, 80]. The signal is obtained only from the dissolved Na, Li and H nuclei because the signal from the nuclei incorporated in the crystals decays too fast to be detected. To obtain a sufficient signal-to-noise ratio 256 a nd 64 a verages of the spin echo measurements are taken for sodium and lithium ions, respectively. The magnetic field gradient was chosen such that the whole droplet is covered in the measurement. A schematic diagram of the set-up is given in Fig. 6.2.

To obtain visual information time lapse microscopy of the crystallization was performed using a Dino-lite$^©$ digital microscope. Four LED's were placed at the bottom of the sample holder to provide additional lighting within the enclosed NMR set-up. The capture of photomicrographs along with the NMR measurements gives the possibility to visualize the drying droplet while simultaneously obtaining information about the amount of dissolved salt ions. From the ratio of the measured NMR signals (Na/H) and (Li/H) the concentration of Na and Li in solution droplet is calculated. Using NMR the average concentration (C_{avg}) is determined over the whole volume (V_{drop}) of the droplet. A cylindrical quartz glass sample holder with an inner diameter of 16 mm w as used. Droplets of 300 µl salt solutions were dried at room temperature using airflow of about 1 l min^{-1} to control the humidity in the Perspex chamber (see Fig. 6.2).
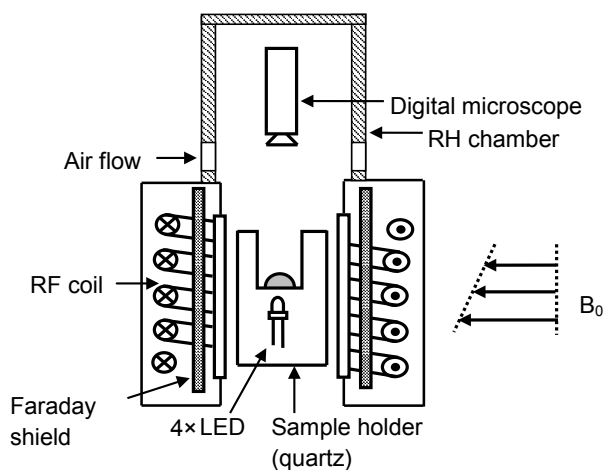
Figure 6.2: *Schematic diagram of NMR set-up used for droplet drying experiments. A 300 μl droplet was placed on a quartz glass holder. Time lapse microscopy of the drying droplet was performed by incorporating a digital microscope in the set-up. Using a Perspex chamber the humidity around the droplet was controlled.*

6.3 Results

6.3.1 NaCl

First, the influence of ferrocyanide inhibitor on NaCl crystallization was studied. For this purpose, a droplet of NaCl solution with and without inhibitor was dried inside the NMR set-up. Using NMR the hydrogen and dissolved sodium content was measured and using the digital microscope the onset of crystallization and crystal morphology were recorded. From the ratio of the Na and H content (Na/H), the NaCl concentration is calculated (for more details see [45]). The supersaturation is calculated as C/C_o, where C is the measured salt ion concentration and C_o is the saturation concentration of NaCl. To test the influence of the inhibitor concentration on t he crystallization, the tests were performed for different concentrations of inhibitor (0.0001m, 0.001m and 0.01m). The results of these experiments are shown in Fig. 6.3, w here the supersaturation (C/C_o) is plotted as a function of inhibitor concentration. For a solution droplet without inhibitor the onset of crystallization was observed at a concentration of 6.2 ± 0.5 m, giving a supersaturation of 1.06 ± 0.04 (see Fig. 6.3). In the presence of inhibitor, the crystallization was observed at a concentration higher than the saturation concentration of NaCl, i.e., the droplet supersaturates. The supersaturation increases with increasing inhibitor concentration. A maximum supersaturation of 1.55 m is observed for 0.01 m inhibitor. These results clearly indicate that ferrocyanide ions act as a strong nucleation inhibitor for NaCl crystallization. The results are in line with other studies, where higher supersaturation in the presence of ferrocyanide ions was reported [43]. The inhibiting action of ferrocyanide ions on N aCl crystallization can be caused by the fact that they can reduce the concentration of available solvent (i.e., water) in the system, thereby

increasing the relative supersaturation, and by adsorbing Na^+ ions they can interfere with ion transport towards more or less developed NaCl clusters with dimensions below the critical radius [43, 81].
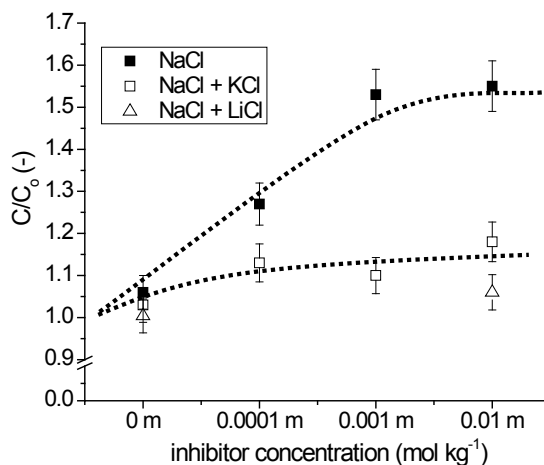

Figure 6.3: Supersaturation plotted as a function of inhibitor concentration for NaCl and for the salt mixtures 3m NaCl - 1m KCl and 3m NaCl - 1m LiCl. The dotted lines are drawn as a guide to eye.

The pictures captured using the digital microscope show that ferrocyanide acts as a habit modifier for NaCl. The NaCl crystal morphology changes from cubic structured crystals to dendritic crystals. Dendritic crystal morphology results from the non-equilibrium growth of the crystals in a supersaturated medium [82]. The non-equilibrium growth is due to the presence of some irregularities on the flat surface of the crystal [83]. These irregularities result from inhibitor adsorption on the growing crystal surface, which causes some parts of the surface to grow faster than the rest of the surface, which leads to budding or protruding on the surface. Higher concentrations can be achieved at these locations causing preferential growth [83]. The net result is that flat growth is unstable, and a crystal will tend to grow into more complex shapes, e.g., dendrites. Some pictures of the NaCl crystal morphology at the end of the drying experiment are shown in Fig. 6.4. As can be seen from Fig. 6.4a, in the absence of inhibitor bigger cubic crystals were formed. However, in the presence of inhibitor (Fig. 6.4b) dendritic crystals were formed and these crystals spread very rapidly all over the available substrate. Spreading of the crystals was more pronounced at higher inhibitor concentrations. The branches of dendritic crystals provide a pathway for spreading the solution to a much larger surface area. This phenomenon is commonly known as 'salt creep'. Because of the enlarged surface area for evaporation at higher inhibitor concentrations an increase in the drying rate was observed [45]. In porous building materials, the phenomenon of salt creep helps to crystallize salt outside the materials as non-destructive efflorescence [45]. The formation of efflorescence prevents blockage of pores inside the material. This in

turn helps to extract more and more salt out of the material. This way efflorescence acts as a sink of ions and is helpful to reduce the amount of salt inside the material.
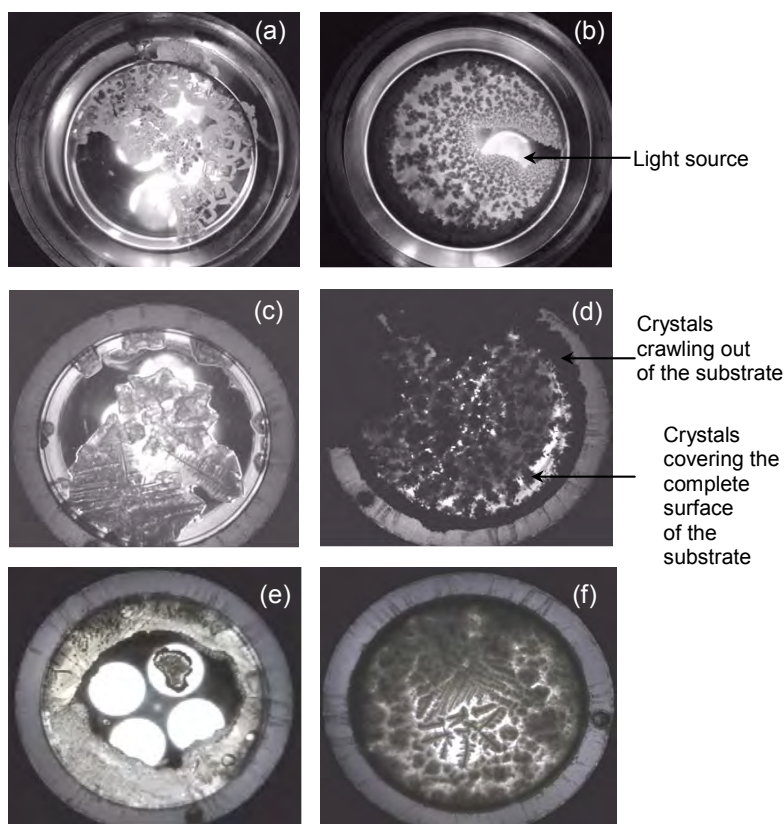

Figure 6.4: *Images showing the crystal morphology at the end of the drying experiment for (a) NaCl (b) NaCl + 0.01m inhibitor (c) NaCl - KCl (d) NaCl - KCl + 0.01m inhibitor (e) NaCl - LiCl (f) NaCl - LiCl + 0.01m inhibitor.*

As mentioned above, in the presence of inhibitor a high supersaturation is attained. This result in a higher number of crystals and therefore [84] the crystal size should become smaller for the same amount of salt. This has been confirmed by ESEM analysis. Using ESEM pictures the average crystal size was determined. The results are given in Fig. 6.5, where the crystal size is plotted as a function of inhibitor concentration. The average crystal size decreased from about 700 μm to 1-2 μm by increasing the inhibitor concentration from 0.0001m to 0.01 m. Moreover, the crystals formed in the presence of inhibitor were more like a fluffy powder covering a much larger surface area and, moreover, they did not strongly adhere to the substrate. In a system with fairly large pores, such small crystals can travel along with the flow without getting deposited on the walls.
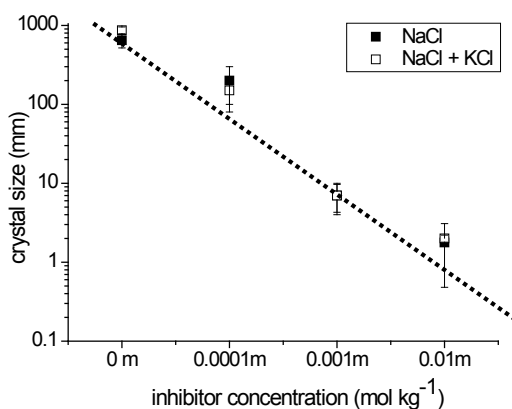
Figure 6.5: *Crystal size plotted as a function of inhibitor concentration for NaCl and for the salt mixture NaCl - KCl. The dotted line is drawn as a guide to eye.*

6.3.2 NaCl-KCl-H_2O

Next, the influence of inhibitor on NaCl crystallization in the salt mixture NaCl - KCl was studied. In order to obtain information about the influence of ferrocyanide ions on potassium chloride (KCl) crystallization a few preliminary tests were performed. These tests were performed outside the NMR set-up, because it is not possible to measure potassium with our set-up, since the sensitivity of potassium nuclei relative to hydrogen is very low.

KCl solution droplets with (0.01 m) and without inhibitor were dried at room temperature at the same drying conditions. The aim was to compare the time for the onset of nucleation and the crystal morphology for the two cases. The onset of nucleation was seen at about the same time in both the cases. Regarding the crystal morphology, bigger and strongly adhered cubic crystals were seen in the absence of inhibitor and smaller and immensely spread dendritic crystals were observed in the presence of inhibitor. The corresponding pictures are shown in Fig. 6.6. These results indicate that ferrocyanide ions act as a habit modifier for KCl crystallization.
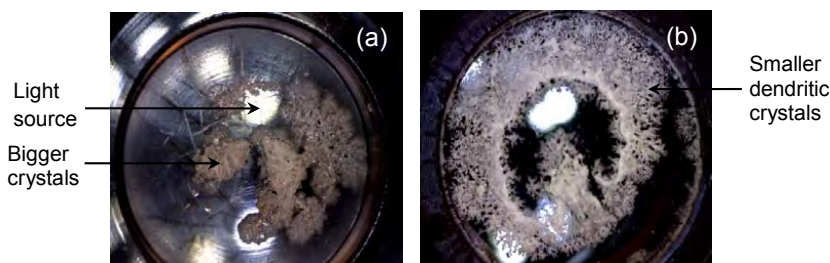

Figure 6.6: *Images showing the crystal morphology at the end of the drying experiment for (a) KCl and (b) KCl + 0.01m inhibitor.*

After these preliminary tests, drying tests were performed on salt mixtures of NaCl - KCl inside the NMR set-up. Two concentrations of the salt mixture were tested, i.e., 2m NaCl - 2m KCl and 3m NaCl - 1m KCl. In the first case, according to the phase diagram, KCl should crystallize first, followed by NaCl crystallization at a concentration of nearly 5.1 m (see Fig. 6.1). In the latter case, NaCl should crystallize first at a concentration of 5.3 m, followed by KCl crystallization. In these measurements, we could only measure sodium concentration. Hence, based on the phase diagram and assuming that the path of 3m NaCl - 1m KCl will be followed during drying, the supersaturation in the presence of inhibitor is determined. The result is included in figure 6.3. The NaCl supersaturation (C/C_o) is plotted as a function of inhibitor concentration for the 3m NaCl - 1m KCl mixture. As can be seen from this figure, the supersaturation increases with increasing inhibitor concentration. However, the increase in supersaturation was much lower than for NaCl only. In case of the salt mixture, at the maximum concentration of inhibitor (0.01 m) a supersaturation of 1.17 is observed compared to 1.55 in case of the single salt. One reason for this relatively low supersaturation may be that KCl can act as nucleation site in the salt mixture and thereby prevents higher supersaturation. Another possible reason can be the fact that ferrocyanide ions act as a growth inhibitor for both NaCl and KCl [41, 43]. Therefore, in the presence of KCl, the amount of available inhibitor for NaCl crystallization reduces. Future research is required for the exact mechanism and a quantitative explanation of this effect.

The pictures of the crystal morphology taken at the end of the experiments are shown Fig. 6.4. Fig. 6.4c and 6.4d show the crystal morphology for the mixture of NaCl - KCl without inhibitor and with inhibitor, respectively. A significant change in crystal morphology was observed in the presence of inhibitor. Dendritic crystals with immense spreading were seen. In the absence of inhibitor bigger and strongly adhered crystals were formed, whereas in the presence of inhibitor dendritic and loosely attached crystals were formed. Because of the dendritic crystal morphology the whole surface of the substrate was filled with salt crystals. The crystals were even seen creeping out of the sample holder (see Fig. 6.4d). The crystal size was again determined using ESEM pictures. The crystal size was found to decrease from ~ 800 μm to 1-2 μm in the presence of inhibitor. The results are included in Fig. 6.5.

6.3.3 NaCl-LiCl-H$_2$O

With the NMR set-up it was not possible to measure the potassium signal, and hence it was not possible to locate the concentration of the NaCl - KCl salt mixture in the phase diagram after the onset of crystallization. Therefore, another mixture, NaCl - LiCl, is tested, where we can measure simultaneously the H, Na and Li ions. From the concentration of both the Na and Li ions we can locate the exact location of the salt mixture in the phase diagram. This way, it was possible to check if the equilibrium solubility line is followed after the onset of crystallization. The ternary phase diagram of a NaCl-LiCl-H$_2$O mixture at 25 ^{o}C is given in Fig. 6.7, where the LiCl concentration (m) is plotted as a function of the NaCl concentration [85]. The solubility equilibrium line is shown by a red line. Everywhere on this line NaCl will crystallize and LiCl will precipitate only at very high concentrations, i.e., 19.84 m LiCl and

0.03m NaCl. As an example, the expected paths during evaporation of a solution are shown by the solid lines A, B and C for three different initial ion concentrations.
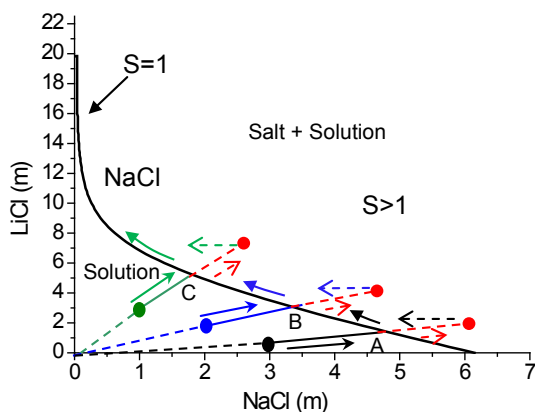

Figure 6.7: *The ternary phase diagram of NaCl-LiCl-H₂O at 25°C. During evaporation the paths A, B and C (shown by solid black, blue and gr een lines) will be followed for salt mixture of compositions 3m NaCl - 1m LiCl, 2m NaCl - 2m LiCl, and 1m NaCl - 3m LiCl, respectively. If no crystal appears at the intersection of path A, B, C and the equilibrium line (S = 1), the concentration will keep on increasing (supersaturation), as indicated by dotted red arrows. After crystallization the system will return to the equilibrium solubility line.*

Initially, the influence of inhibitor is tested on LiCl only. For this purpose droplets of 10m LiCl with (0.01m) and without inhibitor were dried inside the NMR set-up at a room temperature at an air flow of 1 l min⁻¹ and 0% RH. In both the cases, i.e. with and without inhibitor, the salt crystals were formed at the same concentration and no supersaturation was observed. Also, no change in crystal morphology was seen in the presence of inhibitor. The pictures showing the crystal morphology are given in Fig. 6.8. T hese results indicate that ferrocyanide ions have no influence on LiCl nucleation and crystal morphology.

Next, the influence of inhibitor was tested on a mixture of NaCl - LiCl. Three different salt ion concentrations were tested, i.e., 3m NaCl - 1m KCl, 2m NaCl - 2m LiCl, and 1m NaCl - 3m KCl. For all these experiments, 0.01m inhibitor concentration was used. The results are shown in Fig. 6.9. T he solid lines are the expected paths to be followed upon drying of the droplet. As can be seen from the figure, the experimental data points coincide very well with the expected paths. The salt ion concentration first increases to the equilibrium line. At this point a salt crystal appears, as was confirmed from the pictures taken by the digital microscope. After the onset of crystallization the concentration of NaCl will decrease and the equilibrium solubility line is followed, as shown by dotted arrows. These results show that multi-nuclear NMR is a powerful experimental tool to validate the phase diagrams.
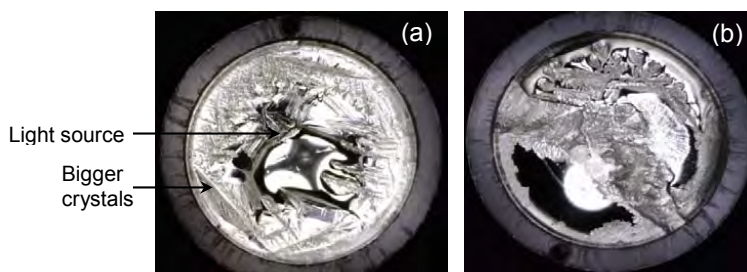
Figure 6.8: *Images showing the crystal morphology at the end of the drying experiment for (a) LiCl and (b) LiCl + 0.01m inhibitor.*

For the mixture of NaCl - LiCl also no significantly higher NaCl supersaturation was observed in the presence of inhibitor. These results indicate that in the presence of another salt, ferrocyanide ions are not able to highly supersaturate NaCl. However, a clear habit modification was also seen in this case. The pictures showing the crystal morphology at the end of the experiments are shown in Fig. 6.4, where Figs. 6.4e and 6.4f represent the crystal morphology in case of the mixture of NaCl - LiCl without and with inhibitor, respectively. As can be seen in Fig. 6.4f, more spreading occurred and dendritic crystals were formed in the presence of inhibitor.
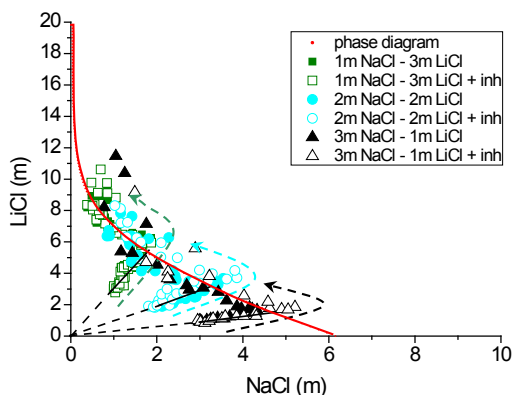

Figure 6.9: *The three tested concentrations of NaCl - LiCl salt mixtures shown in the ternary phase diagram of the NaCl - LiCl - H$_2$O system. The open symbols denote salt mixtures with inhibitor and the closed symbols denote salt mixtures without inhibitor. The solid lines show the expected pathways to be followed before the equilibrium line is reached.*

6.4 Conclusions and discussion

The influence of ferrocyanide ions on NaCl crystallization behavior was studied. The tests were performed on NaCl and on the salt mixtures NaCl - KCl and NaCl - LiCl. The

results show that ferrocyanide ions act as a strong nucleation inhibitor for NaCl. A significantly higher NaCl supersaturation (1.55) was observed in the presence of inhibitor and the supersaturation increases with increasing inhibitor concentration. For salt mixtures it is found that the inhibitor will result in a much lower supersaturation than that of the single salt. For both single salt and salt mixtures, the crystal morphology changes completely from bigger cubic crystals to dendritic crystals in the presence of inhibitor. The crystal size decreases significantly at high inhibitor concentrations.

This dendritic crystal morphology with immense spreading is seen for all the cases. In a porous material, such a type of morphology can promote the formation of efflorescence that causes only little structural damage. The crystals formed in the presence of inhibitor were more powdery and fluffy and were easy to remove from the substrate. Consequently, the ferrocyanide ions may be beneficial for building materials that are contaminated with a salt mixture. Moreover, as the solution does not highly supersaturate in the presence of inhibitor, the risk of damage will be reduced (see Eq. 6.1). If the same type of small crystals is formed inside the material as well, these crystals can easily be flushed with a flow of water, thereby reducing the risk of damage.

However, the results presented here are preliminary tests only; a more detailed study is required to explore all the aspects of the crystallization of salt mixtures inside a porous material. For example, it is important to study the influence of inhibitor on other salts, like sodium sulphate (Na_2SO_4), magnesium sulphate ($MgSO_4$) and sodium nitrate ($NaNO_3$). Also, it is important to explore the effect of ferrocyanide ions on mixtures of these salts. Ultimately, it is required to perform all these tests inside a real porous material.

Chapter 7

Crystallization behavior of NaCl droplet during repeated crystallization and dissolution cycles: an NMR study

Abstract

Repeated cycles of crystallization and dissolution of the salt crystals inside the pores of a building material can provoke damage to that material. To find effective treatment methods against this damage, a better understanding of the crystallization process is required. For this purpose, a microscopic study on a sodium chloride (NaCl) solution droplet is performed. The crystallization behavior of NaCl during repeated cycles of crystallization and dissolution is studied using time lapse microscopy along with Nuclear Magnetic Resonance (NMR). Using NMR non-destructive and simultaneous measurements of hydrogen and dissolved sodium ions were made. The results show that with repeated cycles the number of available foreign nucleation sites for salt crystallization decreases. The resulting decrease of the number of crystals leads to an increase in crystal size. A maximum supersaturation up to 1.16 ± 0.08 was observed.

7.1 Introduction

It has been known for a long time that the presence of salts inside the pores of building materials can give rise to damage [86]. Among the various salts present in building materials sodium chloride (NaCl) is one of the most widely distributed. Sea salt spray, deicing salts and salinization of soil are possible sources of NaCl. Until now, the mechanisms that control the development of damage by crystal growth are poorly understood. The major mechanisms generally assumed to be responsible for damage include crystallization pressure [3, 14].

According to this mechanism, the damage is caused by the growth of salt crystals in a confined space, e.g., a pore. These crystals exert a pressure on the pore walls, which can exceed the tensile strength of the material and therefore lead to damage [3,14]. Thermodynamically, the crystallization pressure can be related to the supersaturation (C/C_o) of the solution [14]:

$$P_C = \frac{vRT}{V_m} ln \frac{C}{C_O} \tag{7.1}$$

Where, P_c is the crystallization pressure, v is the total number of ions released upon dissociation of the salt (e.g. for NaCl = 2), R is the universal gas constant, T is the absolute temperature and V_m is the molar volume of the salt crystal and C and C_o are the concentration in the vicinity of the crystal and the saturation concentration of NaCl (6.14 m) respectively.

In particular for NaCl, the damage mechanism is controversial. Several experiments have been done to show that NaCl has a low tendency to supersaturate [16] inside building materials and to develop a high crystallization pressure to generate damage. In addition, it is known that NaCl has a tendency to crystallize on foreign nucleation sites, e.g., impurities on the pore walls [18]. Therefore, crystallization is more likely to occur at low values of supersaturation. Rijniers [4], has shown that relevant crystallization pressures will develop in nm pore sizes, which are usually absent in traditional building materials, e.g., in fired-clay brick, mortar and limestone. Nevertheless, serious decay occurs in the building materials in the presence of NaCl, leaving an open question with respect to the NaCl damage mechanism. Thus, the actual NaCl damage mechanism is still not clear.

In lieu of this, in the present study, we have investigated crystallization of NaCl induced by drying of a solution with repeated cycles of crystallization and dissolution. The crystallization of NaCl in droplets with repeated crystallization and dissolution cycles has been studied previously by Desarnaud et al. [87]. They have shown that with repeated cycles of crystallization and dissolution a small number of nuclei form which grow to bigger sizes. Also, they have reported that with more cycles higher supersaturation can be reached before nucleation and growth. The salt ion concentration was calculated indirectly. For this purpose the evaporation rate was calculated from the measured radius of the droplet using microscopic images. Knowing the time before nucleation and amount of salt, the salt ion concentration was calculated. However, with the help of a specially designed NMR set-up we can measure the salt ion concentration directly during dynamic drying experiments. In this article, by combining time-lapse microscopy with NMR measurements, we are able to follow

the dynamics of crystallization and to measure the dissolved salt ion concentration simultaneously.

7.2 Experiments

Nuclear Magnetic Resonance (NMR) is used for carrying out non-destructive, quantitative and simultaneous measurements of both the hydrogen and sodium ion content in a sample. NMR is based on the principle that in a magnetic field, nuclei have a specific resonance frequency and can be excited by a radio frequency field. The resonance frequency f (Hz) depends linearly on the magnitude of the magnetic field:

$$f = \frac{\gamma}{2\pi} B_O \qquad (7.2)$$

where $\gamma/2\pi$ (HzT^{-1}) is the gyromagnetic ratio, B_0 (T) is the main magnetic field. For ^1H $\gamma/2\pi =$ 42.58 $MHzT^{-1}$ and for ^{23}Na $\gamma/2\pi = 11.26$ $MHzT^{-1}$. Therefore, by using a specific frequency the method can be made sensitive to a particular type of nucleus, in this case either hydrogen or sodium. The intensity of a spin-echo signal (S) as used in our experiments is given by:

$$S = k\rho \left[1 - exp\left(-\frac{T_r}{T_I} \right) exp\left(-\frac{T_e}{T_2} \right) \right] \qquad (7.3)$$

Where, k is the sensitivity of the nuclei relative to hydrogen, ρ is the density of the nuclei, T_r and T_I are the repetition time of the pulse sequence and the spin-lattice relaxation time, T_e and T_2 are the spin-echo time and spin-spin relaxation time. As the sensitivity of ^{23}Na nuclei is low relative to hydrogen ($k_H = 1$, $k_{Na} = 0.1$), 256 averages of the spin-echo measurements are taken for Na nuclei and four averages for hydrogen nuclei, thereby giving the possibility to obtain a sufficient signal-to-noise ratio. Since the relaxation time for Na in NaCl crystals is of order of 10 µs [73] only dissolved Na ions are measured using the NMR set-up. For the experiments presented here, a home-built NMR scanner with a static magnetic field of 0.78 T and a magnetic field gradient up to 0.16 T/m is used. To perform quantitative measurements a Faraday shield is placed between the coil and the sample [60]. The measurements were done at room temperature. A schematic diagram of the set-up is presented in fig. 7.1.
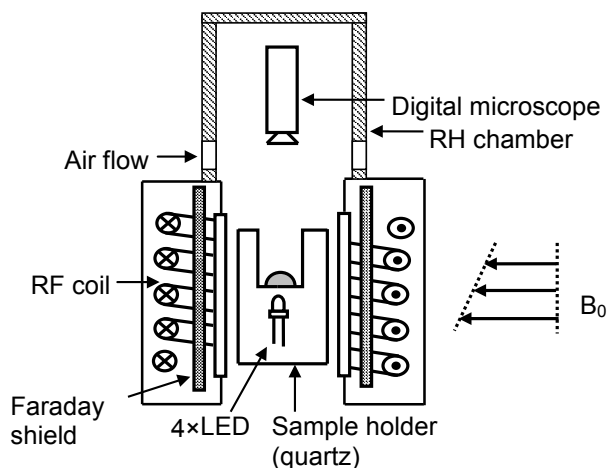
Figure 7.1: A schematic diagram of NMR set-up used for non-destructively measuring the salt ion concentration during droplet drying experiments. A 300 µl droplet of 5m NaCl was placed on a quartz glass holder. Time lapse microscopy of the drying droplet was done by incorporating a di gital microscope in the set-up. Using a Perspex chamber the desired humidity was maintained around the droplet.

Time lapse microscopy of the crystallization was done using a Dino-lite digital microscope ©, with four LED's placed below the substrate as a lighting source for imaging within the NMR setup. Capturing the photomicrograph along with the NMR measurements gives the possibility to visualize drying droplets while simultaneously obtaining information about the NaCl concentration of the droplets. From the ratio of the sodium (Na) and hydrogen (H) signals (Na/H) the concentration of Na in a solution droplet is calculated. Using NMR the average concentration i.e., C_{avg} at a given time t is determined as:

$$C_{avg}(t) = \frac{R_i}{C_i} \times R(t) \tag{7.4}$$

In this equation, R_i is the ratio of the average sodium signal to the average hydrogen signal at time $t=0$, C_i is the initial known concentration (5m) and $R(t)$ is the ratio of the average sodium signal to average hydrogen signal at time $t=t$. Using simultaneous time lapse microscopy, we can see exactly at which concentration the salt crystal appears. Hence, we can relate the onset of crystallization with the Na concentration in the drop. A cylindrical quartz glass sample holder with an inner diameter of 16 mm was used. Droplets of 300 µl salt solutions (5m NaCl) were dried at room temperature using an air flow of about 1 l min^{-1} to maintain the humidity in the chamber. Using a Perspex chamber the humidity around the droplet was controlled (see fig. 7.1).

Crystallized salt in a building material can dissolve by two possible ways; either by uptake of water vapor, e.g., in high humidity regions or by uptake of pure water, e.g., by capillary rise of ground water and infiltration by rain water. To see the effect of both these

dissolution conditions on the dynamics of NaCl crystallization, two series of experiments were performed: dissolution using water vapor and dissolution using pure water. Dissolution using water vapor was done by applying a high RH (98%) in the chamber and dissolution using pure water was done by adding 300μl of water. For both the experiments three cycles of crystallization and dissolution were performed.

7.3 Results and discussion

We have studied the drying of a droplet of salt 5m NaCl (mole/kg) solution on a quartz glass substrate. Repeated crystallization and dissolution cycles using water vapor (section 7.3.1) and using liquid water (section 7.3.2) have been performed at room temperature. Initially, the results from the dissolution using water vapor followed by dissolution using liquid water and then advection diffusion diagram for the droplets will be discussed.

7.3.1 Dissolution using water vapor

In cycle 1, a 5m salt solution droplet was dried by maintaining 45% RH in the sample chamber. The measured normalized sodium and hydrogen content of the droplet as a function of time are given in fig. 7.2a, whereas the calculated dissolved salt ion concentration is given in fig. 7.2b. Immediately after the drying starts the moisture content decreases whereas the dissolved sodium content remains constant (see fig. 7.2a). As a result the concentration in the droplet increases (see fig. 7.2b). After about 1 hour a decrease in the sodium content occurs, indicating crystallization. This onset of crystallization is also observed by direct visualization (see fig. 7.2c) where a large numbers of small cubic crystals are seen near the boundary of the droplet and a few small crystals in the center of droplet. At this time (~ 1h), the average concentration was 5.8 m (see fig. 7.2b). Near the end of the drying cycle, a few bigger NaCl crystals, surrounded by small cubic crystal were seen at the center of the substrate (see fig. 7.2d).
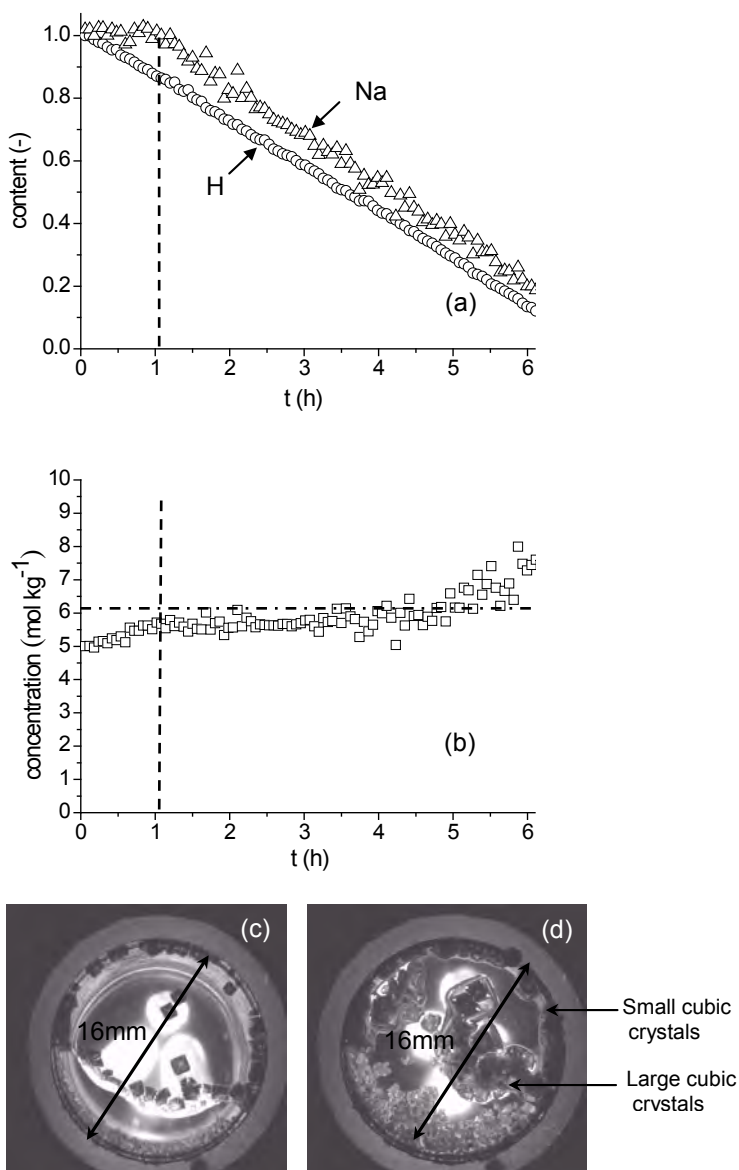
Fig. 7.2: *Results from deliquescence experiments during drying cycle 1. In fig. 7.2a, the measured normalized moisture (H) content (o) and normalized sodium (Na) content (Δ) are plotted as a function of time during drying of the droplet. In fig. 7.2b the calculated NaCl concentration (□) is plotted as a function of time during drying of the droplet. Fig. 7.2c shows the onset of crystallization, where small cubic crystals were seen near the boundary of the droplet, whereas, fig. 7.2d shows the crystals at the end of the drying cycle.*

From the microscopic images the crystal size was determined. The results are shown in fig. 7.3a. The average crystal size was 1.4 mm (see fig. 7.3a). The crystal growth rate was also evaluated from the images taken after the first crystal was seen. For the growth rate calculations the crystal size was determined as a function of time. This was done for four crystals (see fig. 7.3b). The reported growth rate is the average growth rate of the four crystals measured during initial growth rate period (indicated by dotted lines in fig. 7.3b). The growth rate was found to be 0.26 ± 0.03 μm s^{-1} (see fig. 7.3c).

The onset of crystallization was observed at an average concentration of 5.8 m, whereas the saturation concentration of NaCl is 6.14 m. This difference may be caused by the fact that with NMR we measure the average concentration (C_{avg}) over the whole volume of the droplet. Close to the saturation concentration a large number of small cubic crystals were formed near the edge of the droplet (see fig. 7.2c). This is due to the pinning of the contact line near the edge of the droplet [88]. If the contact line is pinned during evaporation process, evaporation drives capillary flow that transports water from the center towards the periphery, the well-known coffee stain effect [88]. This causes a higher salt ion concentration near the edges than in the bulk, causing the first crystals to appear near the edges. Due to this reason the reported average concentration was less than 6.14 m.
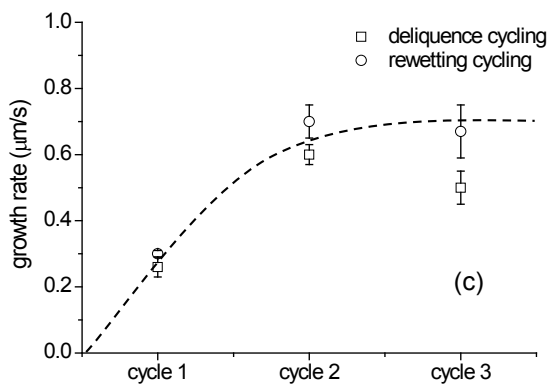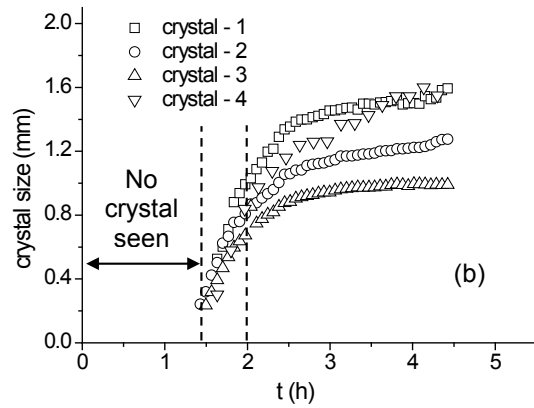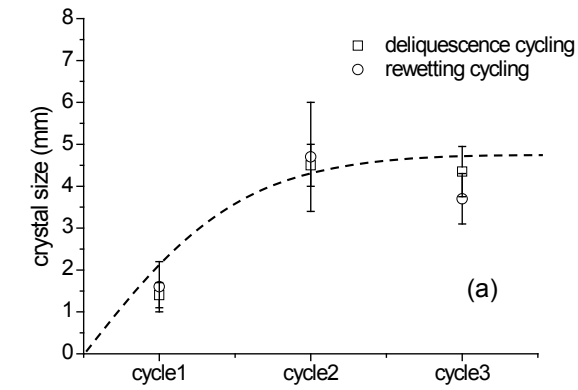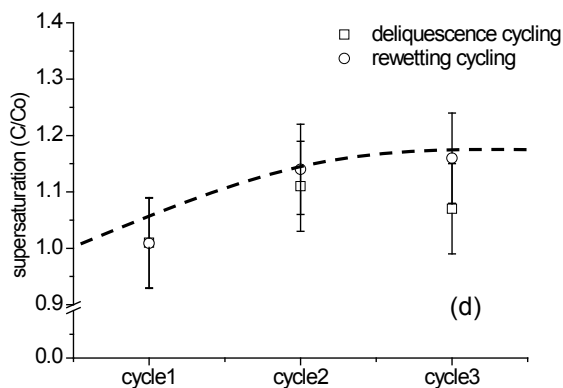
Figure 7.3: *In fig.7.3a, crystal size is plotted as function of different drying cycles given during deliquescence and rewetting experiments, in fig. 7.3b, crystal size is plotted as a function of time for four different crystals during cycle 1 of drying, in fig.7.3c and 7.3d, crystal growth rate and NaCl Supersaturation is plotted as a function of different drying cycles during deliquescence and rewetting experiments.*

After complete drying, the crystals were dissolved by maintaining 98 % RH in the sample chamber. As the equilibrium relative humidity for NaCl is 75 %, the salt crystals will capture the water vapor from the surrounding air followed by their complete dissolution with time. The measured sodium and hydrogen content during dissolution is shown in fig. 7.4a and the calculated concentration is shown in fig. 7.4b. During dissolution a constant increase in the moisture content and the dissolved sodium content was observed and the concentration in the droplet remained constant nearly at the saturation concentration, i.e., 6.14 m. After ~ 40 h, the sodium content became constant indicating the complete dissolution of the salt crystal. However, the moisture content was still increasing at this time. This is due to the relative humidity gradient between the surface of the droplet (75%) and in the surrounding environment (98%). So, the water vapor will condense on the surface of the droplet. Due to this fact, the moisture content was still increasing (see figure 7.4a and a slight decrease in the salt ion concentration is seen (see fig. 7.4b).
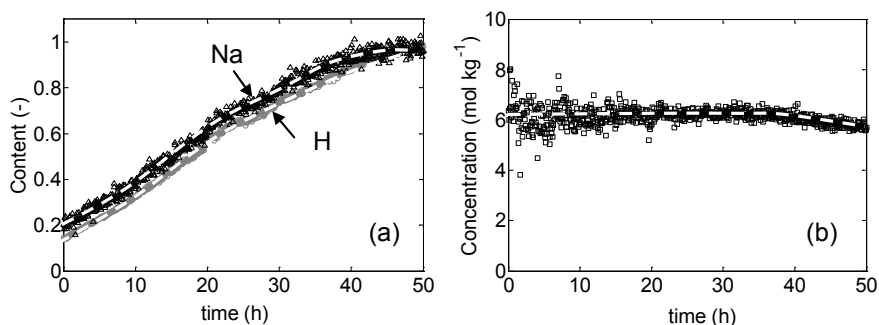
Figure 7.4: *Results from deliquescence experiments during dissolution in cycle 1. In fig. 7.4a, the measured normalized moisture (H) content (o) and nor malized sodium (Na) content (Δ) are plotted as a function of time during drying of the droplet. In fig. 7.4b the calculated NaCl concentration (□) is plotted as a function of time during drying of the droplet.*

By this time, as all NaCl crystals have dissolved, the second cycle (cycle 2) of drying was started. It should be noted that in cycle 2 the starting salt ion concentration is higher (~ 5.6 m) than that of cycle 1 (5 m). For drying of the droplet, the procedure of cycle 1 was repeated. The re-dissolved droplet was dried again at 45% RH. Initially, a single crystal was seen growing. With time, as it grew bigger in size, a lot of small particles/impurities were seen sticking on the surface of the crystal (see fig. 7.5a). This will decrease the number of available foreign nucleation sites (e.g. dust particles) in the droplet itself for the crystals to grow. In cycle 2 during drying a contraction of the droplet contact line was seen. This helps to leave behind the impurities on the surface and will also decrease the number of available nucleation sites [87]. One of the causes of the contraction of the droplet can be that initially the impurities in the droplet may act as a source for the retention of the droplet contact line [89]. However, in cycle 2, because of the smaller number of impurities in the droplet, the contact line can no longer be retained and thus the droplet shrinks.
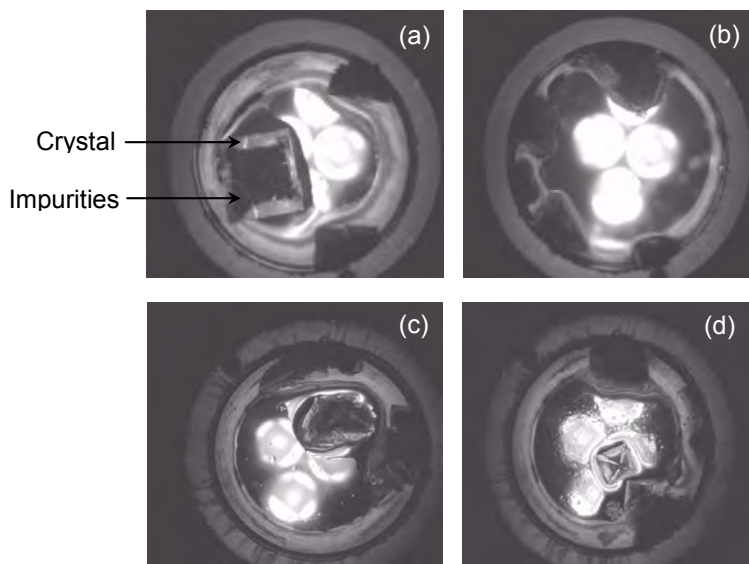
Figure 7.5: *Dissolution using water vapor: NaCl crystals observed at the end of drying cycle 2 (fig. 7.5a) and cycle 3 (fig. 7.5b), Dissolution using liquid water: NaCl crystals observed at the end of drying cycle 2 (fig. 7.5c) and cycle 3 (fig. 7.5d).*

A significant decrease in the number of crystals was seen in cycle 2. Only 3 crystals were observed at the end of the drying cycle (see fig. 7.5a). Because of the formation of fewer nuclei, the crystals formed in this case were much bigger in size (see fig. 7.5a), because the same amount of salt ions has to be consumed by less number of nuclei. The average crystal size in cycle 2 was found to be approx. 4.5 mm, which is more than twice the crystal size in cycle 1 (see fig. 7.3a). The average growth rate of the crystals was 0.6 ± 0.04 µm s^{-1} (see fig. 7.3c). The onset of crystallization was observed at an average concentration of 6.8 ± 0.5m giving a supersaturation of 1.10 ± 0.08 (see fig. 7.3d). After complete drying the crystals were dissolved by applying 98% RH in the sample chamber. The complete dissolution in this case took a longer time than in cycle 1. This is due to the bigger size of the crystals and is in agreement with previous work [87].

After complete dissolution, cycle 3 was started. For this cycle, the same procedure of crystallization and dissolution was performed again. The results show that the system behaves about the same in cycle 2 and cycle 3. The average crystal size observed here was nearly 4.3 mm which is approx. the same order that was observed in cycle 2 (see fig. 7.3a). The onset of crystallization occurred at an average concentration of 6.58 ± 0.5m, giving a supersaturation of 1.07 ± 0.08 (see fig. 7.3d), and the growth rate was found to be 0.41 ± 0.05µm s^{-1} (see fig. 7.3c). After cycle 3, the drying behavior was found to remain the same.

Our observations are in good agreement with a previous study [87]. The authors have reported that with repeated cycles the number of crystals decreases and the growth rate

increases. The retraction of the droplet seen during cycle 2 of our experiment has also been observed by the previous authors [87]. In cycle 2, a larger number of impurities were sticking on the surface of crystal, thereby reducing the available nucleation sites in the droplet. Also retraction of the droplet in cycle 2 shows that the contact line was not pinned in repeated cycles. As a consequence of this we did not observe small cubic crystals growing near the edge of the droplet in cycle 2. A decrease of the number of crystals leads to an increase in the crystal size. Since, the droplet is drying under same external conditions a decrease in the number of crystals leads to an increase of the growth rate of the individual crystal. The increase of the growth rate is only possible when supersaturation is present, as was seen observed in cycle 2 and cycle 3 [87].

7.3.2 Dissolution using pure water

For this series of experiments, three cycles of crystallization and dissolution were performed. For this purpose, pure water was added to dissolve the crystals instead of water vapor. In cycle 1 we started with the drying of a 5m salt solution droplet by maintaining 45% RH in the sample chamber. Once the salt crystals were formed, 300 µl of pure water was added on top of the crystals using a micropipette to dissolve the crystals. This will dilute the droplet more in cycle 2 and cycle 3 compared to cycle 1, where the initial total volume of the droplet was 300 µl , i.e., volume of water + volume of salt. Therefore, the initial dissolved salt ion concentration will be less in cycle 2 and cycle 3 than in cycle 1. After dissolution of crystals, cycle 2 of drying was started by maintaining 45% RH in the sample chamber. This way, three cycles of wetting and drying were performed.

The dissolution of the crystals using pure water was much faster than with water vapor. Immediately after addition of water, a water film was seen spreading initially on the top of the crystals and later filling the space in between the crystals. The crystal size, growth rate and the supersaturation for all three cycles are shown in figure 7.3a, 7.3c and 7.3d respectively. The results show that with repeated cycles the number of crystals decreases and the size of the crystals increases (see fig. 7.3a). The average crystal sizes at the end of the drying cycles were 1.6 mm, 4.7 mm and 3.7 mm. The growth rate of the crystals for cycle 2 and cycle 3 was found to be 0.7 ± 0.05 µm s^{-1} and 0.67 ± 0.08 µm s^{-1} (see fig. 7.3c) and the onset of crystallization occurs at 7 ± 0.5 m giving a supersaturation of 1.14 ± 0.08 in cycle 2 and at 7.1 ± 0.5 m giving a supersaturation of 1.16 ± 0.08 in cycle 3 (see fig. 7.3d). In our results for the deliquescence and dissolution cycles, almost similar behavior was seen in terms of number and size of crystals and in terms of supersaturation.

7.3.3 Analysis of advection-diffusion processes in a droplet

In order to identify the ion transport mechanism in a salt solution droplet the data is plotted in an Advection Diffusion Diagram (ADD) that is somewhat similar to the so-called efflorescence pathway diagram (EPD) [45, 90]. As the droplets geometry is dynamically changing because of the de pinning of the contact line during drying, a direct calculation of the Peclet number is rather complicated. However, an estimation of the Peclet number can be obtained from the experimental data by using ADD. In this diagram, the dissolved sodium

content of the droplet is plotted as a function of the water content of the droplet, normalized with respect to the initial content. The relative sodium content gives a direct indication of the amount of dissolved salt ions in the solution. Therefore, a decrease can only take place when crystallization occurs. On the other hand, the relative water content is directly related to the drying behavior of the system. Hence by plotting the relative sodium content as a function of the relative water content gives us a direct relation between the crystallization and the drying. The results for dissolution using water vapor are given in fig. 7.6a, and for dissolution using liquid water in fig. 7.6b. In this diagram, the competition between advection and diffusion is shown.
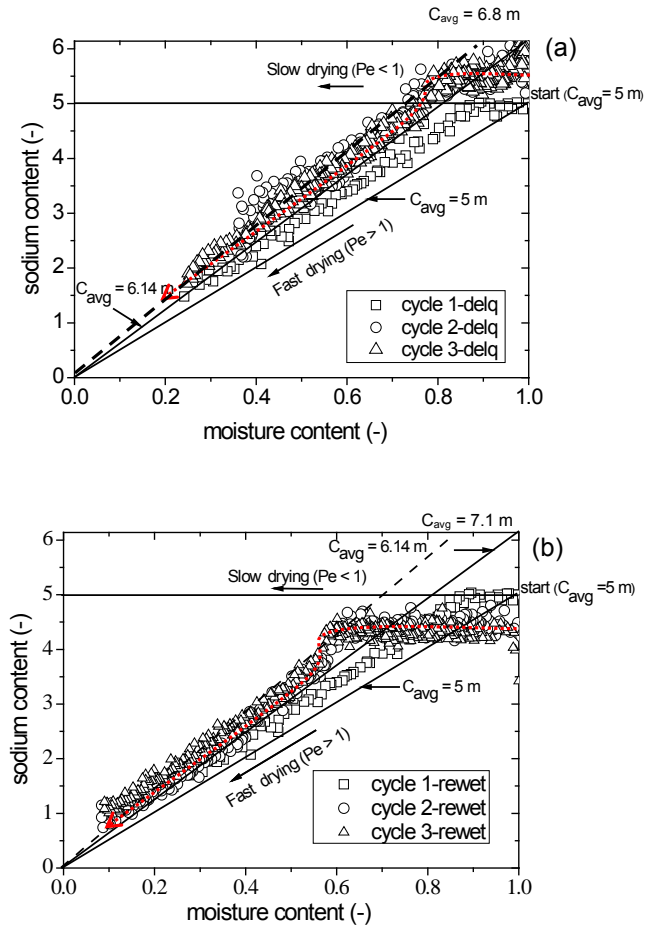

Figure 7.6: *In fig. 7.6a, advection-diffusion analysis diagram for the droplet wetted using water vapor (deliquescence) and in fig. 7.6b, advection-diffusion analysis diagram for the droplet wetted using liquid water vapor (wetting) is given. The total amount of dissolved sodium in the droplet is plotted as a function of the volume of the droplet (V). Both the axes are normalized with respect to the initial volume of the droplet (V_{initial}).*

Two extreme situations can be distinguished. If diffusion dominates ($P_e < 1$), it will result in a homogeneous distribution of ions throughout the droplet. Hence during drying the volume of the droplet will decrease and the concentration will increase homogenously, till the saturation concentration 6.14 m is achieved. From this moment onwards any further drying will cause crystallization and the concentration will stay constant at 6.14 m. If advection dominates ($P_e > 1$), it will result in the concentration gradients in the droplet, e.g., convective flow of the ions towards the periphery, resulting in crystallization patterns somewhat similar to coffee-stain effects. In this case, as soon as the volume of the droplet decreases immediate crystallization of salt will occur if there are enough nucleation sites (e.g. near the periphery). In this case, the ratio of dissolved salt to water and hence the concentration remains almost constant.

Water vapor dissolution

In fig. 7.6a, the data for the dissolution using water vapor for all the three cycles have been plotted. In cycle 1, where we observed something similar to the coffee-stain effect, we expect advection to be the governing process. As can be seen in fig. 7.6a, near the crystallization point a path in between two extreme situations is followed. This indicates that advection was the governing process near the crystallization point. Towards the end of drying, the concentration gradients vanish and the concentration stays constant at the saturation concentration.

In cycle 2 and cycle 3, the starting concentration is higher than the starting concentration in cycle 1. The second cycle of drying was started once all the salt crystals had dissolved. The results show that initially the dissolved salt ion concentration increases up to the saturation concentration. The droplet then supersaturates in cycle 2 and cycle 3, reaching a maximum concentration in the order of 6.8 m. From this moment onwards further drying causes salt crystallization and the dissolved sodium content decreases. After a certain time a path corresponding to Pe < 1 is followed, indicating that diffusion is dominant thus, the salt ion concentration remains homogenous throughout the droplet.

Liquid water dissolution

In fig. 7.6b, the data for dissolution using liquid water for all the three cycles has been plotted. Cycle 1 was the same as for water vapor dissolution. In cycle 2 and cycle 3, the starting concentration was lower than the starting concentration in cycle 1. This is due to the fact that initially the droplet of 300 μl containing 88 vol% (i.e. 264 μl) of water and 12 vol% (i.e. 36μl) of salt, giving a concentration of 5m. For the dissolution 300 μl of water was added instead of 264 μl. This diluted the solution a bit more than in cycle 1, giving an average concentration of 4.6m instead of 5m. Therefore, the initial dissolved salt ion concentration was less in cycle 2 and cycle 3 than in cycle 1. In cycle 2 and cycle 3, initially the dissolved salt ion concentration remains homogenous and increases up to the saturation concentration. The droplet then supersaturates, reaching a maximum concentration of 7.1 m. Due to crystallization the dissolved sodium content decreases. After a certain time a path

with Pe < 1 is followed. Consequently, we observed more or less the same behavior as for water vapor dissolution.

For both cases (deliquescence and dissolution) we found that with repeated cycles the number of crystals reduces and the size of the crystals increases. Our results are in good agreement with a previously reported study. However, we could never reach a supersaturation as high as S = 3, as was reported [87]. The maximum supersaturation in our experiments was around 1.16 ± 0.08. In the previous study it was reported that the process of making less crystals with a bigger size is more efficient by deliquescence cycling than by rewetting using liquid water. However, we observed about the same behavior in terms of number and size of crystals and also in terms of supersaturation for both deliquescence and dissolution cycles. A possible explanation for this difference may originate from the different experimental conditions. In our experiments, we used a volume of 300 µl compared to the volume of 0.1 µl used in [87]. Because of the bigger volume (3000 times) in our case the probability of heterogeneous nucleation on the dust particles or impurities is also higher. This will prevent the system from being highly supersaturated. In order to check this effect a droplet drying experiment was performed on a smaller volume of the droplet. A droplet of 100 µl was dried under the same conditions as were used for 300 µl droplet. Repeated humidity cycles were given. However, in this case also, we saw approx. the same supersaturation behavior as was seen in case of 300 µl droplet. We could never reach a supersaturation higher than 1.16 in our experimental conditions. It should be noted that the droplet volume was still significantly bigger (1000 times) than the volume used in [87]. Besides, dust particles in the air flow in our experiments may act as a source of nucleation sites. From known values of supersaturation in our experiments, the crystallization pressure (P_c) is calculated using eq. (7.1). For a maximum supersaturation of 1.16 seen in our case, the calculated value of P_c = 26.26 MPa (C_o is 6.14 mol kg^{-1} at 298.15 K, ν = 2 for NaCl, V_m = 27.02 cm^3mol^{-1}). If this value of P_c exceeds the critical failure strength of the building material, the damage will occur. However, it must be kept in mind that inside a building material enough surface area is available in the form of pore walls for the heterogeneous nucleation to take place. This may be reason in some studies supersaturation of NaCl inside building materials is never observed [16].

7.4 Conclusions

Repeated cycles of crystallization and dissolution were performed on a NaCl solution droplet. The crystallized salt was rewetted either with water vapor (deliquescence) or with liquid water (wetting). Almost similar behavior in terms of number and size of crystals and in terms of supersaturation was seen for the deliquescence and dissolution cycles. With repeated cycles, larger numbers of impurities were seen sticking on the surface of crystal, thereby reducing the available nucleation sites in the droplet. This leads to a significant decrease of the number of crystals in the later cycles. A decrease of the number of crystals leads to an increase of the growth rate of the individual crystals, since the droplet is drying at the same external conditions and therefore the evaporation rate is the same. The increase of the growth rate is only possible when supersaturation is present, as was seen observed in cycle 2 and

cycle 3. With progression of cycles, an increase of the supersaturation up to 1.16 ± 0.08 was found. If such a high supersaturation can be achieved inside a building material, the resulting crystallization pressure can be harmful.

Chapter 8

Conclusions and outlook

8.1 Conclusions

The aim of the study described in this thesis was to understand the drying behavior of NaCl saturated porous materials and to explore the use of ferrocyanide ions as a preventive method to stop/reduce damage caused by NaCl crystallization. The work presented here is an important step towards better understanding and prediction of NaCl damage.

We have shown that the presence of salt changes the standard drying behavior of porous building materials. For NaCl saturated porous materials, on reducing the external evaporation demand, e.g., by increasing the relative humidity (RH), the drying rate of the material *increases*. Only at very low RH conditions the drying rate decreases. This can be attributed to the type of efflorescence developing at the very beginning of drying. At very low RH conditions, a blocking efflorescence (crust) forms at the initial stage of drying. As a result, the drying rate slows down and hydraulic connections between the drying surface and the solution inside the material remain intact till very low saturation values. For such a case, the critical moisture content is never reached. At high RH conditions, non-blocking efflorescence forms at the initial stage of drying. This type of efflorescence does not affect the initial drying rate of the material. Therefore, a constant drying rate is maintained initially, followed by the appearance of critical moisture content. Obviously, the critical moisture content is not an intrinsic property of the material. It varies depending on the evaporation condition: a lower drying rate results in a lower critical moisture content.

We have investigated the effect of ferrocyanide inhibitor on the crystallization behavior of NaCl both in bulk and in porous material. For a bulk solution, in the presence of inhibitor, a high supersaturation (1.55) was attained. The inhibitor drastically changes crystal morphology. The NaCl crystal morphology changes from bigger cubic to smaller fluffy dendritic crystals. These dendritic salt crystals spread all over the surface of a substrate and can therefore enhance the drying rate. In contrast, no supersaturation was found in porous media in the presence of inhibitor. This is due to the formation of dendritic crystal morphology. The branches of dendritic crystals which develop at the drying surface provide a larger surface area for evaporation at the material/air interface. As a result, advection becomes the governing phenomenon (Pe > 1). Consequently, the dissolved salt ions crystallize as efflorescence on the material surface and no higher supersaturation is generated inside the porous material. As a result, in general, inhibitor will not generate higher stresses in the material induced by crystallization. The influence of ferrocyanide ions on N aCl nucleation behavior is summarized in table 8.1.

The use of inhibitor is found to be more beneficial in preventing salt damage at low than at high humidity conditions. At low humidity conditions and in the absence of inhibitor, advection is dominant (Pe > 1) at the beginning of drying. The salt ions quickly crystallize

and block the drying surface. Blockage slows down the drying rate. Consequently, back diffusion of salt ions from the surface to inside the porous material occurs (Pe < 1) at the later stage of drying. This leads to sub-florescence. In the presence of inhibitor, branches of dendritic crystals provide much larger surface area for evaporation. Therefore, the drying rate enhances and advection (Pe > 1) remains the governing process even at the later stage of drying. This promotes salt crystallization as efflorescence. At high humidity conditions, the addition of inhibitor has no significant effect on either the moisture/ion transport phenomena or the amount of efflorescence formed. Advection remains the governing process at later stage of drying even in the absence of inhibitor. This is because the lower evaporative flux at the beginning of drying causes non-blocking efflorescence. The influence of ferrocyanide ions on m oisture/ion transport and crystallization behavior of NaCl at different relative humidity conditions is summarized in figure 8.1.

In order to use inhibitor in practical situations, the inhibitor solution has to be sprayed on salt contaminated samples. For such a case, it will be necessary to give sufficient time to the inhibitor molecules to diffuse inside the contaminated material, e.g., by covering the salt contaminated material after spraying with inhibitor solution. We have shown that once inhibitor molecules diffuse inside the material, the inhibitor is effective and promotes the formation of non-destructive efflorescence on the surface, which could be brushed off.

In practice always a m ixture of salt will be present; therefore we have investigated the effectiveness of inhibitor on N aCl and on mixtures of NaCl - KCl and NaCl - LiCl. Ferrocyanide still acts as a strong nucleation inhibitor for NaCl crystallization in droplets. NaCl supersaturates (1.55) in the presence of inhibitor. However, in salt mixtures NaCl does not significantly supersaturate (1.17) anymore. For both single salt and salt mixtures, the crystal morphology changes from bigger and strongly adhered cubic crystals to smaller and fluffy dendrtitic crystals in the presence of inhibitor.

In this work, we have shown that NaCl does not supersaturate during a single drying cycle. The supersaturation in salt solution droplets increases up t o 1.16 after repeated crystallization and dissolution cycles. Note that inside a porous building material enough surface area is available in the form of pore walls for heterogeneous nucleation to take place. Therefore, the existence of high supersaturation in porous materials can be doubted. However, this still needs to be tested.

Table 8.1: *Influence of ferrocyanide ions on NaCl nucleation behavior.*

Solution/Medium	Salt	Salt + inhibitor
Bulk	No supersaturation	Supersaturation
Brick	No Supersaturation	No Supersaturation
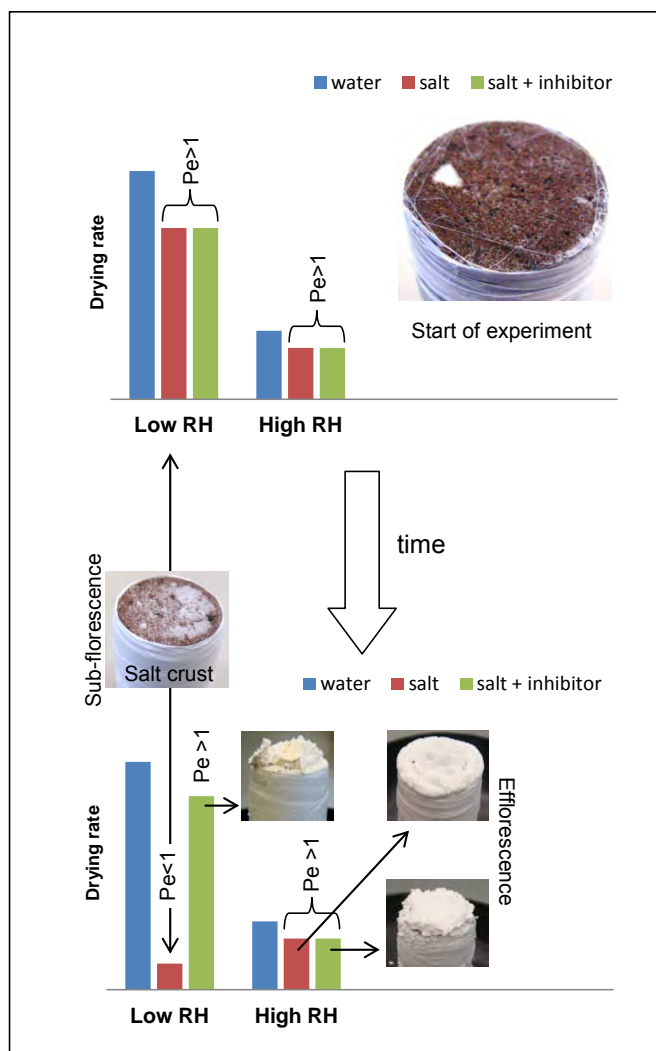
Figure 8.1: *Diagram showing the effect of ferrocyanide ions on moisture/ion transport and crystallization behavior of NaCl at different RH conditions.*

8.2 Outlook

In the previous section, important conclusions are drawn from the work presented in this thesis. However, some issues remain that need to be addressed in the future:

In this work, we mainly focused on moisture and ion transport phenomena of NaCl in porous materials. In practice, the deterioration of porous building materials is caused by the presence of salt mixtures rather than a single salt. A few commonly found salt mixtures in porous media include mixtures of NaCl, Na_2SO_4 and $NaNO_3$. The presence of several different salts together can lead to the formation of complex salt compounds in these materials. The moisture and ion transport phenomena of such compounds need to be studied. Such studies will give insight in the location of salt crystallization inside the material and will take us a step ahead to understand the damage mechanism as well.

In this thesis, the influence of inhibitor on the drying behavior of salt mixtures (NaCl-KCl, NaCl-LiCl) in salt solution droplets has been studied. The influence of inhibitor on other salt mixtures (NaCl-Na_2SO_4, NaCl-$NaNO_3$) needs to be studied in bulk, to provide a basis for more complicated experiments on bricks. Furthermore, the study needs to be extended to other porous building materials that are used in practice. In addition, it is unknown if ferrocyanide, any other inhibitor, or a combination of inhibitors can be an option as a preventive measure against salt damage caused by salt mixtures. This issue needs to be addressed in the future.

The NaCl damage mechanism itself is not clear yet. Supersaturation is considered as one of the probable causes of damage [14]. Our work shows that no NaCl supersaturation was generated inside the material during a single drying cycle. However, it still needs to be investigated if supersaturation can be reached inside a porous material after repeated drying and wetting cycles. In addition, a study of the drying behavior of salt saturated porous media while simultaneously measuring the material expansion caused by in-pore salt crystallization is required. This study will provide information on both the salt concentration and the stresses generated inside the material. This will allow testing the reaction of porous media with certain poro-mechanic properties upon in-pore salt crystallization.

Bibliography

(1) Herodotus, **420 B.C.** History 2.12, Book 2.

(2) Doehne, E. Geol. Soc. Spec. Publ. **2003**, *No. 205*, London.

(3) Scherer, G.W. Cem. Concr. Res. **1999**, *29*, 1347-1358.

(4) Rijniers, L. A.; Huinink, H. P.; Pel, L.; Kopinga, K. Phys. Rev. letters **2005**, *94*, 075503.

(5) Chapman, R. W. Am. J. Sci. **1980**, *280*, 116-129.

(6) Prebble, M. M. Nature **1967**, *216*, 1194-1195.

(7) Lavalle, J. Compt. Rend. Acad. Sci. **1853**, *34*, 493-495.

(8) Taber, S. Am. J. Sci. **1916**, *41*, 532-556.

(9) Becker, G. F.; Day, A. L. J. Geol. XX1V **1916**, *4*, 313-333.

(10) Scherer, G. W. Cem. Concr. Res. **2004**, *34*, 1613–1624.

(11) Correns, W. Disc. Faraday Soc. **1949**, *5*, 267-271.

(12) Everett, D. H. *Trans. Faraday Soc.* **1961**, *57*, 1541–1551.

(13) Steiger, M. J. Cryst. Growth **2005**, *282*, 455- 469.

(14) Steiger, M. J. Cryst. Growth **2005**, *282*, 470- 481.

(15) Coussy, O. J. Mech. Phys. Solids **2006**, 54, 1517-1547.

(16) Pel L.; Huinink H. P.; Kopinga K. Appl. Phys. Lett. **2002**, *81*, 2893-2895.

(17) Rijniers L.; Huinink H. P.; Pel, L.; Kopinga K. Phys. Rev. let.**2005**, *94*, 075503.

(18) Benavente, D.; Garcia del Cura, M. A.; Garcia-Guinea, J.; Sanchez-Moral, S.; Ordonez, S. J. Cryst. Growth **2004**, *260*, 532-544.

(19) Cooke, R. U.; Smalley, I. J. Nature **1968**, *220*, 1226-1227.

(20) Scherer, G. W.; Flatt, R.; Wheeler, G. MRS Bulletin **Jan-2001**.

(21) Lubelli, B.; van Hees, R. P. J.; Huinink, H. P.; Groot, C. J. W. P. Cem. Concr. Res*.* **2006***, 36,* 678-687.

(22) Lewin, S. Z. *In Conservation of historic stone buildings and m onuments*, National Academy Press, Washington D.C., 1982; pp 120-44.

(23) Hall, C.; Hoff, W.D. *Water Transport in Brick, Stone and C oncrete,* Spon Press, London, **2002**; pp 188-194.

(24) Huinink, H.P.; Pel, L.; Michels, M.A. J. Phys. Fluids **2002**, *14*, 1389-1395.

(25) Rodriguez-Navarro, C.; Doehne, E. Surf. Process. Landf. **1999***, 24*, 191-209.

(26) Pel, L.; Sawdy, A.; Voronina, V. J. Cul. Herit. **2010**, *11*, 59-67.

(27) Kamran, K.; Pel, L.; Sawdy, A.; Huinink, H.; Kopinga, K. Mater. Struct. **2012**, *45***,** 297–308.

(28) Sangwal, K. J. Cryst. Growth **1993**, *128*, 1236-1244.

(29) Sangwal, K. Prog. Cryst. Growth charact. **1998**, *36*, 163-248.

(30) Hutter, J. I.; Hudson, S.; Smith, C.; Tetervak, A.; Zhang, J. J. Cryst. Growth **2004**, *273*, 292-302.

(31) Butt, F. H.; Rahman, F.; Baduruthamal, U. Desalination **1995**, *103*, 189-198.

(32) Hernandez, A.; Rocca, A.; Power, H.; Graupner, U.; Ziegenbalg, G. J. Cryst. Growth **2006**, *295*, 217-230.

(33) Black, S. N.; Bromley, L. A.; Cottier, D.; Davey, R.; Dobbs, B.; Rout , J. E. J. Chem. Soc. Faraday Trans. **1991**, 87, 3409.

(34) Garcia, C.; Courbin, G.; Ropital, F.; Fiaud, C. Electrochem. Acta **2001**, 46, 973.

(35) Zafiropoulou, A.; Dala, E. S. J. Cryst. Growth **2000**, 219, 477.

(36) He, S.; Kan, A. T.; Tomson, M. B. Appl. Geochem. **1999**, 14, 17.

(37) Li. H.Y.; Ma. W.; Wang, L.; Liu, R.; Wei, L. S.; Wang, Q. desalination **2006**, 196, 237-247.

(38) Rome de L'Isle, J. B. L. Cristallographie, Iimpremiere du Monsieur, Paris, 1783.

(39) Pastero, L.; Aquilano, D.; Moret, M. J. Cryst. Growth Des. **2012**, *12*, 2306-2314.

(40) Van Damme-van Weele I. M. A. Influence of additives on the Growth and Dissolution of Sodium Chloride Crystals, Ph.D. Thesis, Technical University Twente, Enschede, The Netherlands, 1965.

(41) Steinike, U.; Anrog, Z. Allg. Chem. **1962**, *317*, 186.

(42) Glasner, A.; Zidon, M. J. Crys. Growth **1974**, 21, 294.

(43) Navarro, C. R.; Fernandez, L. L.; Doehne, E.; Sebastian, E. J. Cryst. Growth **2002**, *243*, 503-516.

(44) Bode, A.A. C.; Vonk, V.; Van den Bruele, F. J.; Kok, D. J.; Kerkenaar, A. M.; Mantilla, M. F.; Jiang, S.; Meijer, J. A. M.; Van Enckevort, W. J. P.; Vlieg, E. J. Cryst. Growth Des. **2012**, *12 (4)*, 1919–1924.

(45) Gupta, S.; Terheiden, K. H.; Pel, L.; Sawdy, H. J. Cryst Growth Des. **2012**, *12*(8), 3888-3898.

(46) Linnow, K. Salt damage in porous materials: an RH-XRD investigation. Ph.D. thesis, Universität Hamburg, Germany, 2007.

(47) Sawdy, A.; Heritage, A. Envior. Geol **2007**, *52:303*, 315.

(48) Franzen, C.; Mirwald, P. W. Chemie der Erde **2009**, 69, 91–98.

(49) Linnow, K.; Steiger, M.; Lemster, C.; Clercq, H.D.; Jovanović, M. Environ. Earth Sci. **2013**, *69*, 1609-1620.

(50) Clercq, H. D.; Jovanovic, M.; Linnow, M.; Steiger, M. Environ. Earth Sci. **2013**, *69*, 1751–1761.

(51) Pel, L. Moisture Transport in porous building materials. Ph.D. thesis, Eindhoven University of Technology, The Netherlands, 1995.

(52) Nachshon, U.; Weisbrod, N.; Dragila, M.I.; Grader, A. Water Resour. Res. **2011**, *47* W03513.

(53) Peysson, Y.; Bazin, B.; Magnier, C.; Kohler, E.; Youssef, S. Energy Procedia **2011**, *4*, 4387-4394.

(54) Prat, M. J. Heat Mass Tr. **2007**, *50*, 1455-1468.

(55) Prat, M.; Bouleux, F. Phys. Rev. E **1999**, *60*, 5647.

(56) Chauvet, F.; Duru, P; Geoffroy, S; Prat, M. Phys. Rev. Lett. **2009**, *103*, 124502.

(57) Laurindo, J.M.; Prat, M. Chem. Eng. Sci. **1998**, *53*, 2257.

(58) Eloukabi, H.; Sghaier, N.; Nasrallah, S. Ben; Prat, M. Intern. J. Heat Mass Tr. **2013**, *56*, 80-93.

(59) Veran-Tissoires, S.; Prat, M. Formation of salt efflorescence and impact on evaporation from a saturated porous medium, submitted 2013.

(60) Kopinga, K.; Pel, L. Rev. Sci. Instrum. **1994**, *65*, 3673-3681.

(61) Mujumdar, A. S. (Ed.), *Handbook of industrial drying*, 2nd edition, Marcel Dekker, New York, **1995**.

(62) Veran-Tissoires S.; Marcoux, M.; Prat, M. Phys. Rev. Letters **2012**, *108*, 054502.

(63) Veran-Tissoires S.; Marcoux, M.; Prat, M. Europhysics Letters **2012**, *98,* 34005.

(64) R.M.; Scherer, G.W. Environ. Earth. Sci. **2013**, *69*, 2657-2669.

(65) Carmeliet, J.; Roels. S.J. Thermal Env. Build. Sci. **2002**, *25*, 209-237.

(66) Van Genuchten, M. T. J. Am. Soc. Sci. Soil. **1980**, *44*, 892-898.

(67) Mualem Y. Water Resour. Res. **1976**, *12*, 513.

(68) Le Bray Y.; Prat, M, Int. J. of Heat Mass Tr. **1999**, *42*, 4207-4224.

(69) Lubelli, B.; Van Hees, R.P.J. J. Cult. Herit. **2007**, *8*, 223-234.

(70) Bear, J.; Bachmat, Y. *Introduction to modeling of transport phenomena in porous media*; Klumer: Dordrecht, The Netherlands, 1990.

(71) Wilke, C.R. *Diffusion in gases and liquids*, McGraw-Hill, London, 1988.

(72) Navarro, C.R.; Ruiz-Agudo, E. Internal report of European Project SALT CONTROL (Project no 501517 (Contract SSP1-CT-2003-501571)) (EU project no. 501571, Prevention of salt damage to the built cultural heritage by the use of crystallization inhibitors).

(73) Pel, L.; Huinink, H.; Kopinga, K. Magn. Reson. Imaging **2003**, *21*, 317-320.

(74) Sghaler, N.; Prat, M. Transport Porous Med. **2009**, *80*, 441-454.

(75) Eloukabi, H.; Sghaier, N.; Ben Nasrallah, S.; Prat, M. J. Heat Mass Transfer **2013**, *56*, 80-93.

(76) Gupta, S.; Pel, L.; Sawdy, A. Proceedings of 12th International Congress on the Deterioration and Conservation of Stone, New York 2012.

(77) Harwood, W.S.; Herring, F.G.; Madura, J.D.; Petrucci, R.H. *General chemistry principles and modern applications 9th ed*, New Jersy, Prentice Hall, **2007**, 670-682.

(78) An expert chemical model for determining the environmental condition needed to prevent salt damage in porous materials, European Commission studies: Research Report, Archetype Publication Ltd. (Dec. 2, 2000), C. Price.

(79) Cardell, C.; Benavente, D.; Rodríguez Gordillo. J. Mater. Charact. **2008**, *59*, 1371-1385.

(80) Petkovic, J.; Huinink, H.P.; Pel, L.; Kopinga, K.; Van Hees, R.P.J. Mater. Struct. **2007**, *40*, 475-490.

(81) Twu, Y.J.; Conover, C.W.S.; Yang, Y.A. ; Bloomfield, L.A. Phys. Rev. **1990**, *42*, 5306.

(82) Nicolis, G.; Prigogine,I. *Self-Organization in Non-equilibrium Systems*, Wiley, New York, **1977**.

(83) Mullins, W.W.; Sekerka, R.F. J. Appl. Phys. **1963**, 34, 323.

(84) Abraham, F. F. *Homogeneous nucleation theory,* Academic Press, NY, 1974.

(85) NaCl-LiCl-H_2O phase diagram, received in private communication with Prof. Michael Steiger, University of Hamburg, Germany.

(86) Luquer, L. M. *Am. Soc. Civil Engg. Transac.* **1895**, *33*, 235-256.

(87) Desarnaud, J.; Shahidzadeh-Bonn, N. Europ. Phys. Letters **2011**, *95*, 48002-48002.

(88) Deegan, R.D.; Bakajin, O.; Dupont, T.F.; Huber, G.; Nagel, S. R.; Witten, T.A. Nature **1997**, *389*, 827-829.

(89) Chen, Y.L.; Helm, C.A.; Israelachvili, J. N. J. Phys. Chem. **1991**, 95, 10736-10747.

(90) Saidov, T.; Shahidzadeh, N.; Pel, L. Europ. Phys. Letters **2013**, *102*, 28003.

Summary

Salt weathering is one of the biggest threats to the long-term survival of porous building materials, historic structures and stone monuments worldwide. Soluble salts such as chloride, sulphate and nitrates are widely recognized as a cause of damage to porous building materials. Among the various salts present in building materials sodium chloride is one of the most widely distributed. The damage caused by NaCl crystallization inside porous building materials is ubiquitous. In order to stop/prevent damage caused by salt crystallization, a better understanding of the moisture and ion transport processes inside these building materials is required, as these processes governs the location of salt crystallization. In addition, effective treatment methods need to be explored to stop/reduce the damage by salts. In this thesis, the drying behavior of sodium chloride saturated porous media and the effectiveness of ferrocyanide ions as a preventive method to stop/reduce damage due to crystallization of NaCl has been studied. Ferrocyanide ions are tested as crystallization inhibitor against NaCl damage. The salt ion concentration was measured non-destructively during dynamic measurements using a specially designed NMR set-up.

Initially, the drying behavior of NaCl saturated porous media was studied and is discussed in chapter 2. It has been shown that the presence of NaCl changes the standard drying behavior of porous media. In the presence of NaCl at fast drying conditions no critical moisture content is present anymore. It has been shown that the critical moisture content varies depending on the evaporation rate. In case of NaCl solution saturated fired-clay bricks, at low humidity conditions a crust like efflorescence blocks the drying surface and reduces the drying rate. This lower drying rate helps to maintain the hydraulic connections between the drying surface and the solution which is still present inside the material and as a result no critical moisture content is present. However, at high humidity conditions, the non-blocking efflorescence which is formed keeps the system open. This maintains the initial drying rate, followed by the appearance of receding drying front and a critical moisture content is observed again.

In chapter 3, the influence of inhibitor on the moisture/ion transport and salt crystallization processes at low humidity conditions is explored. In the presence of an inhibitor a higher supersaturation and dendritic crystal morphology were found for bulk solutions of NaCl. If such a high supersaturation can be attained inside a building material it can be dangerous for the material. Therefore, the use of inhibitor was tested inside real porous materials. No supersaturation was attained inside these materials. Dendritic crystals formed in the presence of inhibitor enhanced the drying rate. As a result advection remained the governing process during drying and promoted salt crystallization outside the material as non-destructive efflorescence.

The effectiveness of inhibitor has also been tested at different relative humidity conditions and is discussed in chapter 4. The use of inhibitor is more beneficial in preventing damage at low relative humidity conditions than at high humidity conditions. At low humidity conditions the presence of inhibitor converts destructive sub-florescence to non-destructive efflorescence. This is caused by the formation of dendritic NaCl crystals at the

material/air interface. For such a case, advection remained the governing process and promotes salt crystallization outside the material. At high humidity, due to the low vapor flux at the surface of the material, the drying front is located at the surface of the material. Therefore, during drying NaCl salt ions crystallize on the surface of the material as efflorescence, even in the absence of inhibitor. For such a case the addition of an inhibitor has no influence either on the formation of efflorescence or on moisture/ion transport processes within the material.

In view of the use of inhibitor in practice, a study was performed where inhibitor solution was sprayed on NaCl contaminated materials. The results are discussed in chapter 5. It has been shown that for inhibitor to be effective, it is important to give sufficient time for the inhibitor molecules to diffuse into the material over a sufficiently large distance. This can be done by covering the material after spraying with inhibitor solution. Once the inhibitor penetrates into the material it will promote efflorescence formation.

The influence of inhibitor has been tested on salt mixtures and is discussed in chapter 6. This study has been performed in bulk salt solution droplets. In a salt mixture, NaCl does not significantly supersaturate in the presence of inhibitor, in contrast to single NaCl salt. The crystal morphology is changed to more fluffy and dendritic for both single salt and salt mixture.

The possibility of NaCl to supersaturate upon repeated crystallization and dissolution cycles has been tested in salt solution droplets and is discussed in chapter 7. An increase in crystal size and supersaturation (1.16) was seen after repeated cycles. If such a high supersaturation can be attained inside a porous material it might be dangerous for the material. However, if such a supersaturation actually occurs inside a porous media still needs to be checked.

Samenvatting

Zoutverwering vormt wereldwijd een van de grootste bedreigingen voor de duurzaamheid van poreuze bouwmaterialen, historische gebouwen en monumenten. In het algemeen worden oplosbare zouten zoals chlorides, sulfaten en nitraten gezien als de oorzaak van schade aan poreuze bouwmaterialen. Van alle zouten die in deze materialen aanwezig zijn, komt natrium chloride (NaCl) het meest voor. Schade aan poreuze bouwmaterialen veroorzaakt door NaCl is daarom wijd verspreid. Om schade door kristallisatie te voorkomen of te stoppen is een beter begrip van het vocht- en ionentransport in bouwmaterialen noodzakelijk, omdat deze processen de plaats waar zoutkristallisatie optreedt beïnvloeden. Daarnaast dienen effectieve behandelmethodes te worden ontwikkeld om de schade door zouten te stoppen of te verminderen. In dit proefschrift is het drooggedrag van poreuze materialen die verzadigd zijn met een natrium chloride oplossing bestudeerd. Daarnaast is de effectiviteit van ijzercyanide ionen als kristallisatieremmer voor NaCl onderzocht. De zoutconcentratie in het materiaal werd niet-destructief gemeten met behulp van een voor dit doel speciaal ontwikkelde NMR opstelling.

Eerst is het drooggedrag van een met NaCl verzadigd poreus materiaal bestudeerd. De resultaten van deze studie worden besproken in hoofdstuk 2. Hieruit blijkt dat de aanwezigheid van NaCl het drooggedrag van poreuze materialen significant verandert. Als NaCl aanwezig is treedt bij hoge droogsnelheden geen kritisch vochtgehalte meer op. Nader onderzoek heeft aangetoond dat het kritische vochtgehalte afhankelijk is van de verdampingssnelheid. In het geval van een met NaCl verzadigde baksteen vormt zich bij lage relatieve luchtvochtigheid een korst van zout-uitbloei die het transport door het drogende oppervlak blokkeert. Als gevolg hiervan vermindert de droogsnelheid. Deze lage droogsnelheid maakt dat het hydraulische contact tussen het drogende oppervlak en de oplossing in het materiaal in stand blijft, met als resultaat dat er geen kritisch vochtgehalte meer optreedt. Bij hoge relatieve luchtvochtigheid ontstaat er echter een niet blokkerende zout-uitbloei, waardoor het drogende oppervlak open blijft. Hierdoor blijft de initiële droogsnelheid bestaan, wat resulteert in een intrekkend droogfront en de aanwezigheid van een kritisch vochtgehalte.

In hoofdstuk 3 wordt de invloed van een kristallisatieremmer op het vocht- en ionentransport en de zoutkristallisatie bij lage relatieve luchtvochtigheid bestudeerd. Voor een bulk NaCl oplossing leidt de aanwezigheid van een kristallisatieremmer tot een hogere oververzadiging en een dendritische kristalmorfologie. Als een dergelijke oververzadiging zou worden bereikt in een bouwmateriaal kan beschadiging van dat materiaal optreden. Daarom is de kristallisatieremmer ook getest in een representatief poreus materiaal. In dit geval is geen oververzadiging gemeten. De dendritische kristallen die gevormd worden geven aanleiding tot een verhoogde droogsnelheid. Het resultaat hiervan is dat tijdens het drogen advectie het dominante transportmechanisme blijft en dat zoutkristallisatie buiten het poreuze materiaal plaatsvindt als niet-destructieve uitbloei.

Tests van de effectiviteit van een kristallisatieremmer die zijn uitgevoerd bij verschillende relatieve luchtvochtigheden worden bediscussieerd in hoofdstuk 4. Het gebruik

van een kristallisatieremmer om zoutschade te voorkomen blijkt meer effect te hebben bij lage relatieve luchtvochtigheden dan bij hoge. Bij lage luchtvochtigheden verandert de aanwezigheid van kristallisatieremmer schadelijke kristallisatie binnen in het poreuze materiaal in niet schadelijke zout-uitbloei buiten het poreuze materiaal. Dit komt door de vorming van dendritische NaCl kristallen op het drogende materiaaloppervlak. In dit geval overheerst transport door advectie, wat zoutkristallisatie buiten het materiaal bevordert. Bij hoge luchtvochtigheid bevindt als gevolg van de lage verdampingssnelheid het droogfront zich aan het oppervlak van het materiaal. Hierdoor kristalliseren de NaCl ionen aan het oppervlak van het materiaal in de vorm van zout-uitbloei, ook als er geen kristallisatieremmers aanwezig zijn. Daarom heeft in dit geval het gebruik van een kristallisatieremmer geen invloed op het vocht- en ionen transport in het materiaal.

Met het oog op het gebruik van kristallisatieremmers in de praktijk is een studie gedaan waarbij de kristallisatie remmers zijn gesproeid op NaCl verzadigde materialen. De resultaten worden besproken in hoofdstuk 5. Hier is aangetoond dat voordat een kristallisatieremmer effectief is, de moleculen van de kristallisatieremmer genoeg tijd moeten hebben om het materiaal over een voldoende afstand in te diffunderen. Dit kan bereikt worden door het afdekken van het materiaal na het besproeien met kristallisatieremmer. Nadat de kristallisatieremmer het materiaal is ingedrongen zal zout-uitbloei aan het oppervlak bevorderd worden.

De invloed van een kristallisatieremmers op een mengsel van verschillende zouten wordt besproken in hoofdstuk 6. Deze studie is uitgevoerd aan druppels zoutoplossing. In een mengsel van zouten is in aanwezigheid van een kristallisatieremmer geen significante oververzadiging van NaCl gemeten, in tegenstelling tot oplossingen met alleen NaCl. Wel verandert de kristalmorfologie in een meer pluizige en dendritische structuur, zowel voor NaCl alleen als voor een mengsel van zouten.

De mogelijkheid om oververzadiging van NaCl oplossingen te bereiken met behulp van herhaalde cycli van kristallisatie en oplossen is onderzocht met druppels zoutoplossing. De resultaten worden besproken in hoofdstuk 7. Waargenomen werd een toename van de kristalgrootte en de oververzadiging (1.16). Als deze oververzadiging zou optreden in een poreus materiaal kan dit materiaal worden beschadigd. Verder onderzoek moet uitwijzen of een dergelijke oververzadiging ook in werkelijkheid in een poreus materiaal optreedt.

List of Publications

Gupta, S.; Terheiden, K.H.; Pel, L.; Sawdy, H., Influence of ferrocyanide inhibitors on the transport and crystallization processes of sodium chloride in porous building materials, J. *Cryst Growth Des.* **2012**, *12*(8), 3888-3898.

Gupta, S.; Pel, L.; Sawdy, H. Effect of spraying Ferrocyanide on NaCl contaminated samples, Proceedings of 12th International Congress on the Deterioration and Conservation of Stone, New York **2012**.

Scherer, G.W.; Gupta, S. Pressure from Crystallization in Pore Channels, Poromechanics V: Proceedings of the Fifth Biot Conference on Poromechanics **2013**, 766-771.

Gupta, S.; Huinink, H.P.; Pel, L.; Kopinga, K., How ferrocyanide influences NaCl crystallization under different humidity conditions, Submitted in J. of Crystal Growth and Design.

Gupta, S.; Pel, L.; Kopinga, K., Crystallization behavior of NaCl droplet during repeated crystallization and dissolution cycles: an NMR study, Submitted in Euro Physics Letters.

Gupta, S.; Huinink, H.P.; Prat, M.; Pel, L.; Kopinga, K. Paradoxical drying due to salt crystallization, Submitted in J. of Chemical Engineering Science.

Gupta, S.; Pel, L.; Steiger, M.; Kopinga, K., The effect of ferrocyanide ions on sodium chloride crystallization in salt mixtures, to be submitted.

Acknowledgements

First of all, I am thankful to my daily supervisor and co-promoter Leo Pel for giving me the opportunity to work in TPM, Applied physics group. I am grateful to him for his constant support and guidance during my PhD project. Leo, you were always easily available to talk whenever I had a question. This helped me a lot to do several things in time. I learnt lot of skills from you like thinking of simple but informative experiments and aesthetically presenting your research work in scientific world. Also, your constant 'nagging' about India helped to develop defensive skills in me. Thanks for introducing me to each and every corner of New York during my internship period at Princeton University.

I am thankful to my promoter Klass Kopinga for the useful discussion during my thesis writing. Thank you for teaching me important things about technical writing. Our small discussions during the university borrel were always informative.

I would like to thank Henk Huinink. I learnt a lot from our energetic and comprehensive discussions in the last one and a half year. Henk, whenever I came to you with a question or meeting request you always gave me time despite your busy schedule. Thank you for translating Dutch to English during our group outings.

Bart and Olaf thanks for your encouraging remarks during the group meetings. I am thankful to my co-promoter Prof. Marc Prat for his useful inputs and suggestions during the preparation of my thesis. I would like to thank all my committee members for being a part of my PhD defense ceremony and for their valuable feedback on the manuscript.

I am grateful to Prof. G.W. Scherer for his constant guidance during my internship in his group at Princeton. Prof. Scherer besides your help and suggestions in research related problems, thank you for introducing me to good wines and for inviting me to a very special Thanks Giving and Christmas dinner. I had a memorable time at Princeton.

I am grateful to Prof. Michael Golombok for his guidance about dutch culture and PhD environment in the beginning of my stay in The Netherlands. Mike, chats with you were always inspiring

Stef, thanks for the technical assistance with the NMR equipments and many friendly discussions. Special thanks for supporting me always at the coffee table. I will always support your slogan 'Helmond is the place to be'. Hans, thank you for technical assistance with various instruments in the lab. Special thanks for helping and making the humidity unit next to TMA.

Raheleh, Jingping and Stefan thanks for the friendly discussions and nice outings after work. Raheleh, thanks for inviting me to delicious Iranian food and chocolate cakes several times. Thanks for time to time lunch and coffee break invitations. Jinping, thanks for introducing me to the Chinese food and traditions.

Victor, Nico and Pim, it was prettig sharing a room with you. Thanks to all of you for technical discussions and helping me out with NMR problems. Victor, thanks for theory related discussions and sharing some secret ice-cream recipes. Nico, our few after lunch walks were always nice. Thanks for introducing me to the Dutch culture several times and helping me to understand Dutch letters. Pim, sharing a room with you will always be

CURRICULUM VITAE

Sonia Gupta

18 Dec.1983   Born in Ludhiana, Punjab, India

2001-2004   B.Sc. from Government College for Women Ludhiana, Punjab, India

2004-2006   M.Sc. in chemistry from Panjab University, Chandigarh, India.

2007-2008   M.Phil. at Himachal Pradesh University, Department of inorganic chemistry, Shimla, Himachal Pradesh, India
M.Phil. thesis: Synthesis of nano crystalline spatulae of Lead Zirconate Titanate

2009-2013   Ph.D. at Eindhoven University of Technology, Department of Applied Physics, group Transport in Permeable Media (TPM), The Netherlands
Ph.D. thesis: Sodium chloride crystallization in drying porous media: the influence of inhibitor

Oct.2012-Jan.2013   Internship at Princeton University, Department of Civil and Environmental Engineering, group Materials Research, Princeton, New Jersey, USA

Sep.2013-Oct.2013   Postdoc. at Eindhoven University of Technology, Department of Applied Physics, group Transport in Permeable Media (TPM), The Netherlands
Research Project: Ferrocyanide for the longer life of cultural heritage